

Course of Geothermics

Dr. Magdala Tesauro

Course Outline:

1. Thermal conditions of the early Earth and present-day Earth's structure
2. Thermal parameters of the rocks
3. **Thermal structure of the lithospheric continental areas (steady state)**
4. Thermal structure of the lithospheric oceanic areas
5. Thermal structure of the lithosphere for transient conditions in various tectonic settings
6. Heat balance of the Earth
7. Thermal structure of the sedimentary basins
8. Thermal maturity of sediments
9. Mantle convection and hot spots
10. Magmatic processes and volcanoes
11. Heat transfer in hydrogeological settings
12. Geothermal Systems

Heat

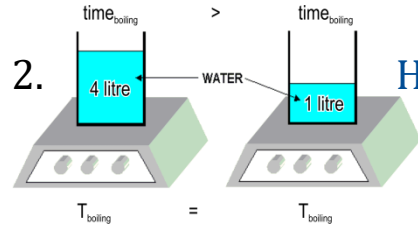
EXAMPLE 1.



MORE HEAT = HIGHER TEMPERATURE

$$Q = T$$

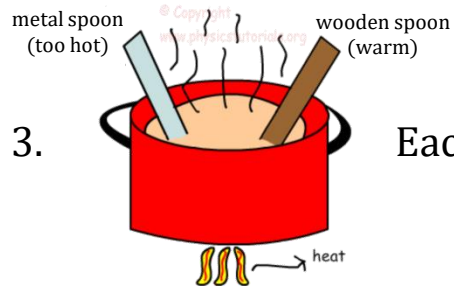
EXAMPLE 2.



HEAT depends on the MASS, TEMPERATURE NO

$$Q = m T$$

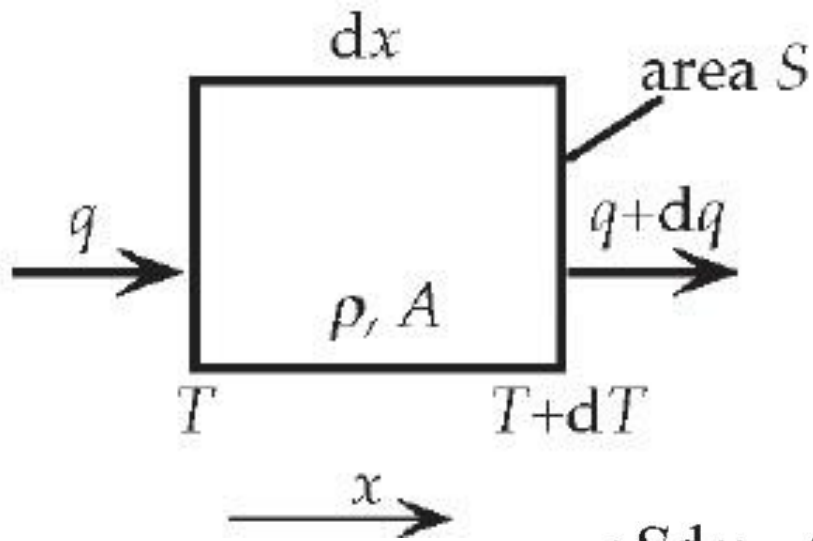
EXAMPLE 3.



Each material has its own characteristic to absorb HEAT

$$Q = m c_p T$$

Conductive Heat Transfer



The change in heat content of the block during a time interval will be equal to the heat conducted in minus the heat conducted out plus the heat generated internally (A).

$$dH = \rho S dx \cdot C_p \cdot dT$$

$$\rho S dx \cdot C_p \cdot dT = q S dt - (q + dq) S dt + A \cdot S dx \cdot dt$$

Heat Conservation Equation:
$$\rho C_p \frac{\partial T}{\partial t} = -\frac{\partial q}{\partial x} + A$$

H = heat content, ρ = density, S = area of the end surfaces of the block ($\rho S dx$ = mass of the block), and C_p = specific heat at constant pressure, which measures the capacity of a material to hold heat, and for mantle minerals it has a value of the order of 1000 J/kg K.

Poisson Equation

$$\frac{\partial T}{\partial t} = \kappa \frac{\partial^2 T}{\partial x^2} + a \quad \kappa = K/\rho C_p \quad \text{and} \quad a = A/\rho C_p \quad \frac{\partial T}{\partial t} = 0 \quad \frac{\partial^2 T}{\partial z^2} = -\frac{A}{K} \quad \text{or} \quad \nabla^2 T = -\frac{H}{\lambda} \quad A=H$$

The ratio $-A/K$ represents the change of the vertical geothermal gradient with depth

Temperature variations with depth (steady state conditions)

If there are no heat sources ($A=0$), the Poisson's equation is known as Laplace's equation: $\nabla^2 T = 0$

$$T'_0 = -q_0/K \approx 20^\circ\text{C/km.}$$

For a constant gradient, at 60 km depth the temperature would be 1200 °C (it would approach the melting point)

$$\frac{\partial^2 T}{\partial y^2} = -\frac{A}{K} \quad \text{First integration gives} \quad \frac{\partial T}{\partial y} = -\frac{A}{K}y + c_1$$

To find c_1 value: $T=T_0$ at $y=0$, then: $\partial T/\partial y = Q_0/K$ at $y = 0$

$$\text{Second integration} \quad T = -\frac{A}{2K}y^2 + \frac{Q_0}{K}y + c_2 \quad \text{since } T=T_0 \text{ at } y=0, c_2=T_0 \quad T = T_0 + \frac{Q_0}{K}y - \frac{A}{2K}y^2$$

With the boundary conditions $T=T_0$ at $y=0$ and $Q=Q_m$ (basal heat flow from the mantle) at $y=y_c$ (base of the crust)

$$\text{since } \partial T/\partial y = Q_m/K \quad \text{at } y=y_c \quad c_1 = \frac{Q_m}{K} + \frac{A}{K}y_c$$

$$T = -\frac{A}{2K}y^2 + \frac{(Q_m + Ay_c)}{K}y + c_2 \quad \text{since } T=T_0 \text{ at } y=0, c_2=T_0 \quad T = T_0 + \frac{(Q_m + Ay_c)}{K}y - \frac{A}{2K}y^2$$

Temperature variations with depth (steady state conditions)

Heat Generation changes exponentially with depth

If q_0 varies linearly with q_a :

$$q_0 = q_a + A_0 D \quad A(z) = A_0 \exp\left(-\frac{z}{D}\right)$$

$$\partial T / \partial t = 0$$

First Integration

q_a = mantle heat flow

$$\frac{\partial^2 T}{\partial z^2} = -\frac{A}{K}$$

$$k \frac{d^2 T}{dz^2} + A_0 \exp\left(-\frac{z}{D}\right) = 0 \quad k \frac{dT}{dz} - D A_0 \exp\left(-\frac{z}{D}\right) = c_1$$

c_1 is the heat flow from the asthenosphere q_a

$$q = -q_a - D A_0 \exp\left(-\frac{z}{D}\right)$$

Second Integration

$$k T + D^2 A_0 \exp\left(-\frac{z}{D}\right) - q_a z = c_2$$

$$T = T_0 \text{ at } z = 0 \quad c_2 = k T_0 + D^2 A_0$$

$$T = T_0 + \frac{D^2 A_0}{k} \left[1 - \exp\left(-\frac{z}{D}\right) \right] + \frac{q_a}{k} z$$

If A_0 is unknown we can substitute DA_0 with $Q_0 - Q_a$, since $q_0 = q_a + A_0 D$

Temperature variations with Heat Generation

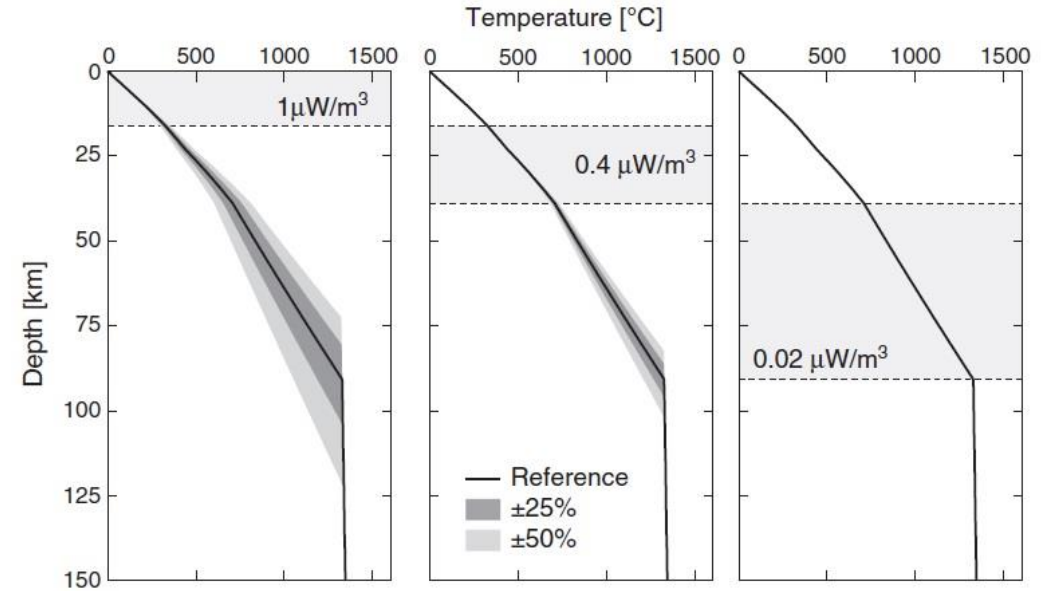
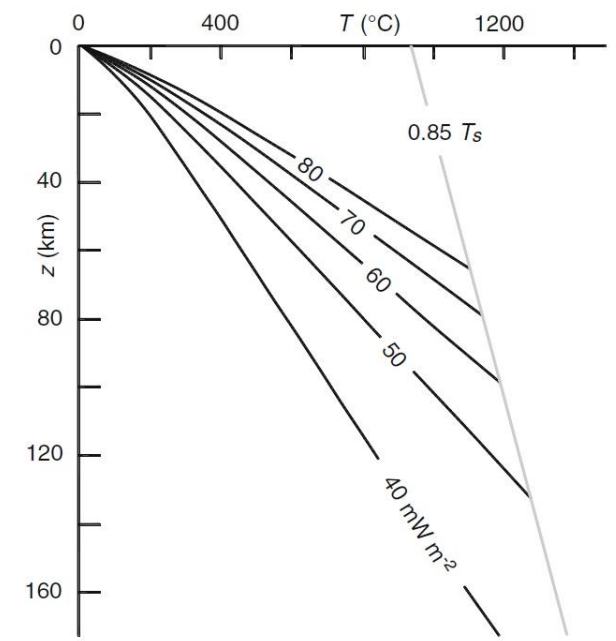
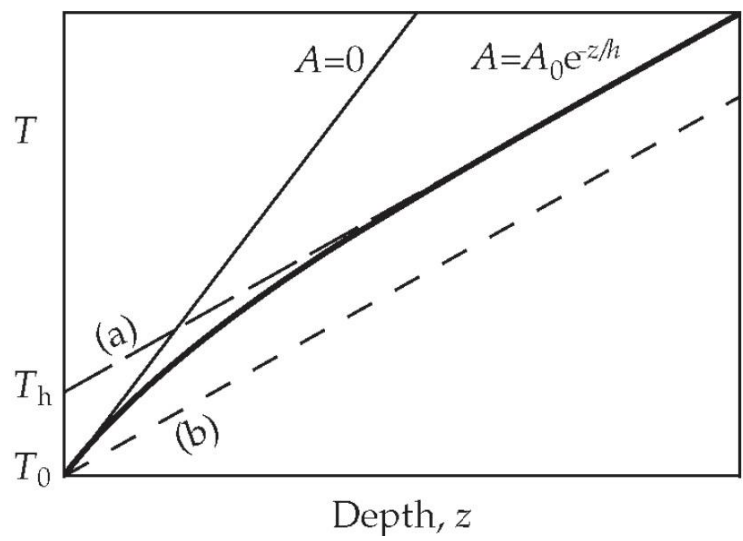
$$T = T_0 + \frac{D^2 A_0}{k} \left[1 - \exp\left(-\frac{z}{D}\right) \right] + \frac{q_a}{k} z \quad D=h \quad T'_m = T'_0 - A_0 h / K \quad T_h = A_0 h^2 / K$$

$$q_a = q_m \quad q_m = K T'_m$$

$$T = T_0 + \frac{A_0 h^2}{K} \left(1 - e^{-z/h} \right) + \left(T'_0 - \frac{A_0 h}{K} \right) z = T_0 + T_h \left(1 - e^{-z/h} \right) + T'_m z$$

$$T = (T_0 + T_h) + T'_m z \quad (\text{since at 40 km depth the term } e^{-z/h} \text{ is already as small as 0.018})$$

Temperature sensitivity to 25 and 50% variations in heat production



$Q_s = 60 \text{ mWm}^{-2}$ UC=16 km, Moho = 39 km

Hasterock and Chapman, 2011, EPSL, 307

Line (a) = asymptote of the heavy curve.

Line (b) = geotherm with $A = 0$ that would match the T at the surface and the T gradient below the zone of radioactive heating.

Internal Heating

Radiogenic Heat Production: is due to the decay of radioactive elements that are present in rocks. The amount of radioactive heat production depends strongly on the type of rocks. Typical values are 2×10^{-6} W/m³ for granites, 2×10^{-7} W/m³ for basalts and 2×10^{-8} W/m³ for mantle rocks.

Shear heat production H_s : is related to dissipation of the mechanical energy during irreversible non-elastic (e.g., viscous) deformation and is calculated via the deviatoric stresses σ'_{ij} and strain rates $\dot{\epsilon}_{ij}$:

$$H_s = \sigma'_{ij} \dot{\epsilon}_{ij} \quad \text{In 3D} \quad H_s = \sigma'_{xx} \dot{\epsilon}_{xx} + \sigma'_{yy} \dot{\epsilon}_{yy} + \sigma'_{zz} \dot{\epsilon}_{zz} + 2(\sigma_{xy} \dot{\epsilon}_{xy} + \sigma_{xz} \dot{\epsilon}_{xz} + \sigma_{yz} \dot{\epsilon}_{yz})$$

- As viscosity links strain rate to shear stress, the responsible shear stress diminishes while generating heat and thermal softening tends to impede the system.
- if shear stress is maintained constant, then the shear strain rate increases with decreasing viscosity and H_s increases with time.

Adiabatic heat production/consumption (adiabatic heating/cooling) H_a : The energy of the rock increases by the product of the applied lithostatic force and the distance of shortening during the volume change. If no change of the heat content of the system is allowed, then the rock must get warmer. Adiabatic heat production is calculated via pressure changes:

$$H_a = T \alpha \frac{DP}{Dt}, \quad \text{with } \frac{DP}{Dt} \quad \text{positive or negative}$$

Latent heat production/consumption H_L : It is due to the phase transformations in rocks subjected to changes in P and T . $H_L < 0$ for melting (heat addition) and $H_L > 0$ for crystallization (heat release).

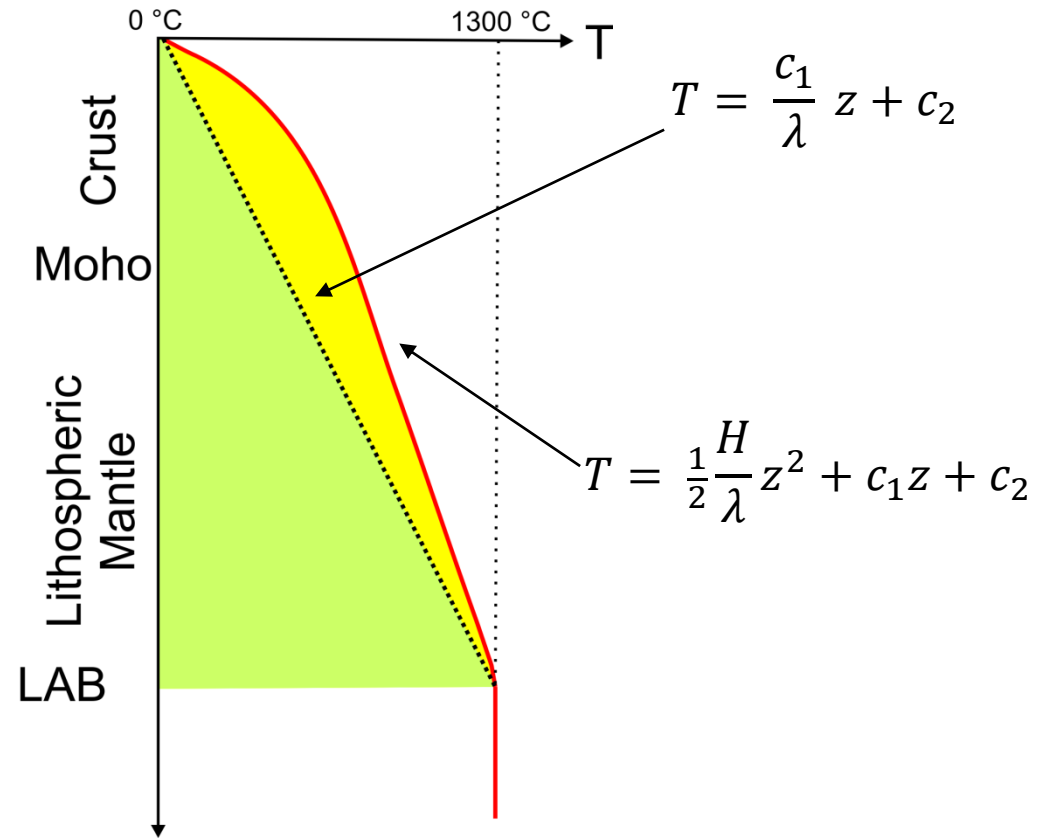
Steady-state geotherms

(valid if heat flux < 90mWm²)

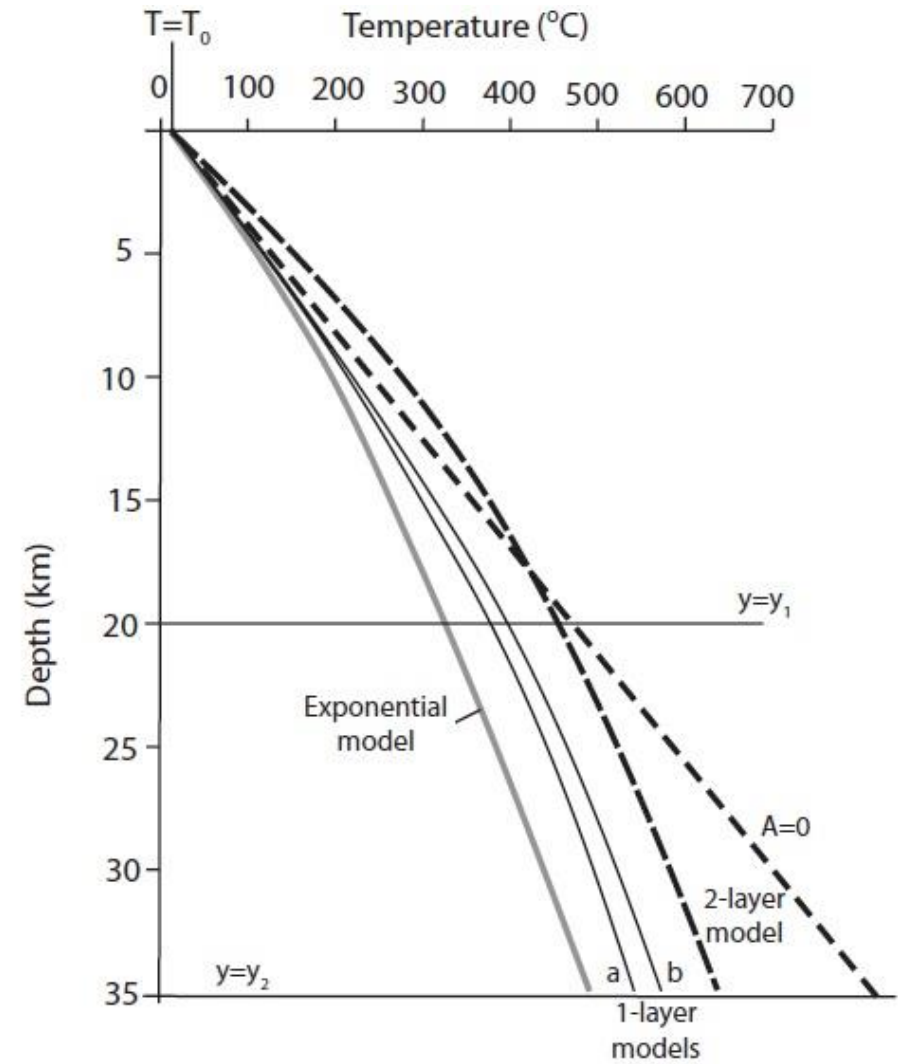
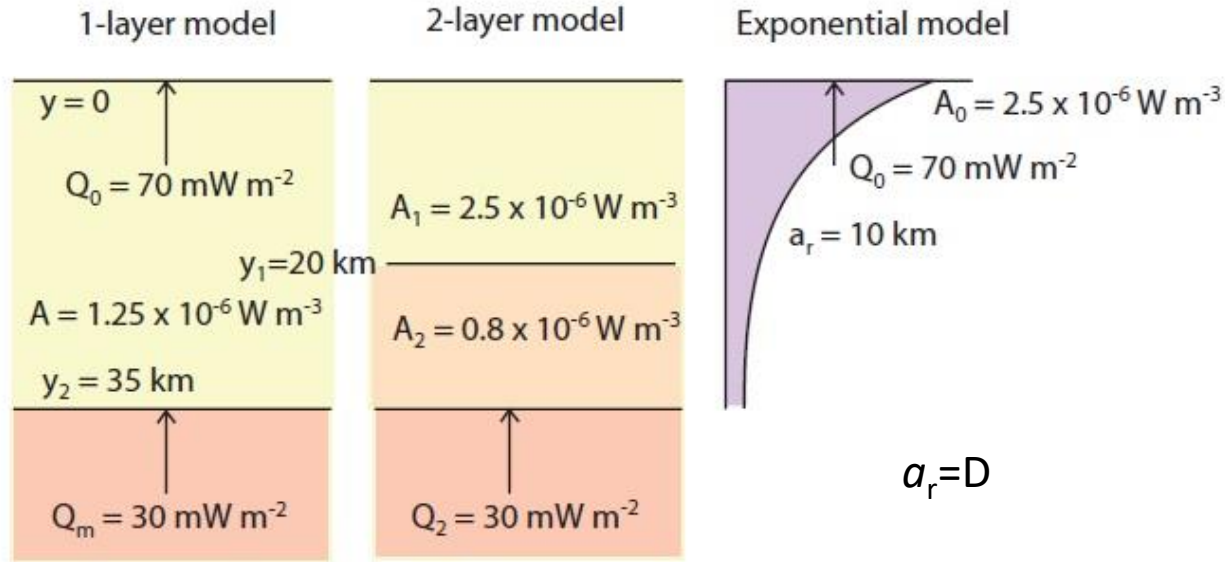
Temperature vs depth profile under steady state conditions

$$\frac{\partial}{\partial z} \left(\lambda \frac{\partial T}{\partial z} \right) = 0$$

$$\frac{\partial}{\partial z} \left(\lambda \frac{\partial T}{\partial z} \right) + H = 0$$



Temperature variations with Heat Generation



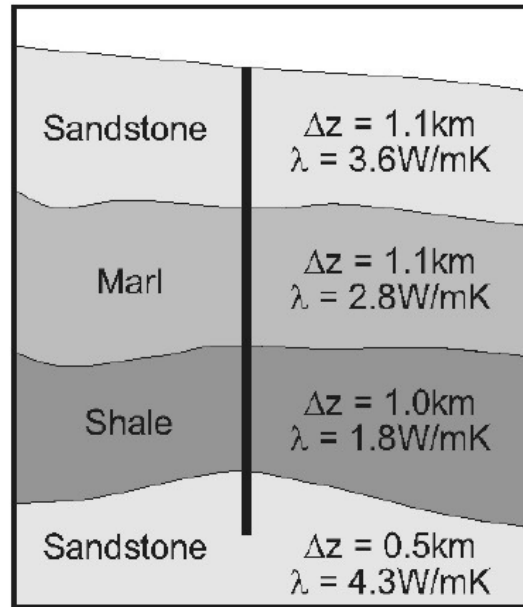
Temperature profile

The average heat flow over an interval is the product of the average thermal gradient (temperature at the top and bottom of the layer, no linear regression is used) and average thermal conductivity (e.g., harmonic mean) over the same interval.

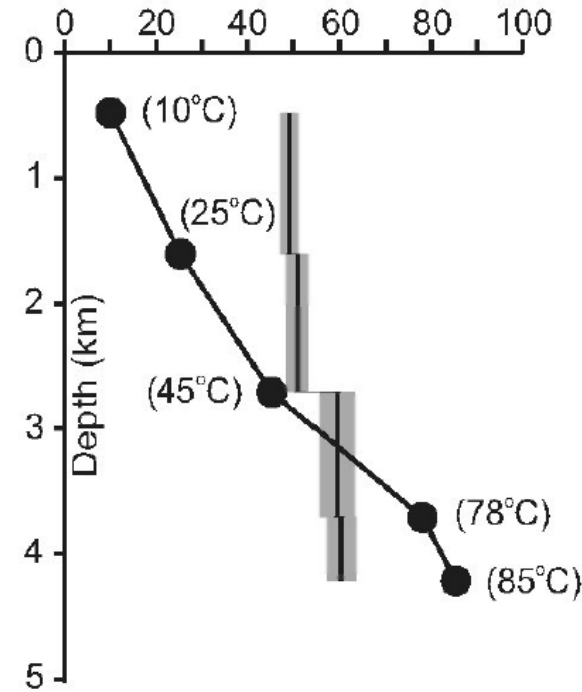
d=specific depth

$$Q_0 = Q_d + \int A(z) \partial z = \lambda_d \left[\frac{\partial T}{\partial z} \right]_d + \int A(z) \partial z$$

Stratigraphy



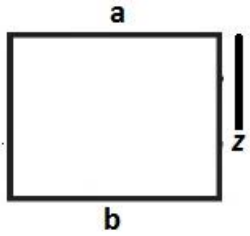
Temperature ($^{\circ}\text{C}$), Heat flow (mWm^{-2})



Temperature
Interval heat flow

Steady-state geotherms

(valid if heat flux < 90mWm²)



For a layer $a < z < b$

$$\frac{d}{dz} \left(\lambda \frac{dT}{dz} \right) = -H.$$

$$-\frac{dq}{dz} + H = 0$$

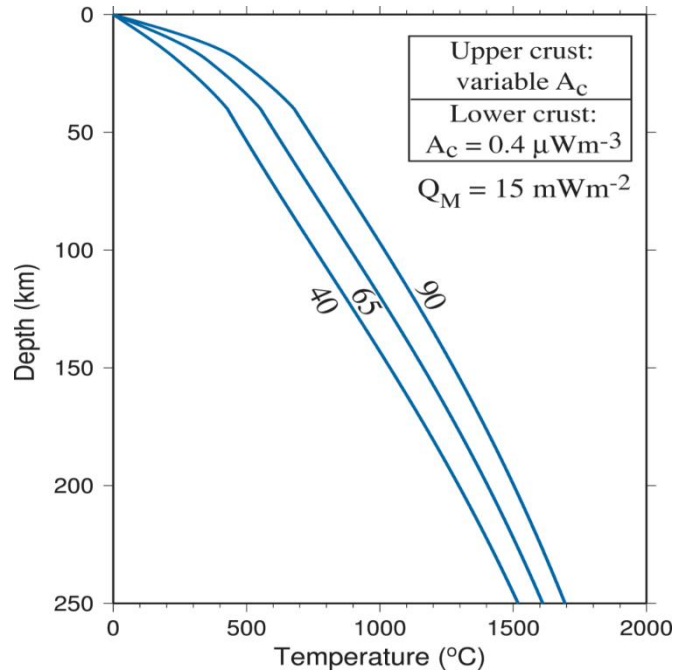
$$q(a) = q(b) + \int_a^b H dz = q(b) - H(b - a)$$

$H=A$

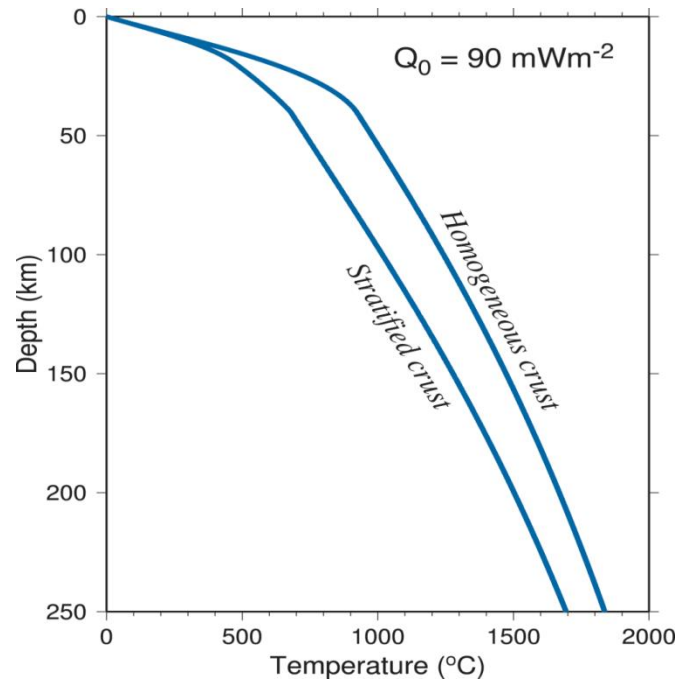
The heat flux at the top of a radiogenic layer is that at the base augmented by heat production

$$Q_0 = Q_m + \int_0^{z_m} A(z') dz'. \quad \lambda(T) \frac{dT}{dz} = Q_0 - \int_0^z A(z') dz'$$

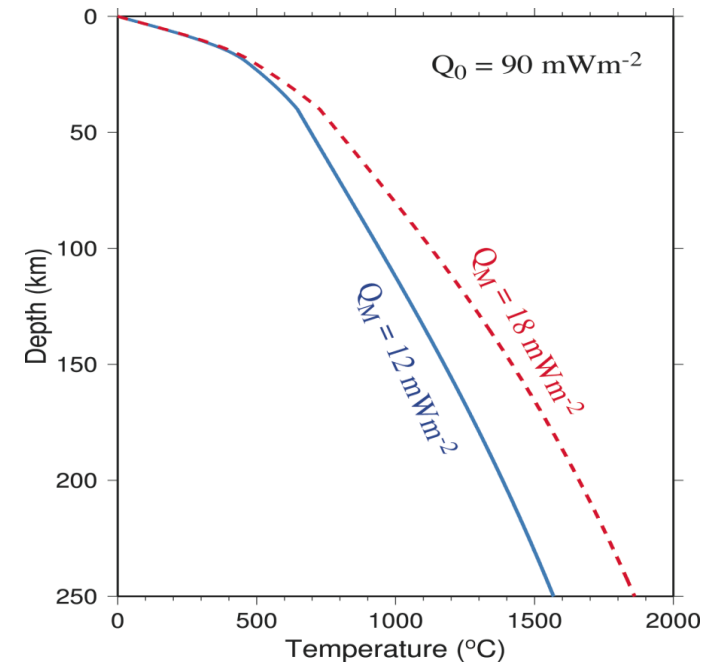
Effect of variable heat flow with a variable amounts of A_{uc}



Effect of crustal stratification

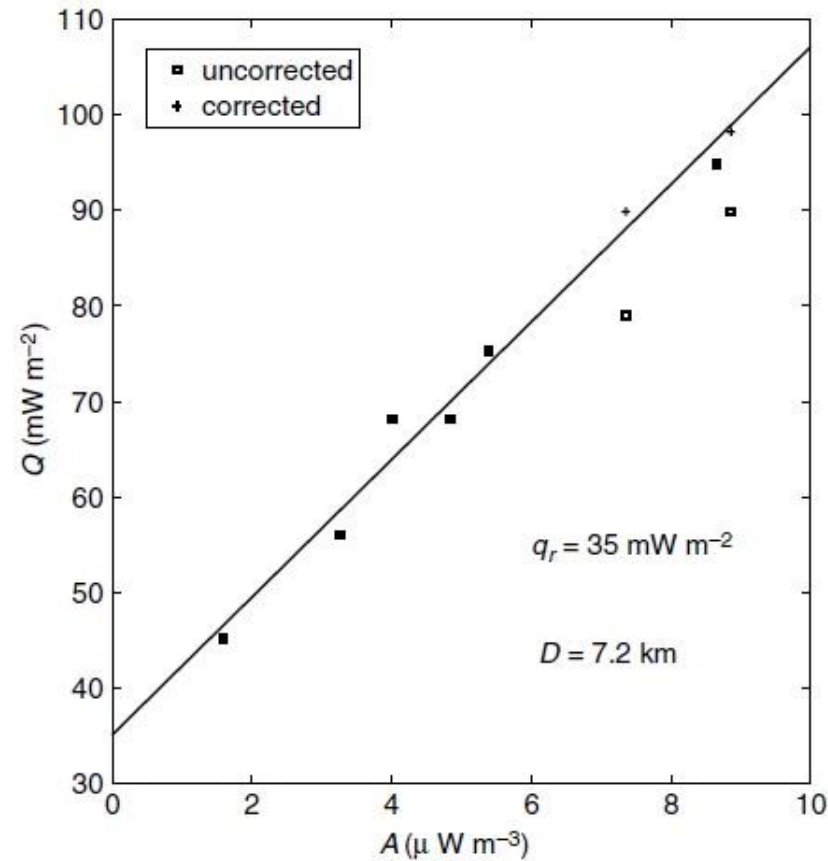


Changes of Moho heat flux



Correlation between heat generation and surface heat flow

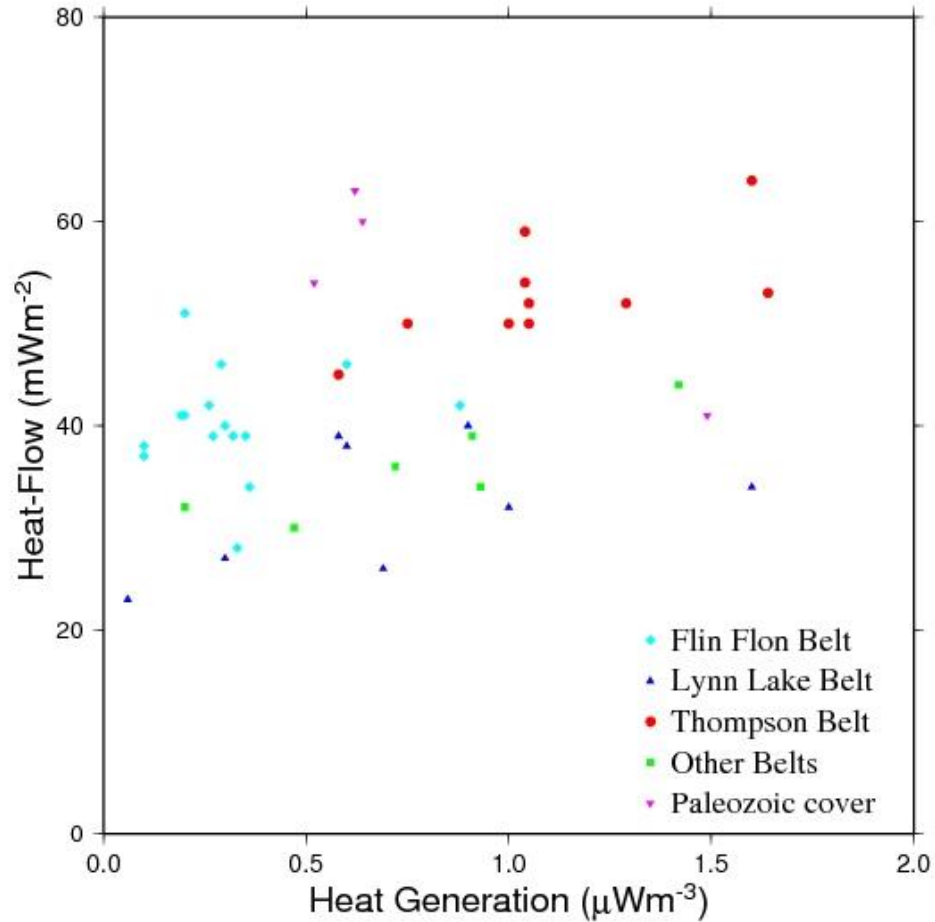
$$q_o = q_a + A_o D$$



New England

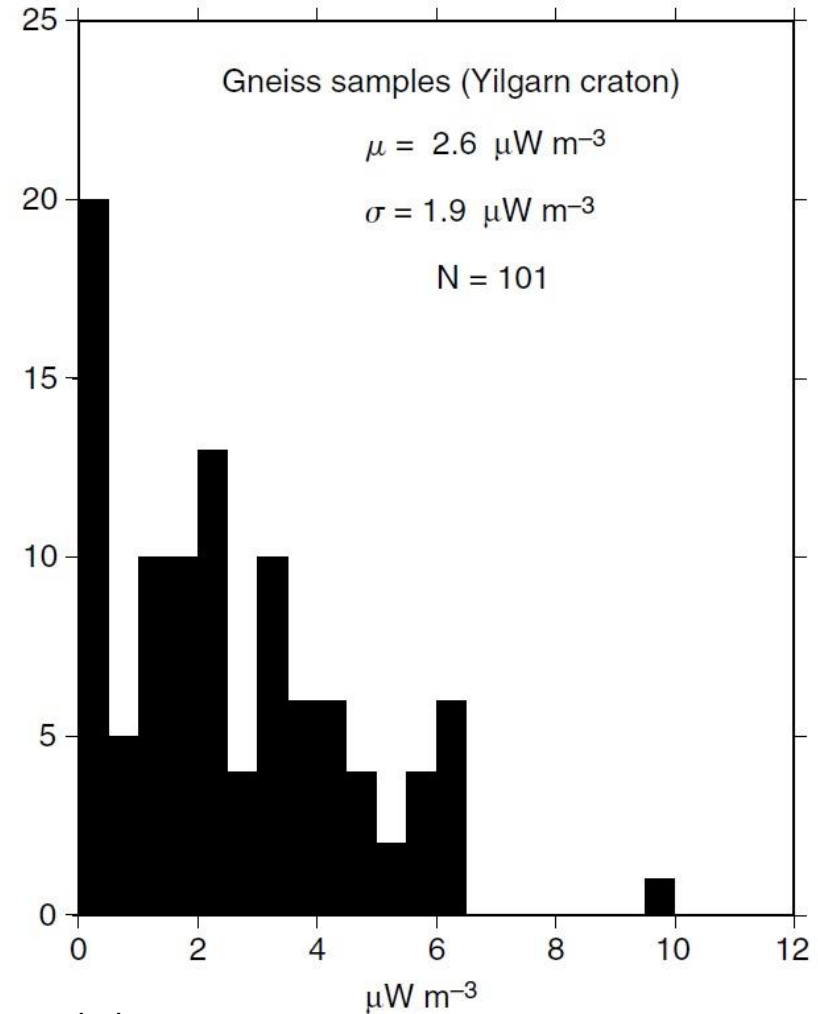
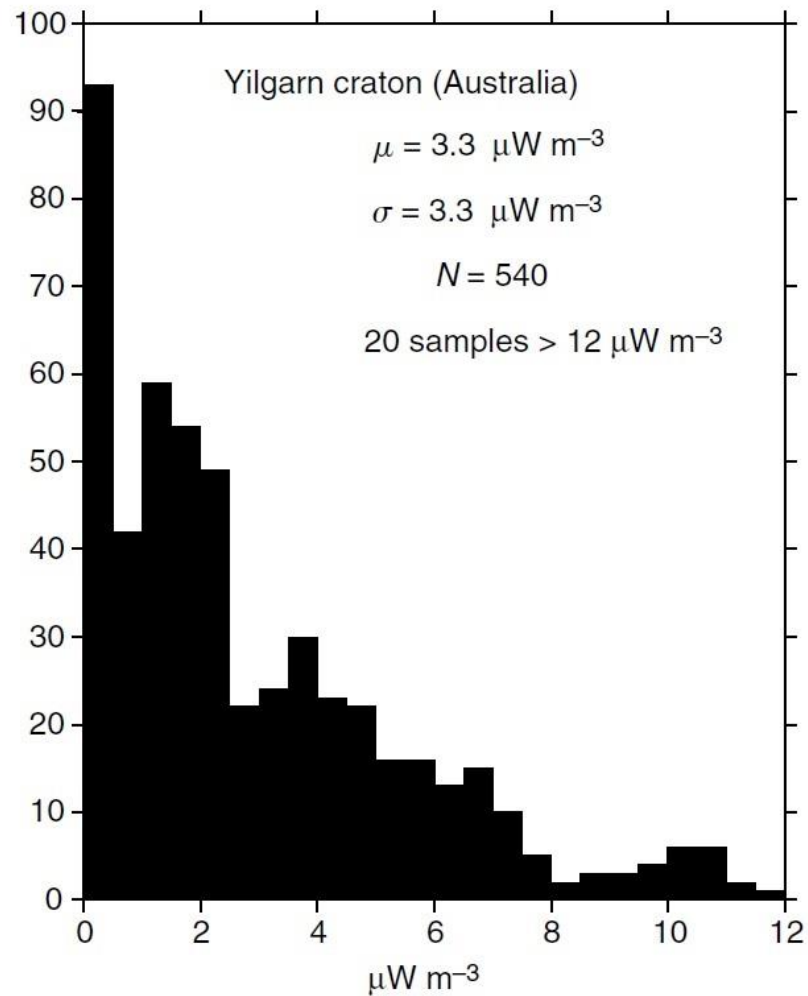
- Heat flow-heat production correlation is generally weak.
- In New England this correlation could work, since the crust has been intruded by highly radioactive plutons.

Relationship between local heat flow and heat production values ? Test : Trans Hudson Orogen



- No clear heat flow – heat production relationship for the entire THO nor for its individual belts.
- No meaningful relationship for any province of the Canadian Shield.

Lateral Variability of Heat Generation



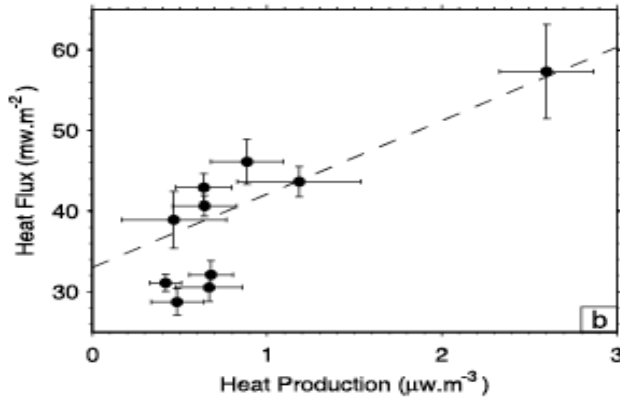
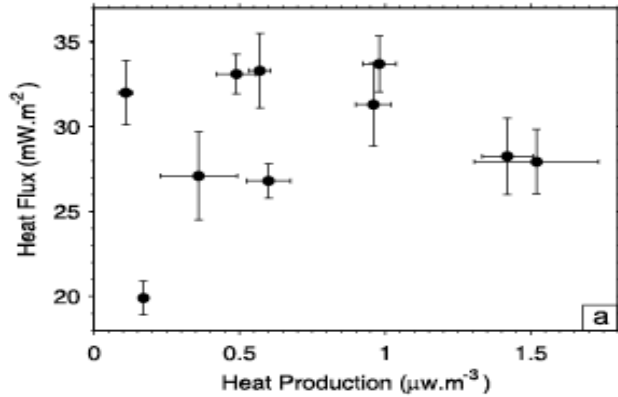
Jaupart and Mareshal, 2010

Heat Generation may vary by a factor of 5 over horizontal distances of few tens of meters, due to rocks heterogeneity, fluid migration, and phase changes.

Scale for a representative heat production model

Individual measurements

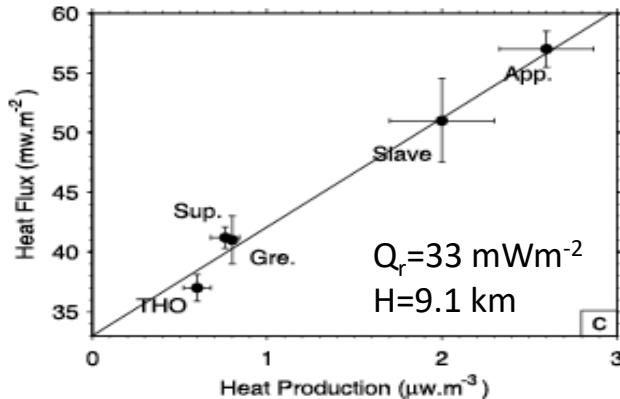
- On a large scale there is a relationship between heat flux and heat production when they are averaged on a province.
- Variations in surface heat flux between geological province occur on a short distance (< 50 km, due to variations of surface heat flow in the crust)



≈ 200x200 km windows

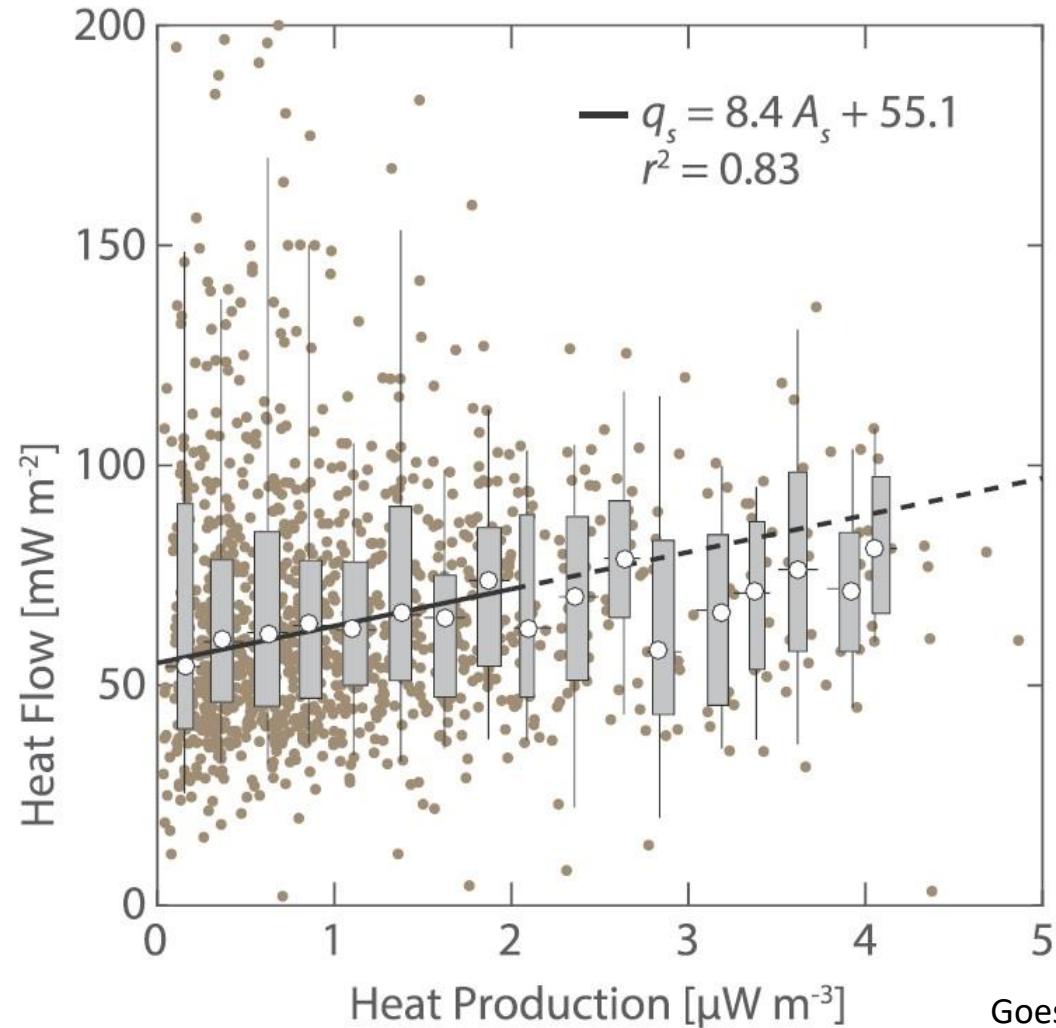
On a large scale, three key control variables on lithospheric temperatures are correlated:

- average surface heat flux,
- average crustal heat production,
- vertical variation of heat production.
- variations in the basal heat flux are small (3 mWm²).



≈ 500x500 km windows

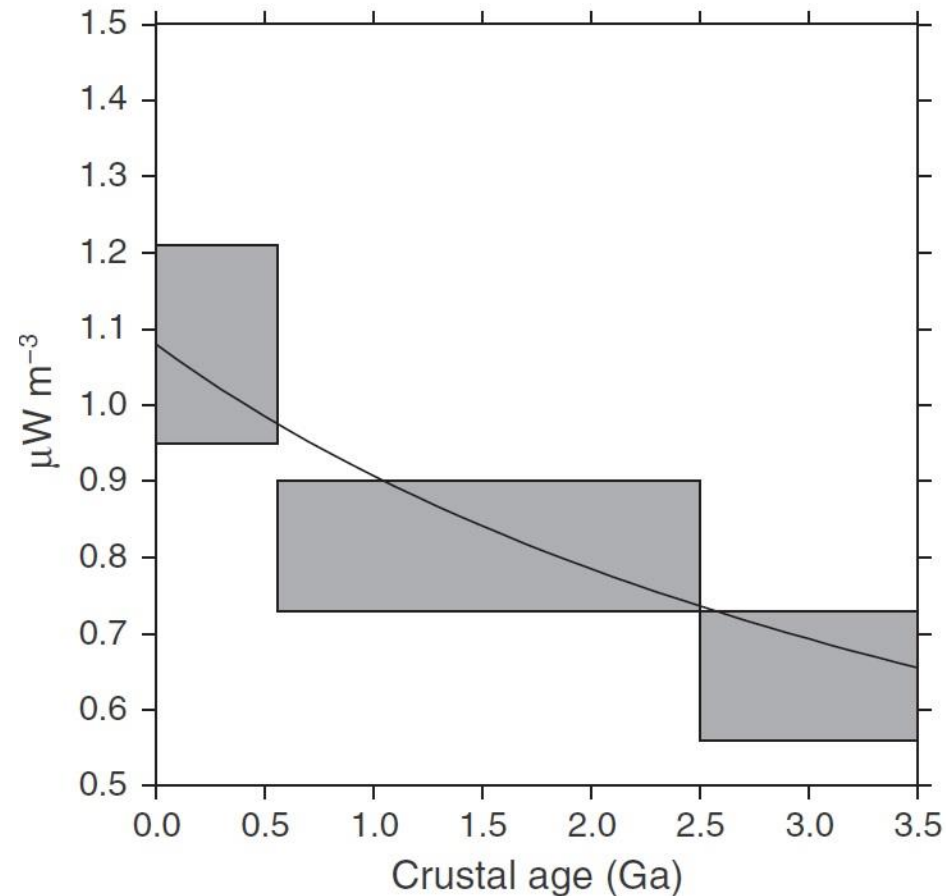
Heat Flow vs Heat Production



Goes et al., 2020, Pepi, 306

- On average a systematic increase in heat flow with increasing heat production is observed.
- Crustal heat production accounts for 25 to 40% of surface heat flow.
- Average heat flow (white circles) systematically increases up to $2 \mu\text{W m}^{-3}$ at which point there are too few points to produce reliable averages.

Heat Production and Crustal Age

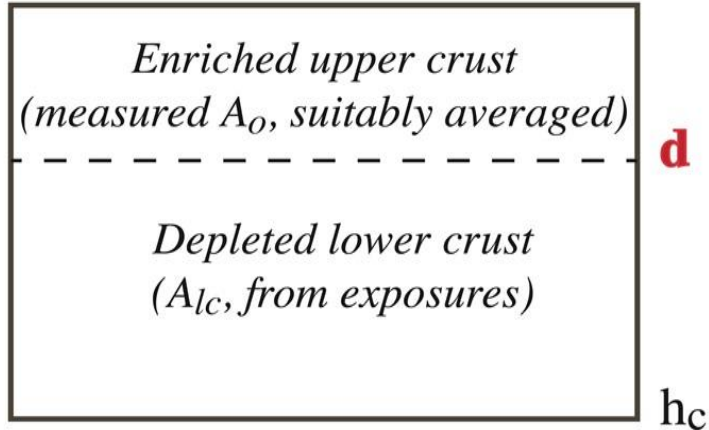


Jaupart et al., 2016, Lithos, 262

- Using a large data base of heat flow and heat production data, we can observe a trend in the distribution of crustal heat production with age.
- However, accounting for the rundown of heat producing elements due to radioactive decay, there is little change in the value of heat production at the time of crustal stabilization: present average heat production of Archean crust is about $0.7 \mu\text{W m}^{-3}$, corresponding to $1.5 \mu\text{W m}^{-3}$ at the time of crustal stabilization occurred about 2.7 Gyr.
- Therefore, heat production values in some Archean granites and gneisses are comparable to (or sometimes greater than) that of younger provinces.

Estimating the degree of enrichment in the upper crust (Differentiation index)

Measured Q_0 (suitably averaged)



Q_m (estimated)

A_s = average surface heat production

A_c = average crustal heat production

$A_c = (Q_0 - Q_m) / Z_m$

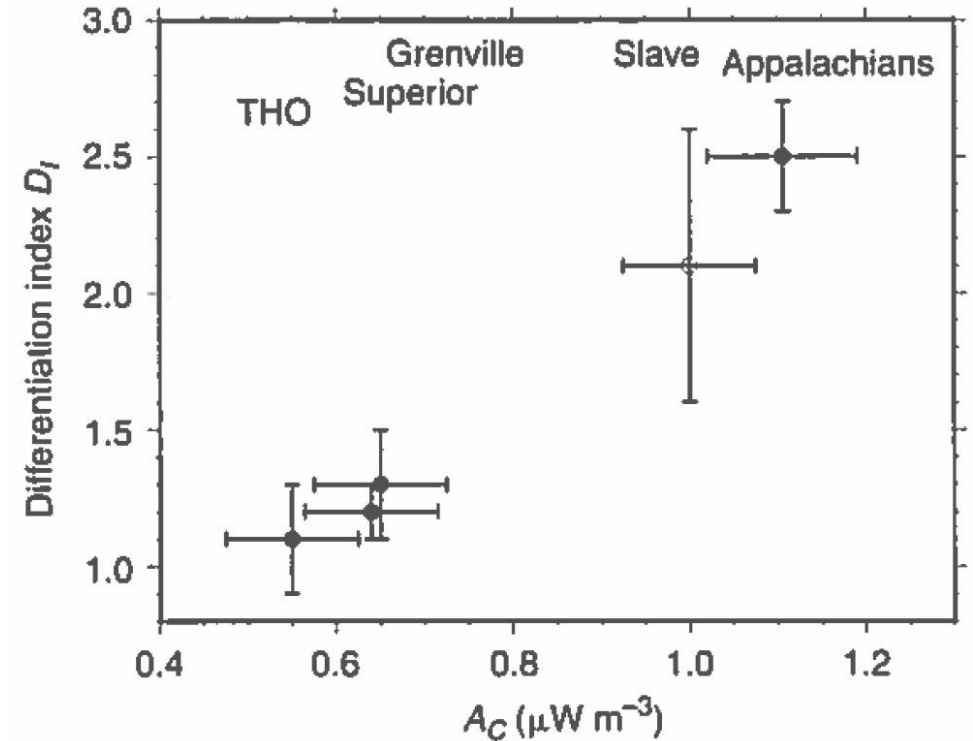
z_m = Moho depth

$$-\frac{dq}{dz} + H = 0$$

$$H=A$$

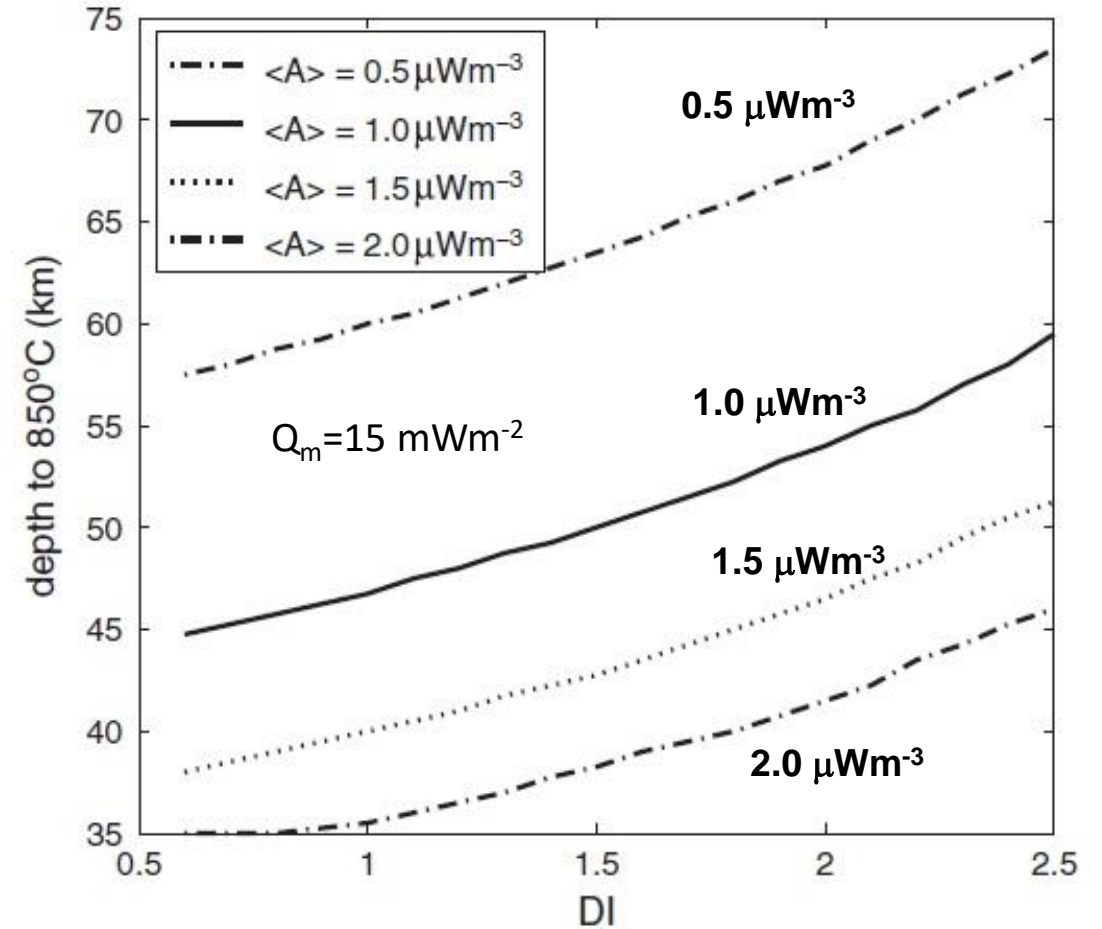
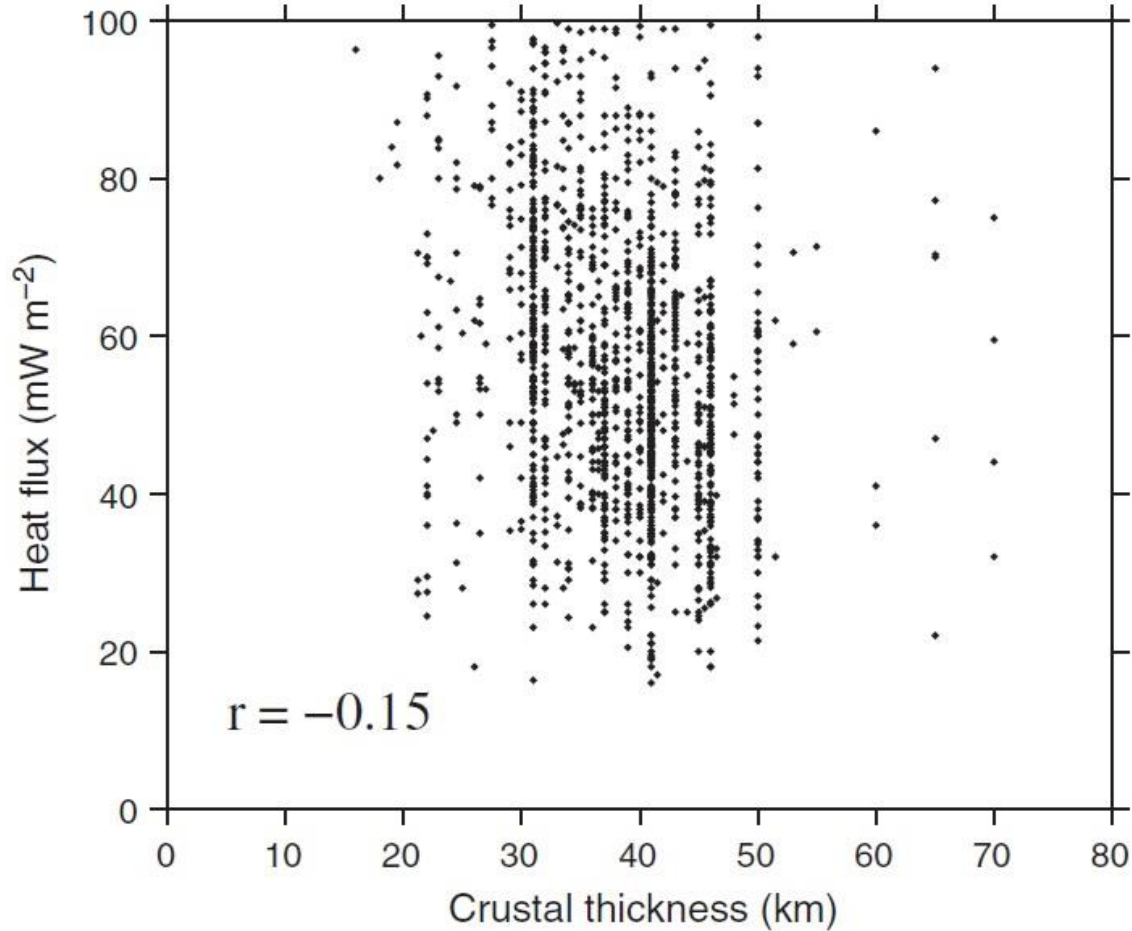
$$D_i = \frac{A_s}{A_c} = \frac{A_s z_m}{Q_0 - Q_m}$$

$$q(a) = q(b) + \int_a^b H dz = q(b) - H(b - a)$$



- Moho temperature increases with increasing A_c and decreases with increasing D_i .
- Usually $D_i > 1$, e.g., $D_i \sim 1$ for Proterozoic Grenville and $D_i \sim 3$ for Phanerozoic Appalachian. The Appalachians crust is stratified today, but its stratification is partly due to crustal melting and magma transport to the upper crust (consequence of the orogenic event).
- $D_i=0.4$ at Kola peninsula (Baltic Shield), since Proterozoic rocks were tectonically transported over Archean basement (more radiogenic).

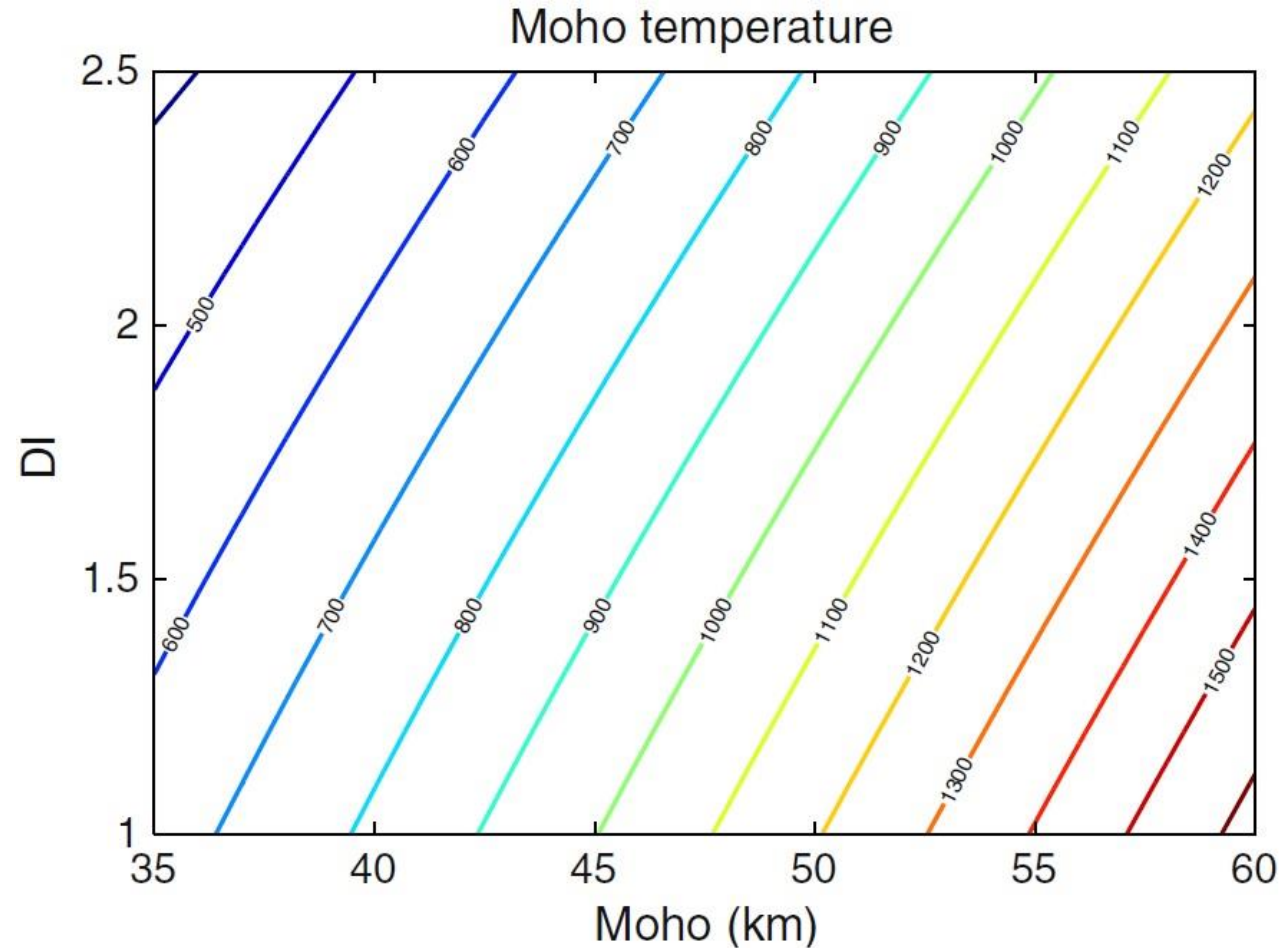
Moho Temperatures and Heat Production Distribution



(Mareschal and Jaupart, 2013, Tectonophysics 609)

No correlation between surface heat flux and Moho depth, since the crust is differentiated

Moho Temperatures and Heat Production Distribution



Jaupart et al., 2016, Lithos, 262

Mean crustal heat production = $1.5 \mu\text{Wm}^{-3}$ (Archean conditions)

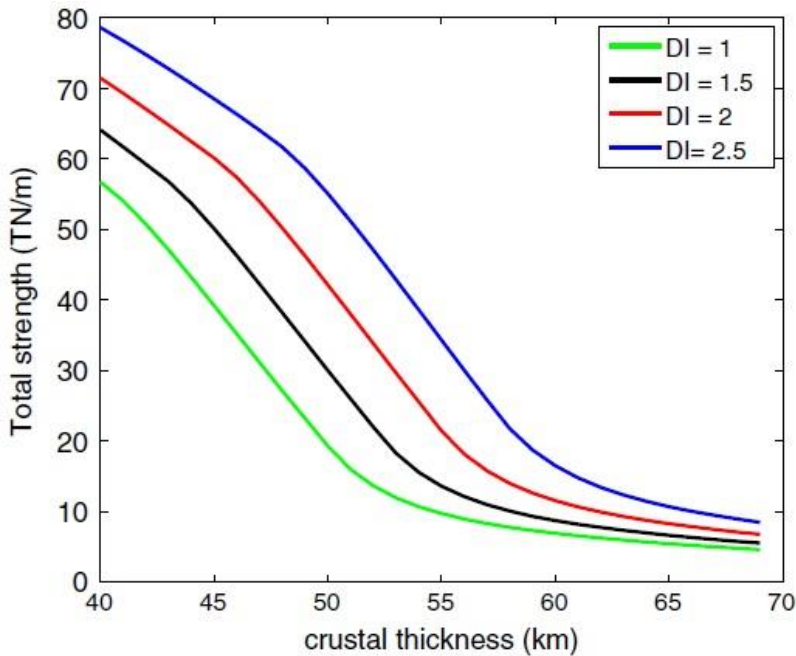
- In case the heat sources are concentrated in an enriched upper layer, the temperatures lower in the layers below.
- Independently of the degree of intra-crustal differentiation, the Moho temperature remains elevated when the crust thickens (for a 50 km deep Moho, the temperature remains $>900 \text{ }^\circ\text{C}$ for highly differentiated crust).
- Crustal heat production imposes an upper limit on crustal thickness in Precambrian time.

Strength of the Lithosphere, Crustal Thickness, and Differentiation Index (DI)

- Crustal differentiation effectively lowers the temperature at the base of the crust, allowing stabilization of a thicker crust.
- The effect of temperature on thermal conductivity results in higher Moho temperature than in calculations with uniform conductivity.

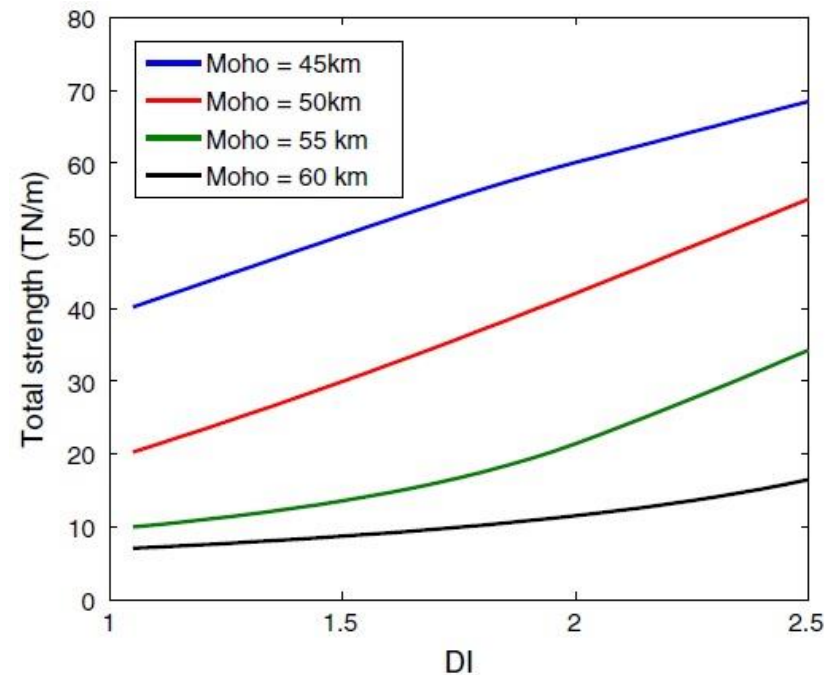
Low Integrated Strength $< 1 \times 10^{13}$ N/m (Pa m)

High Integrated Strength $> 1 \times 10^{13}$ N/m (Pa m)

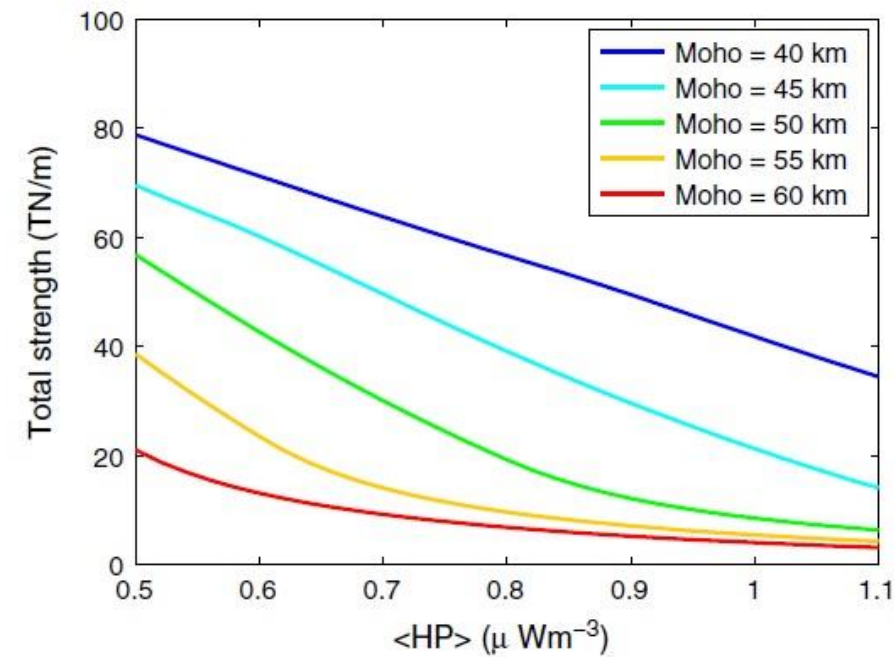


$$A_{CRUST} = 0.8 \mu W m^{-3}$$

Enriched Crustal Thickness of HPE, D=15 km



(Mareschal and Jaupart, 2013, Tectonophysics 609)

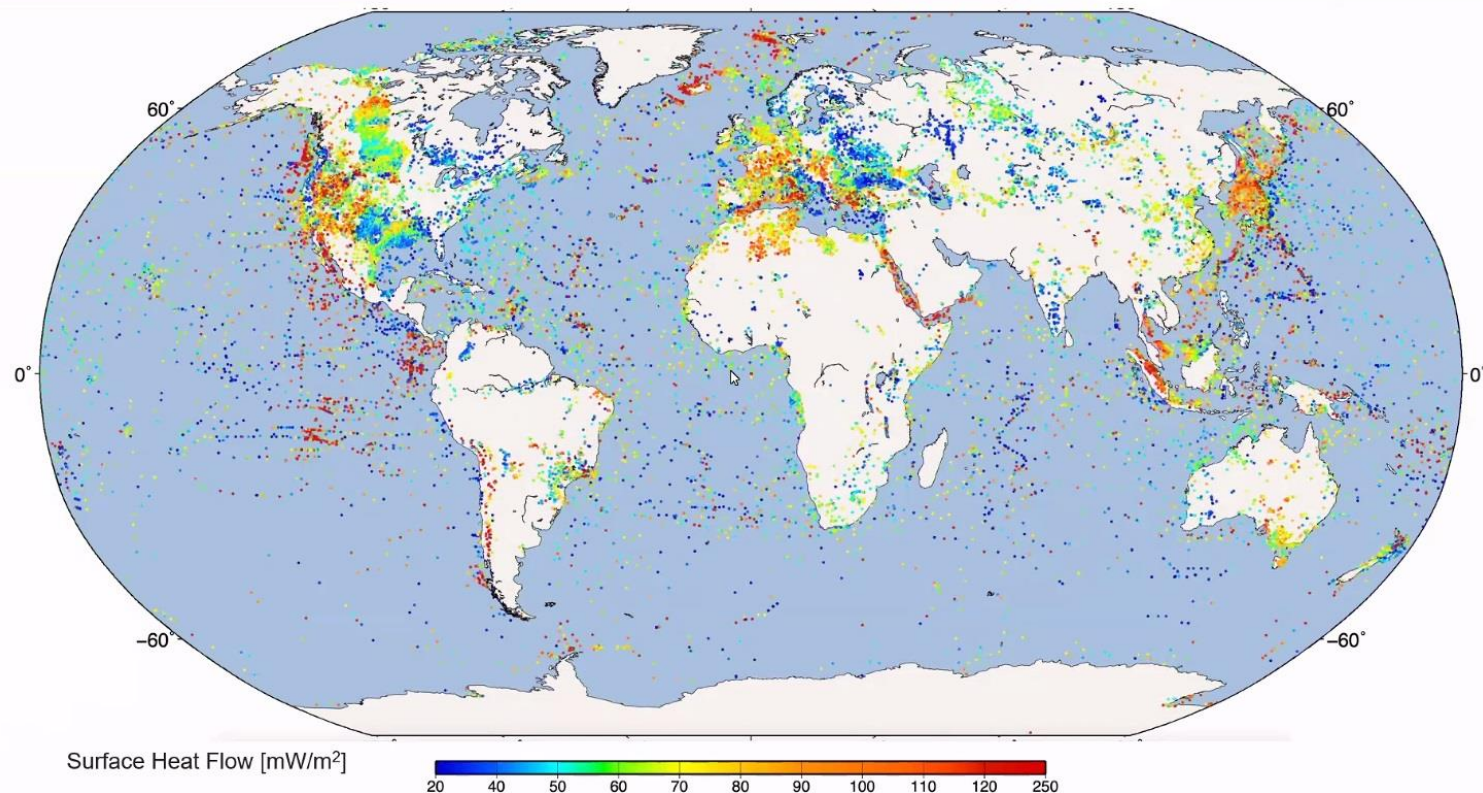


DI=1.

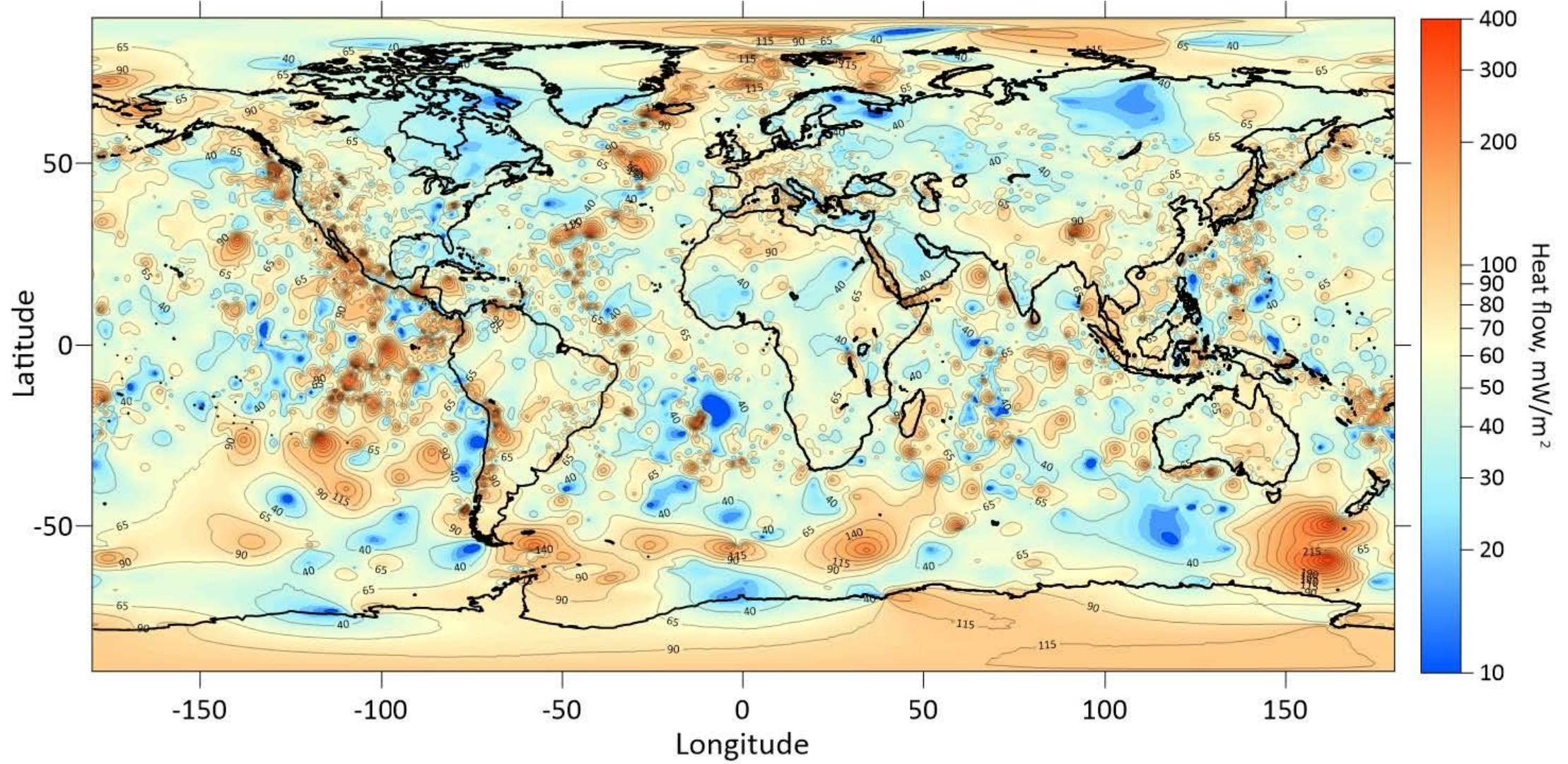
Surface Heat Flow

- Oceanic heat flux follows a decreasing trend as a function of age, average: 67 mWm^{-2} (only due to conduction), 101 mWm^{-2} (including heat loss from hot fluids).
- Oceanic lithosphere is in a transient thermal state
- Over 96% of heat flow originates from beneath the crust, poor of ^{238}U , ^{235}U , ^{40}K , and ^{232}Th .
- In the continents there is not a clear trend of heat flux with age (due to their longer evolution and complicated structure), average: 65 mWm^{-2} .
- Old continental lithosphere is close to thermal steady state.
- A large percentage of the heat flow is generated in the upper crust (10-20 km), rich of ^{238}U , ^{235}U , ^{40}K , and ^{232}Th .
- Mantle thermal anomalies cause surface heat flow perturbation with wavelength of several hundred km.

Surface Heat Flow Measurements, IHFC

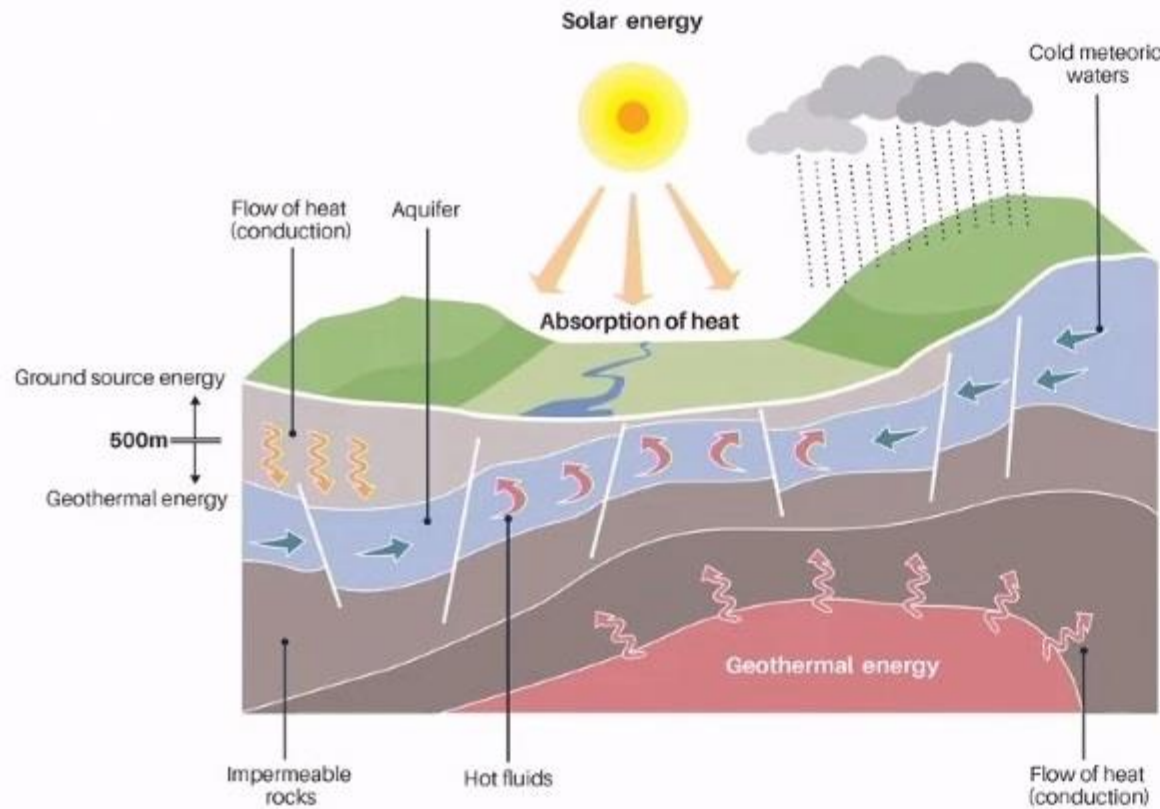


Global Surface Heat Flow



<https://www.heatflow.world>

Processes influencing the Surface Heat Flow



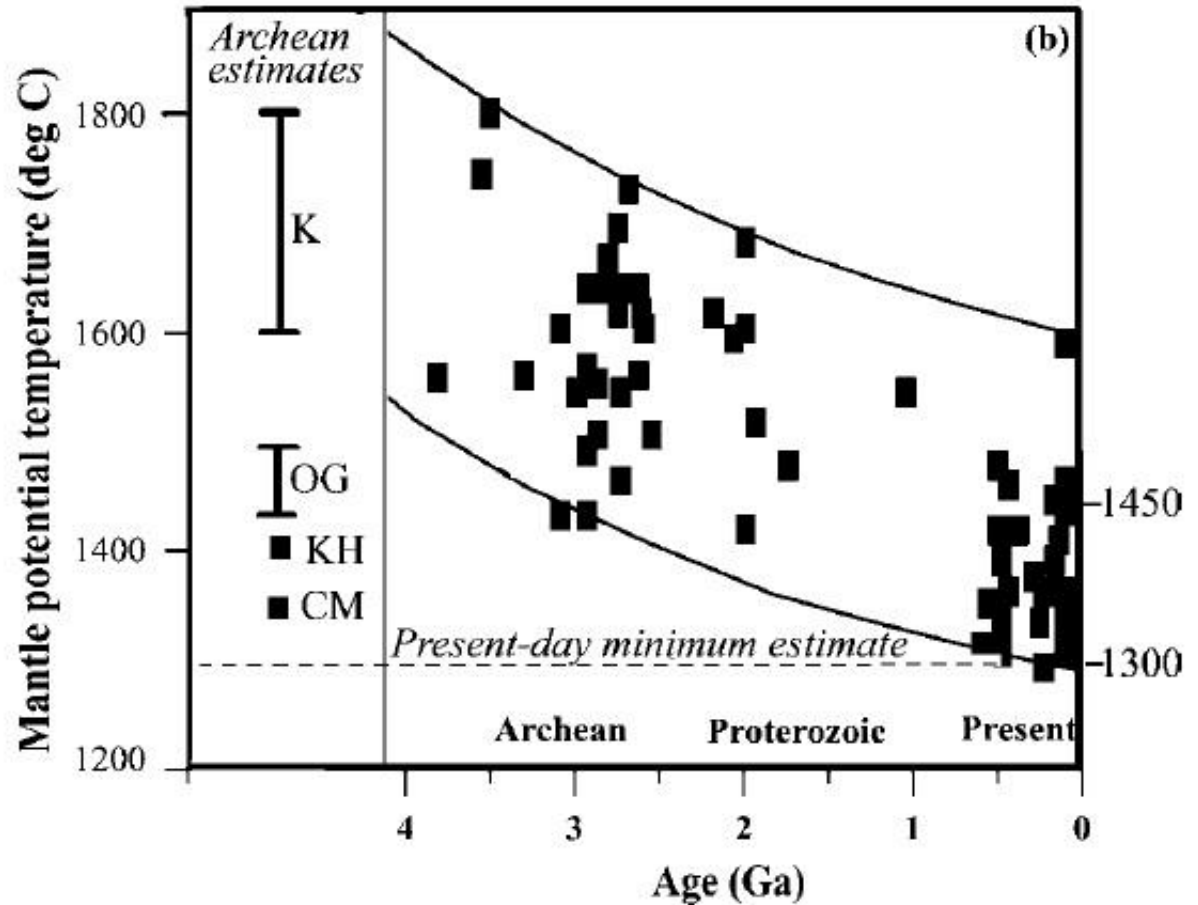
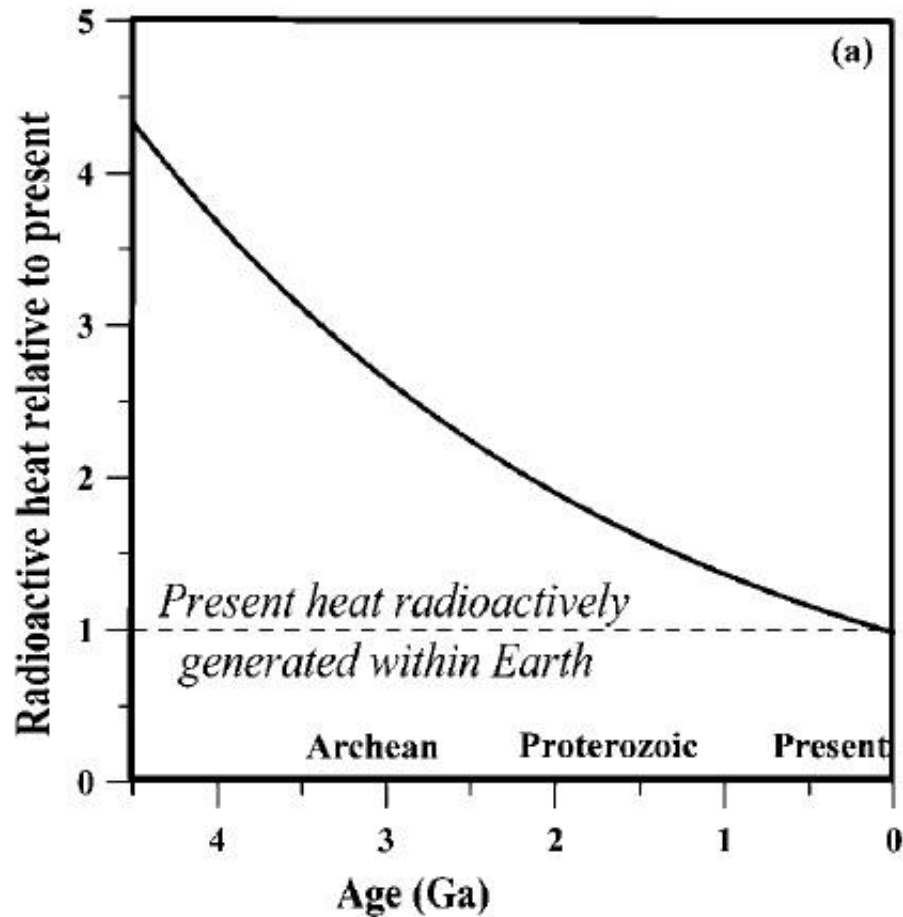
BGS, 2024

(British Geological Survey)

Heat flow values can be affected by several external processes, including:

- ✓ Groundwater circulation
- ✓ Topography
- ✓ Climatic history
- ✓ Lithological contrasts
- ✓ Borehole conditions

Thermal history of the Earth



K=Komatiite

KH=Hydrous Komatiites

OG=Ophiolites and Greenstone belts

CM=Mantle convection models

Heat flux and age: is there any trend?

Archean

Paleozoic

Regional variations of the heat flow in some Archean Cratons

Province, Craton	HFD range (mW m ⁻²)	References
Superior Province	22–48	Mareschal and Jaupart (2006)
Australian Cratons	34–54	Mareschal and Jaupart (2006)
Baltic Shield	15–39	Mareschal and Jaupart (2006)
Siberian Shields	18–46	Mareschal and Jaupart (2006)
Anabar Shield	15–25	Duchkov (1991)
Ukrainian Shield	30–50	Galushkin et al. (1991)
Karelia, Baltic Shield	35–40	Slagstad et al. (2009)
Dharwar Craton, India	25–51	Roy and Rao (2000)
eastern Dharwar Craton, India	33–73	Kumar et al. (2007a)
Karelian and Belomorian prov., Baltic Shield	20–30	Shwartsman (2001)
Belomorian Belt, Baltic Shield	20–30	Čermák et al. (1993)
Karelia and Kola Peninsula, Baltic Shield	<20–35	Čermák et al. (1993)
Laponian supracrustals	20–30	Čermák et al. (1993)

Regional mean heat flows in different Paleozoic regions

Region	Average HFD (mW m ⁻²)	References
The Appalachians	57	Jaupart and Mareschal (1999)
Mainland United Kingdom	54	Lee et al. (1987)
Dnieper aulacogen, the Ukraine	45	Čermák (1993)
Pripyat Depression, Belorussia	66	Čermák (1993)
Russian Platform	68	Čermák (1993)
Caledonian	~50	Čermák et al. (1993)
Hercynian	~70	Čermák et al. (1993)
Altay-Ergula Belt (China)	60	Hu et al. (2000)
Junggar-Higgan Belt (China)	47	Hu et al. (2000)
The Urals	30	Kukkonen et al. (1997)
Ural Foredeep ^a	29	Kukkonen et al. (1997)
West Ural Folded Zone ^a	28	Kukkonen et al. (1997)
Central Ural Uplift ^a	24	Kukkonen et al. (1997)
Tagil-Magnitogorsk Zone ^a	14	Kukkonen et al. (1997)
East Ural Uplift ^a	18	Kukkonen et al. (1997)
East Ural Depression ^a	27	Kukkonen et al. (1997)
Trans-Ural Uplift ^a	20	Kukkonen et al. (1997)
Tyumen-Kustanay Depression ^a	26	Kukkonen et al. (1997)

^a Different regions of the Urals

Range of Heat Flux:

Archean: 36–50mWm⁻²

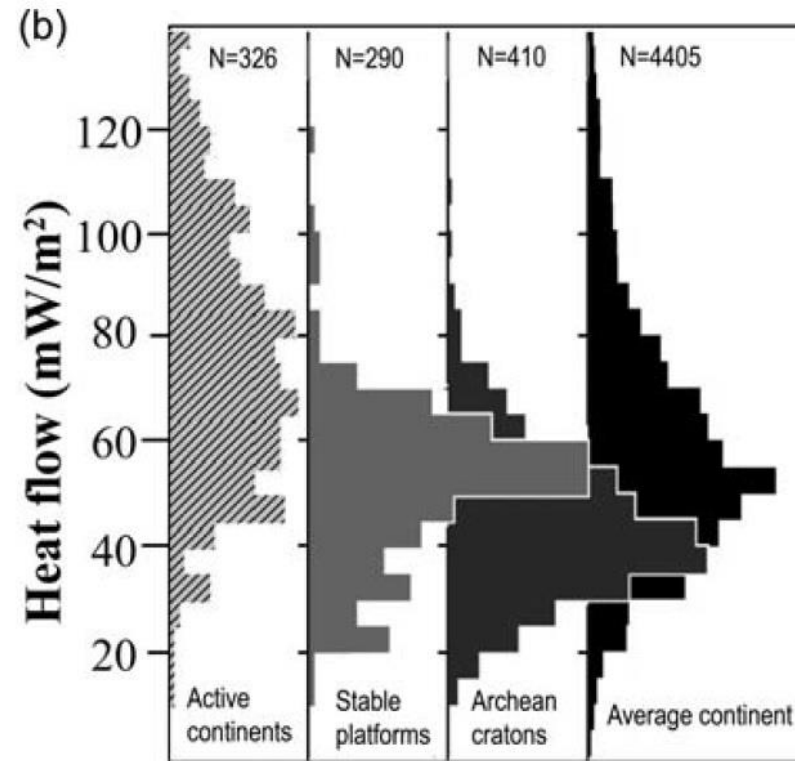
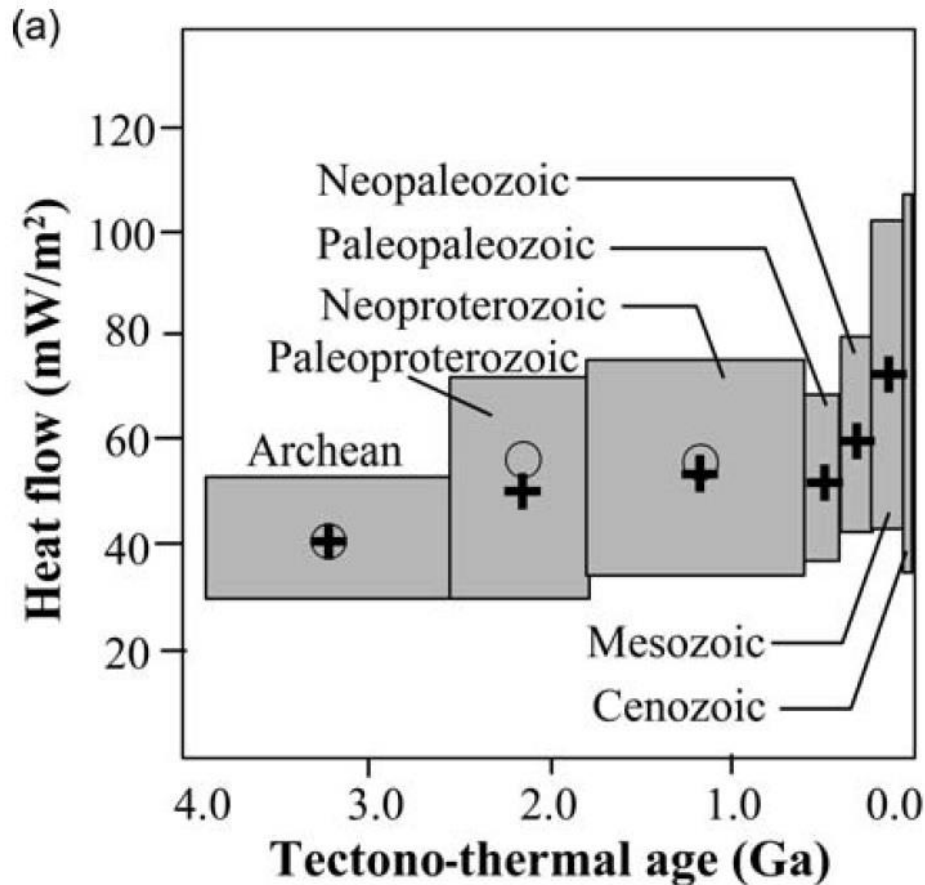
Proterozoic: 36–94mWm⁻²

Paleozoic: 30–57 mWm⁻²

Surface (Q_0) Heat Flux vs Age

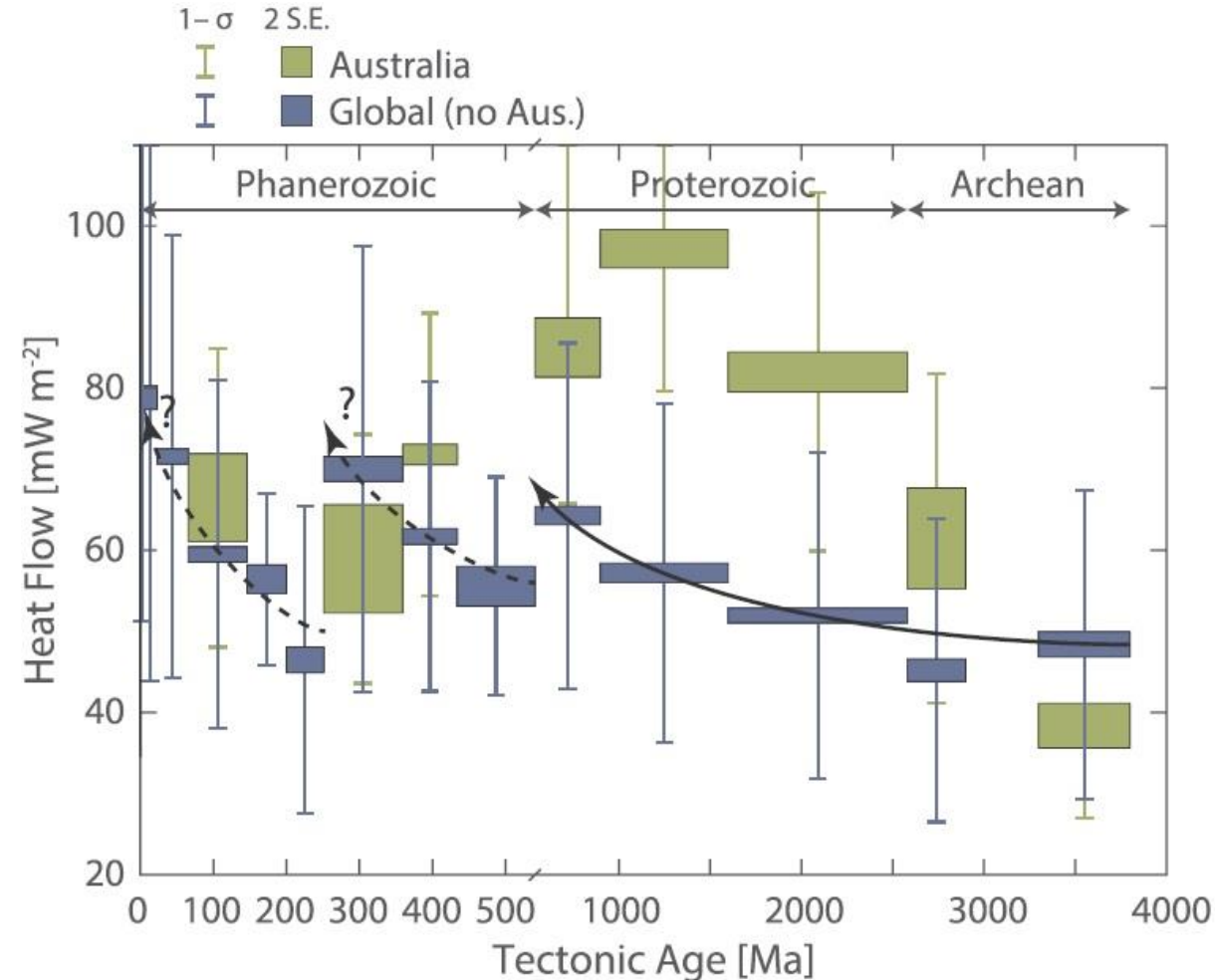
The global age trend of the heat flux can be expressed by: $Q_0=65-9t$ (Gyr) and can be attributed to:

- The relaxation time of the lithosphere after a major tectono-thermal event
- A systematic variation in crustal heat production with age (e.g., the Archean crust is prevalently composed of *Na*-granitoid, with respect to the Phanerozoic crust rich of *K*-granitoid rocks, enrichment of the younger upper crust by radioactive isotopes during orogenic event, secular changes in crust-forming processes).
- A systematic variation in lithospheric thickness and mantle heat flow with age.



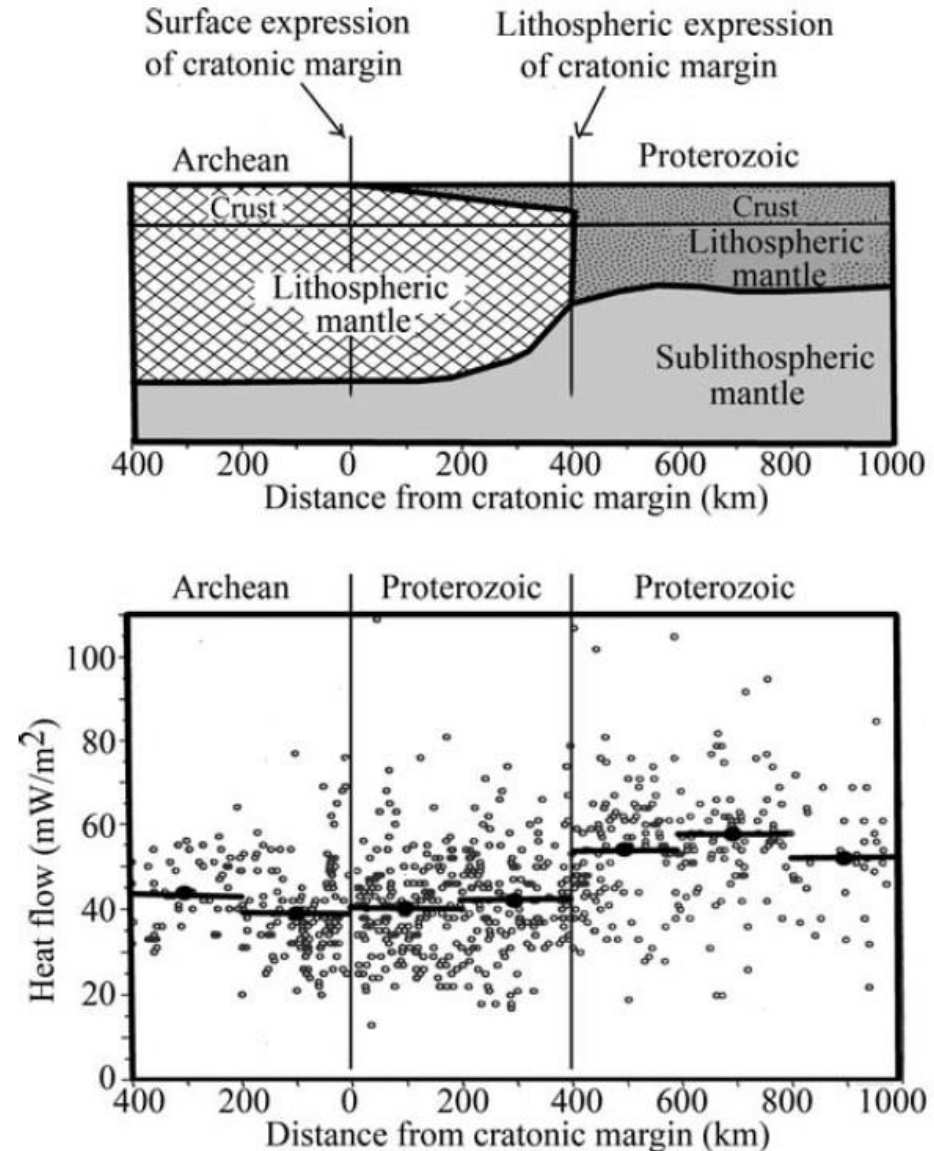
Surface (Q_0) Heat Flux vs Age

- Many of the variations at ages < 2.0 Ga appear to correlate well to the relative proportion of ferroan (more fractionated and higher heat producing) than magnesian granites.
- Ancient granites (> 2.0 Ga) are more calcic and significantly less heat producing and may be associated with trondhjemite-tonalite-granodiorite (TTG) related processes



Surface (Q_0) Heat Flux vs Age

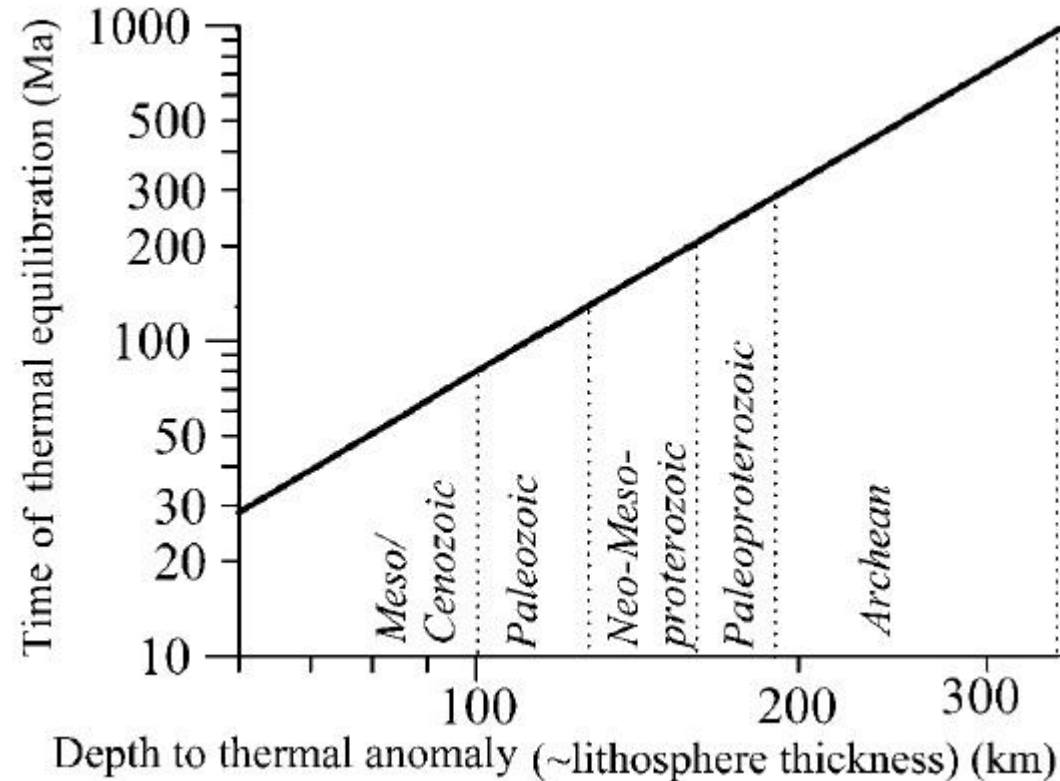
The change in heat flow pattern does not necessarily correspond to the surface expression of the cratonic margin (e.g., in case of overthrusting of terranes of different age).



Surface (Q_0) Heat Flux vs Age

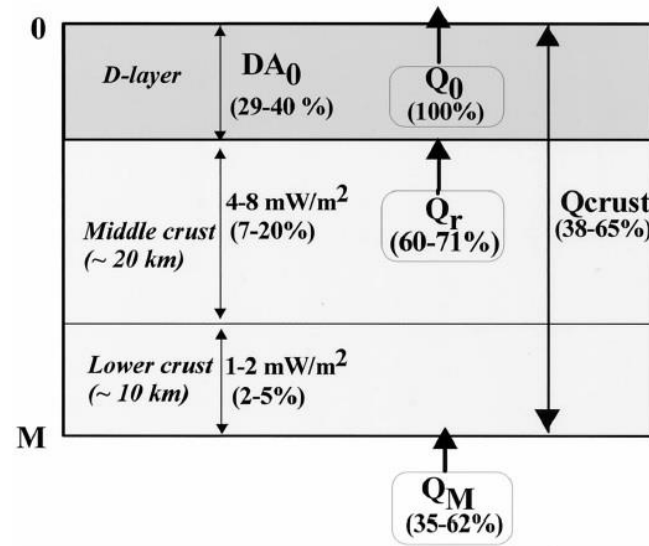
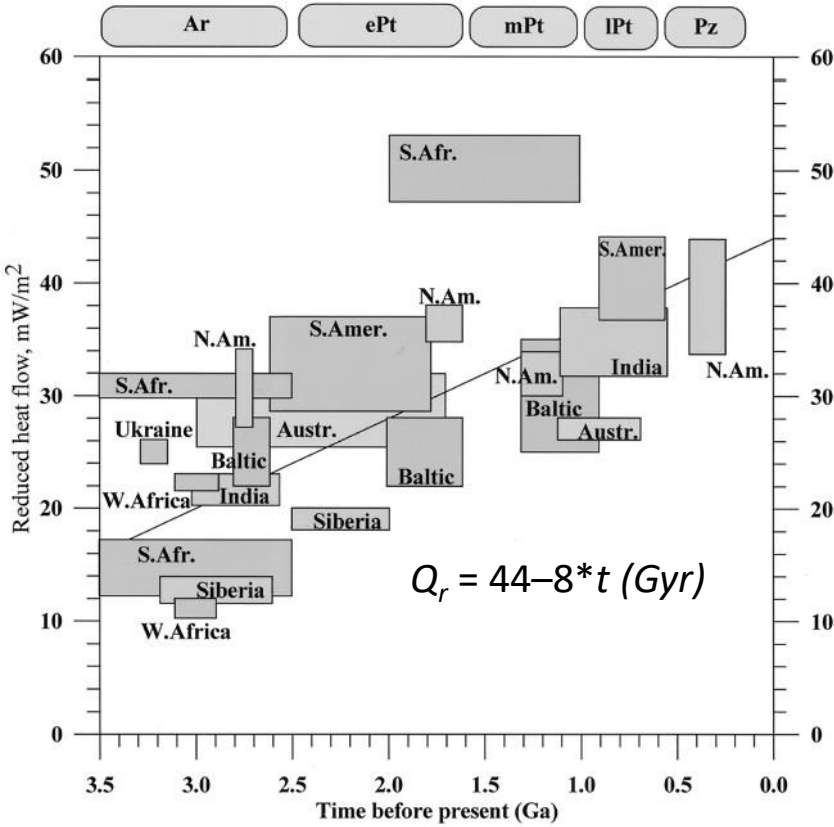
The change in heat flow pattern does not necessarily correspond to the surface expression of the cratonic margin:

- In case of the time delay of a thermal front propagation: $\tau \sim L^2/\kappa$ $\kappa=10^{-6} \text{ m}^2\text{s}^{-1}$ or $1\text{mm}^2/\text{s}^{-1} \sim 31.5 \text{ km}^2\text{Myr}^{-1}$



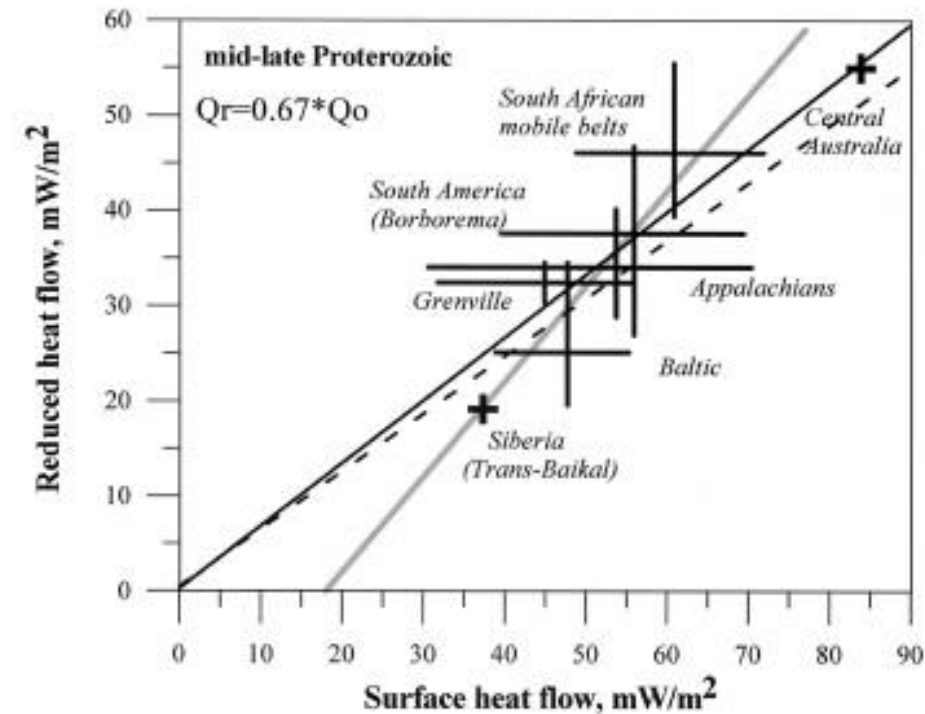
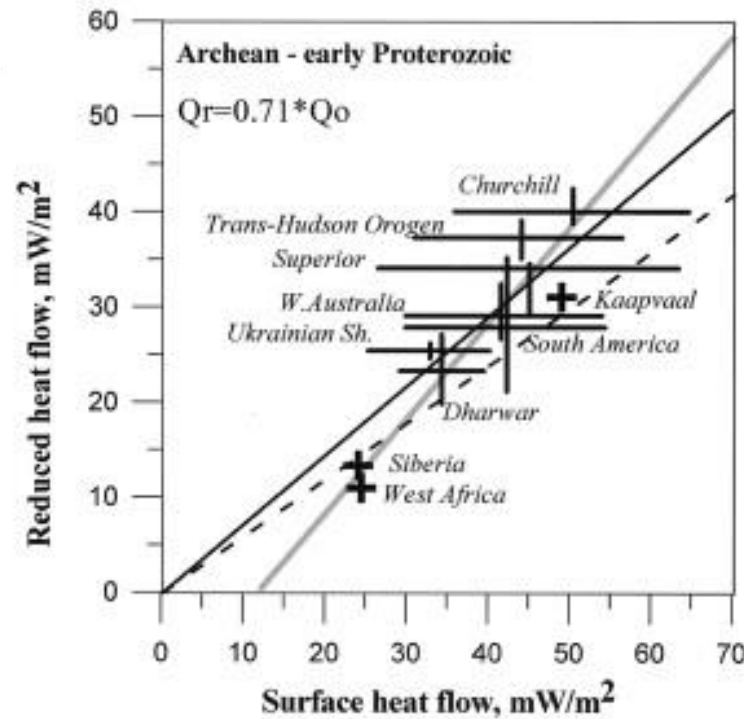
Surface heat flux in boreholes may reflect the past thermal regime, due to the slow rate of conductive heat transfer (transient conditions)

Surface (Q_0) and Reduced (Q_r) Heat Flux vs Age



$$Q_0 = 40-55 mW/m^2$$

(Artemieva and Mooney, 2001, JGR, 106, B8)



— Best fit

- - - $Q_r = 0.60 * Q$

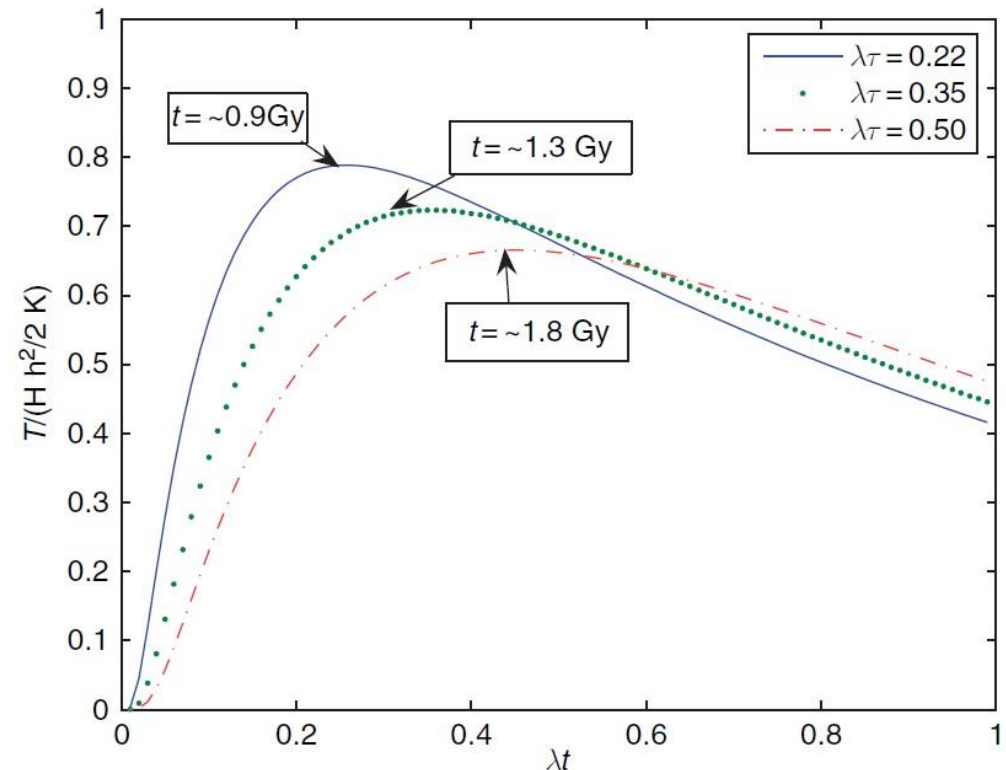
— Contribution of the upper crustal (D) layer to $Q = 12 mW/m^2$ in Archean-early Proterozoic regions and $18 mW/m^2$ in mid-late Proterozoic regions.

Archean conditions

- Crustal heat generation during the Archean time was higher than today for the first few tens Myr, due to the decay of short half-life radioactive elements (e.g. $^{36}\text{Cl} \longrightarrow 3.0 \times 10^5 \text{yr}$ $^{26}\text{Al} \longrightarrow 7.2 \times 10^5 \text{yr}$), but high-temperature-low-pressure metamorphic rocks are maybe related to widespread magmatic perturbation.
- Crustal radioactivity heats the crust in a geologically short time, but a much longer time is required to heat up the lower lithosphere.
- When the half-life of crustal radioactivity is of the same order as the thermal time of the lithosphere, lithospheric temperatures cannot adjust to the time dependent radiogenic heat production.
- The ‘radiogenic’ temperature component at the base of the lithosphere reaches a maximum after 1–2 Gyr.

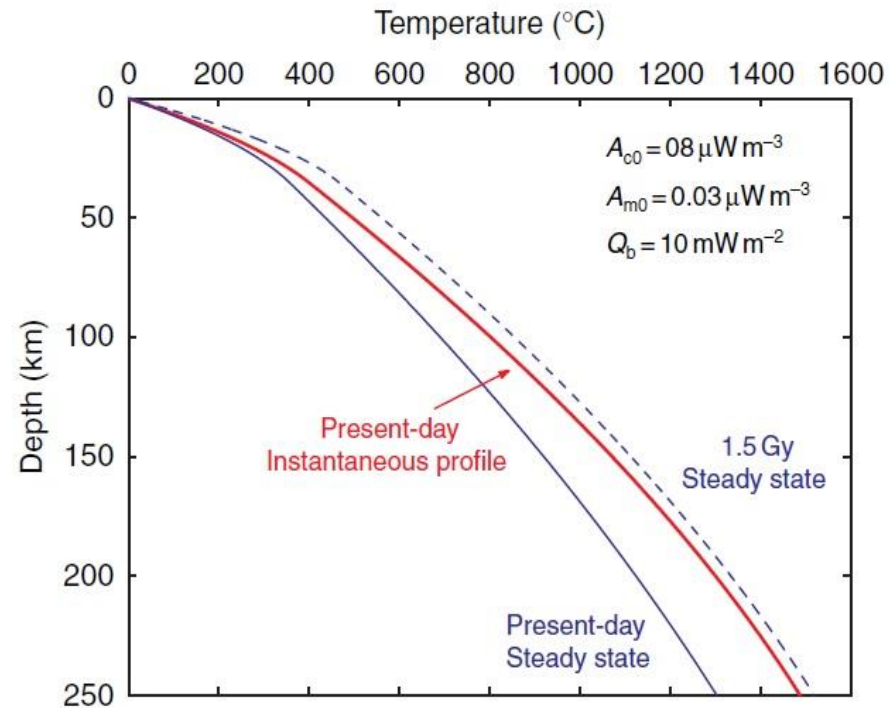
Temperature at the base of the lithospheric root after its stabilization beneath the crust

H =heat generation
 h =crustal thickness
 K =thermal conductivity
 τ =thermal relaxation time of the lithosphere ($\tau=L^2/\kappa$)
 κ =thermal diffusivity ($10^{-6} \text{ m}^2/\text{s}$)
 λ =decay constant ($\lambda=\ln 2/\alpha$ with $\alpha=2.5 \text{ Gyr}$)
 α =half-time life
 $\lambda\tau$ corresponds to a lithosphere thick 160, 200, and 240 km



Secular cooling in the lithosphere

- In thick lithosphere the timescale for diffusive heat transport is comparable to the halflives of U, Th, and K, implying that temperatures are not in equilibrium with the instantaneous rate of radiogenic heat generation.
- In lithosphere that is thicker than 200 km, the geotherm is transient and sensitive to past heat generation.
- The deeper part of the temperature profile largely diverges from a steady-state calculation (because of the long time to transport heat to the upper boundary).
- Small values of heat production lead to significant transient effects in a thick lithosphere (anomalous heat flow remains for longer time in case of a thick lithosphere).
- Predicting cooling rates for the lithosphere are in the range of 50-150 K Gyr⁻¹.
- If the thermal perturbation is narrow, a large thickness enhance lateral heat transfer.



Since $\tau \sim \alpha$ the lithosphere cannot be in equilibrium with present H

Moho Heat Flux (Q_M)

The contribution of the Moho heat flux can be estimated in the regions characterized by low surface heat flux (22-23 mWm⁻²) assuming:

- Heat production estimates cannot be lower than 0.1-0.3 μWm^{-3}
- Over the average thickness of ~ 40 km, the crustal contribution must be at least 4mWm⁻².
- Other methods include mantle xenolith analyses.

e.g.: In Greenville province, the average crustal heat production was determined to be 0.65 μWm^{-3} for an average Q_0 of 41 mWm⁻², which yields a Moho heat flux of 15 mWm⁻².

Average value of Moho heat flux data are ~ 15 mWm⁻²
(lower or larger range may be inconsistent with xenolith and heat flux/heat production data)

Various estimates of the heat flux at Moho in stable continental regions

Region	Moho heat flux (mW m ⁻²)	References
Norwegian Shield	11 †	Pinet and Jaupart, 1987
Vredefort (South Africa)	18 †	Nicolaysen <i>et al.</i> , 1981
Kapuskasing (Canadian Shield)	11–13 †	Ashwal <i>et al.</i> , 1987; Pinet <i>et al.</i> , 1991
Greenville (Canadian Shield)	13 †	Pinet <i>et al.</i> , 1991
Abitibi (Canadian Shield)	10–14 †	Guillou <i>et al.</i> , 1994
Siberian craton	10–12 †	Duchkov, 1991
Dharwar craton (India)	12–19 †	Roy and Rao, 2003
Trans-Hudson orogen (Canadian Shield)	11–16 †*	Rolandone <i>et al.</i> , 2002
Slave province (Canada)	12–24 ‡	Russell <i>et al.</i> , 2001
Baltic Shield	7–15 ‡	Kukkonen and Peltonen, 1999
Kalahari craton (South Africa)	17–25 ‡	Rudnick and Nyblade, 1999

† Estimated from surface heat flux and crustal heat production.

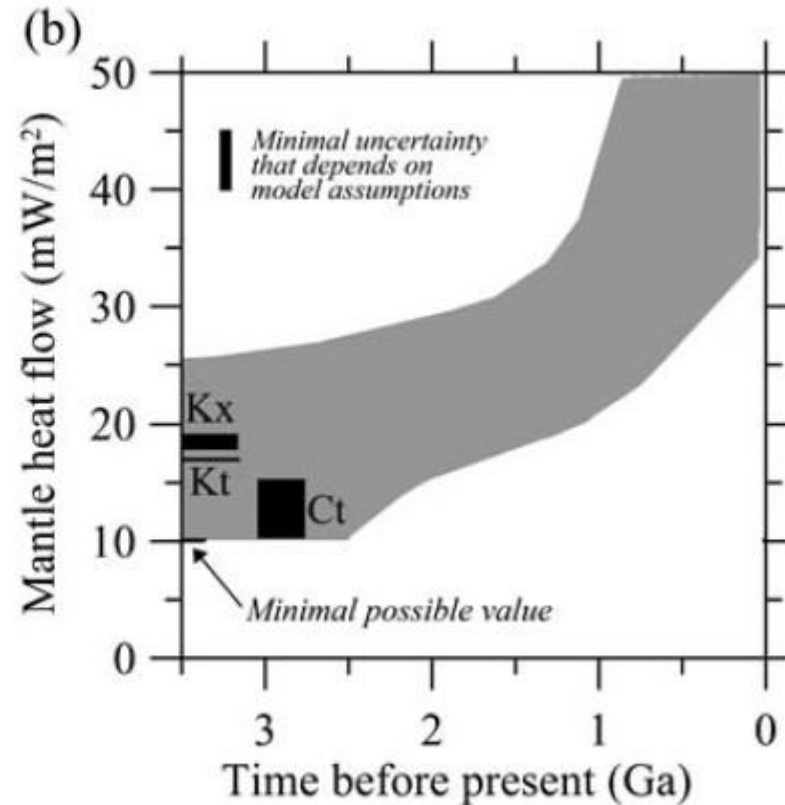
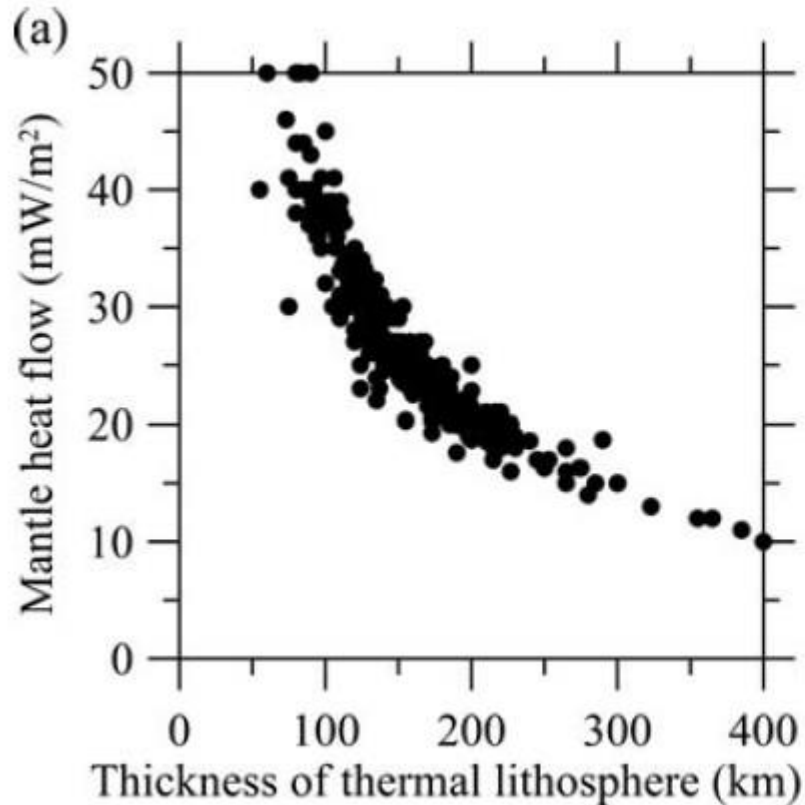
* Estimated from condition of no melting in the lower crust at the time of stabilization.

‡ Estimated from geothermobarometry on mantle xenoliths.

Moho Heat Flux (Q_M)

From pure thermal conductive equation: $Q_M = \lambda(T_L - T_M) / (Z_L - Z_M)$

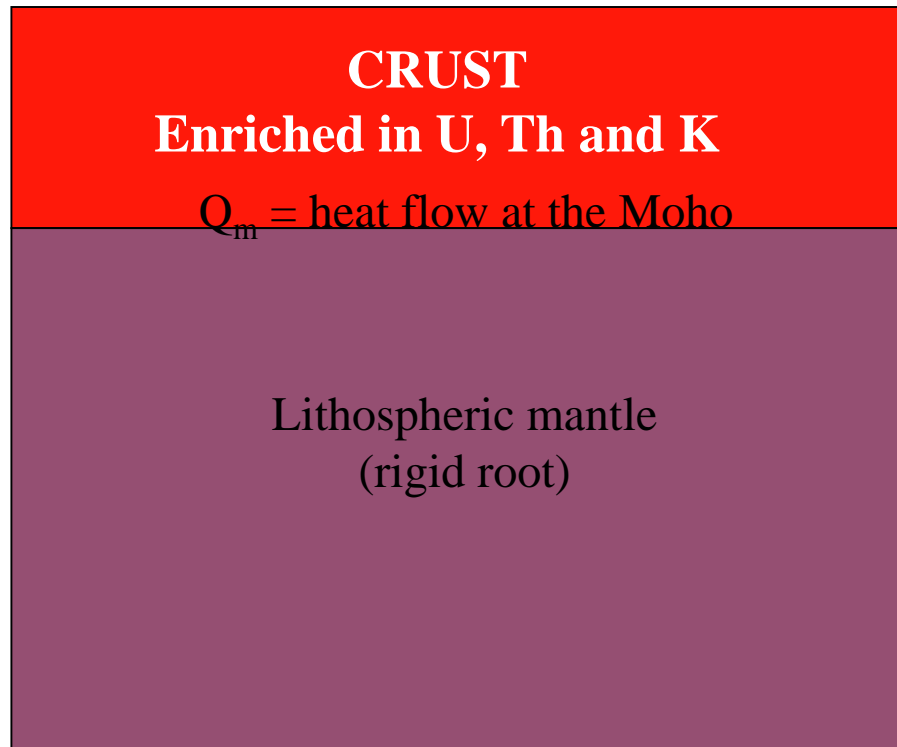
$T_L = 1350^\circ\text{C}$ $Z_L = 300 \text{ km}$ $T_M = 600^\circ\text{C}$ $Z_M = 40 \text{ km}$ $\lambda = 3.5 \text{ Wm}^{-1}\text{K}^{-1}$ $Q_M \sim 10 \text{ mWm}^{-2}$



Kt = Kaapvaal craton
Ct = Canadian Shield
Kx = Kaapvaal xenolith data

Mantle Heat Flux

$$Q_o = \Delta Q_c + \Delta Q_{LM} + Q_b$$



Basal heat flux Q_b

Basal heat flux variation (ΔQ_b) is attenuated and thus it is not significantly reflected in the surface:

L = lithosphere thickness and
 λ = wavelength of the variation

$$\Delta Q_o = \frac{\Delta Q_b}{\cosh(2\pi L/\lambda)}$$

ΔQ_b is an average value over 500 Myr

ΔQ_c

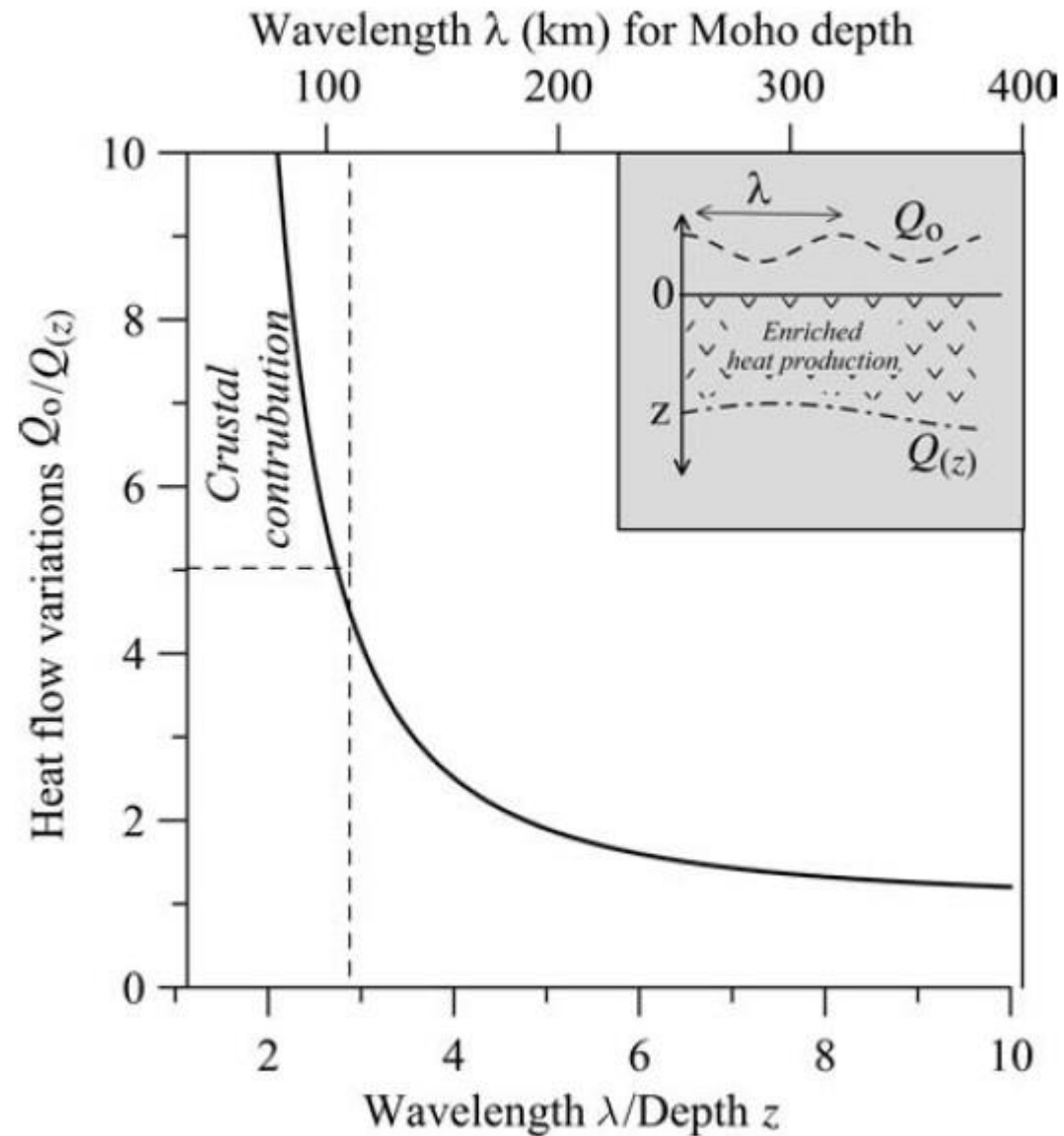
$\Delta Q_{LM} \approx 0$

Changes in the basal heat flux accounts for less than $\pm 2 \text{mWm}^{-2}$ of the surface heat flux variations.

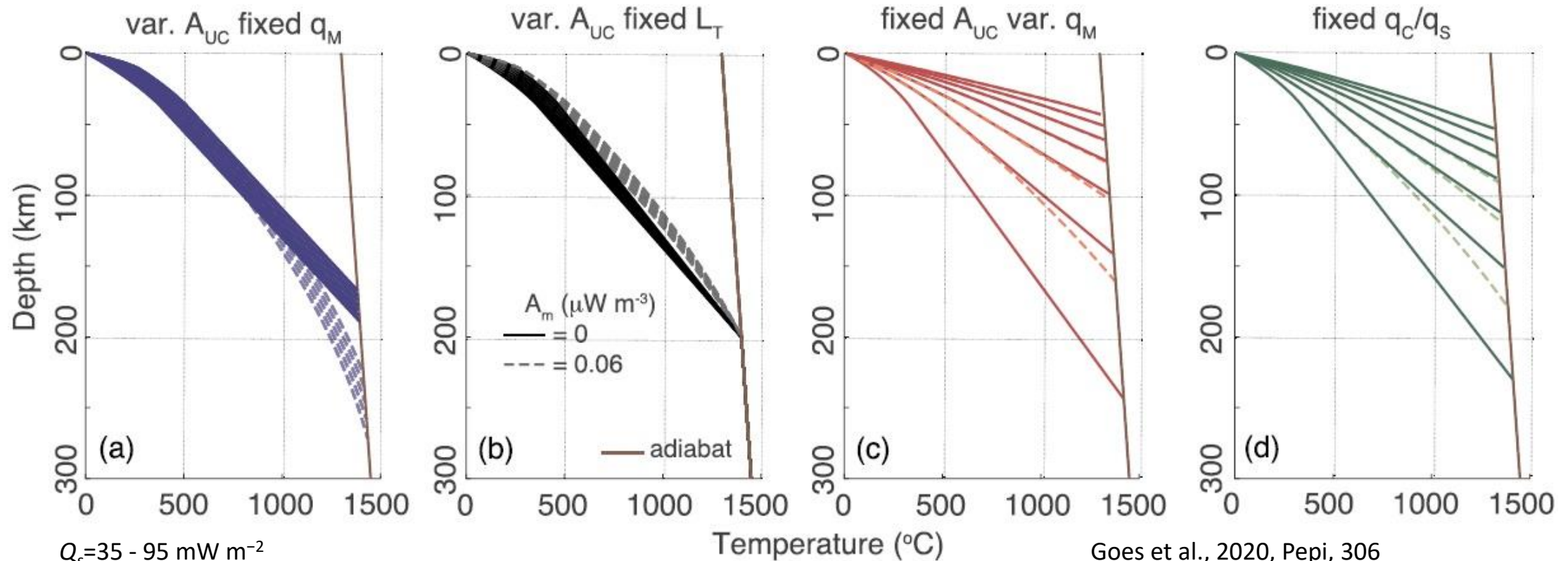
Variations in the basal heat flux accounts $< 3 \text{mWm}^{-2}$

Thermal anomaly depth

Crustal and mantle thermal anomalies cause surface heat flow perturbation with different wavelength



Range of Steady-State Geotherms (for standard thermal lithospheric parameters)



$Q_s = 35 - 95 \text{ mW m}^{-2}$

Crustal Thickness = 36 km, UC = 12 km, LC = 24 km

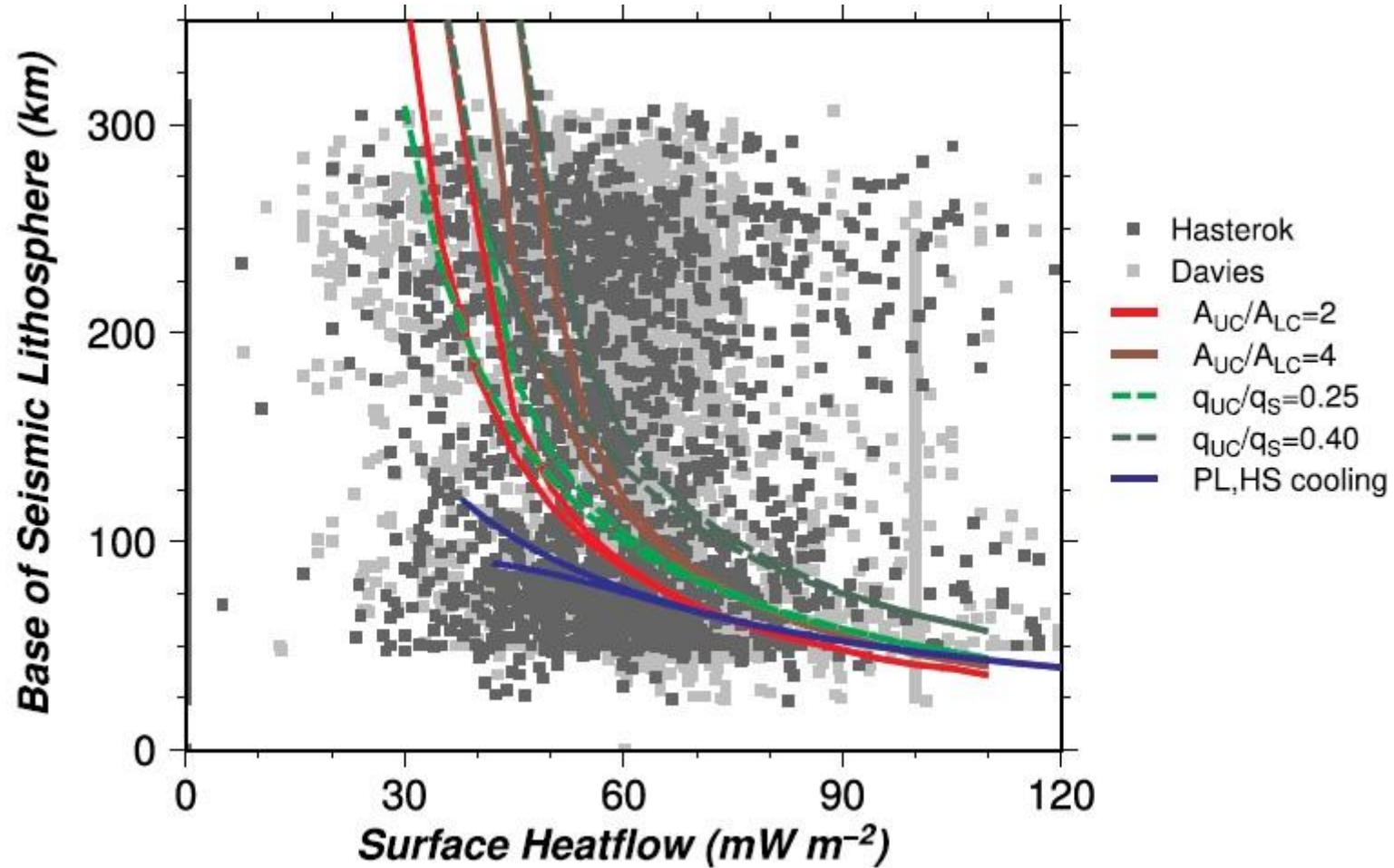
$A_{LC} = 0.4 \text{ } \mu\text{W m}^{-3}$, Solid coloured lines: $A_m = 0$, Lighter coloured dashed lines: $A_m = 0.06 \text{ } \mu\text{W m}^{-3}$

$\lambda_c = 2.7 \text{ W m}^{-1}\text{K}^{-1}$ $\lambda_m = 3.0 \text{ W m}^{-1}\text{K}^{-1}$

(a) Constant Moho heat flow geotherms, $q_M = 20 \text{ mW m}^{-2}$. (b) Same crustal heat production as (a), but for fixed $L_T = 200 \text{ km}$. (c) Constant crustal heat production, $A_{UC} = 3 A_{LC}$ (d) Coupled heat flow-heat production

- For old lithosphere it has been inferred that Moho heat flow should vary in a range of 10 to 20 mW m^{-2} , which actually corresponds to a variation in lithospheric thickness from over 350 to 200 km. These fluctuations influence the mantle lithospheric temperatures.

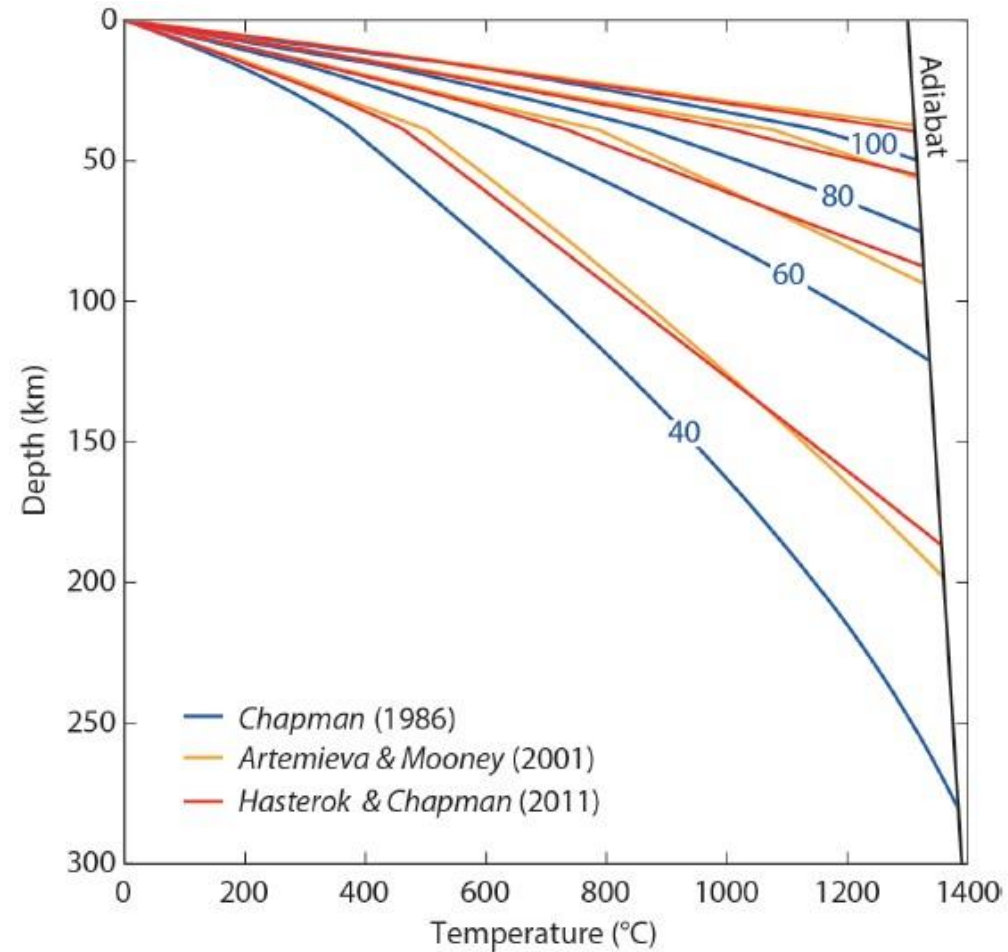
Surface Heat Flow and Seismic Lithosphere



Goes et al., 2020, Pepi, 306

- Lithospheric thickness on surface heat flow is consistent with the distribution of continental seismic lithospheric thickness vs surface heat flow data.
- Steady-state continental trends for constant heat production do overlay the thick-lithosphere part of cloud, while the thin lithosphere-low heat flow points are more like what might be expected from oceanic cooling models.

Global Geotherms (for standard thermal lithospheric parameters)

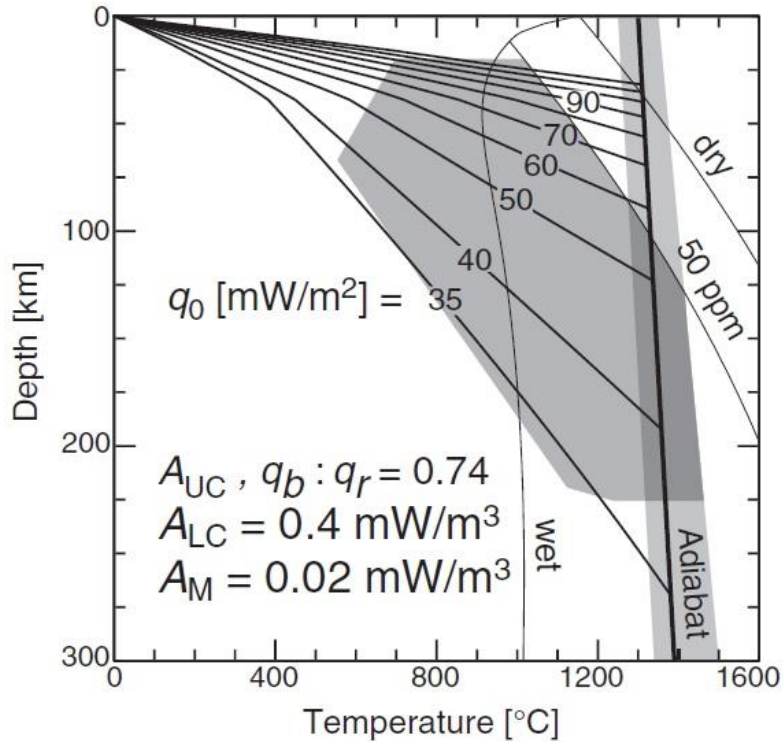


F=Partition Coefficient

F=0.4 (Chapman, 1986), 0.26 (Hasterok and Chapman, 2011), and 0.33 - 0.29 (Artemieva and Mooney, 2001)

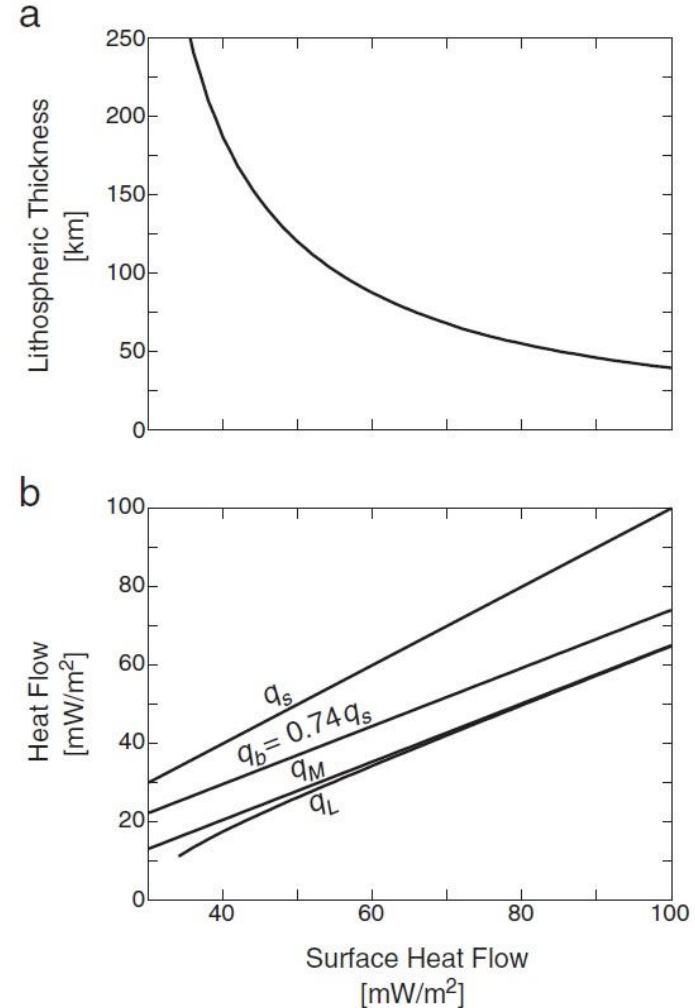
Global Geotherms (for standard thermal lithospheric parameters)

Lithospheric thickness for the partition model with coefficient $F=0.74$, and proton mantle composition



$$A_{UC} = (q_s - q_b) / D \quad q_b = Fq_s \quad A_{UC} = (1 - F)q_s / D$$

Hasterock and Chapman, 2011, EPSL, 307



Heat flow across lithospheric layers: surface, q_s ; middle to upper crust, q_b ; Moho, q_M ; and lithosphere–asthenosphere boundary, q_L .

Effect of uncertainties of thermal parameters on temperature

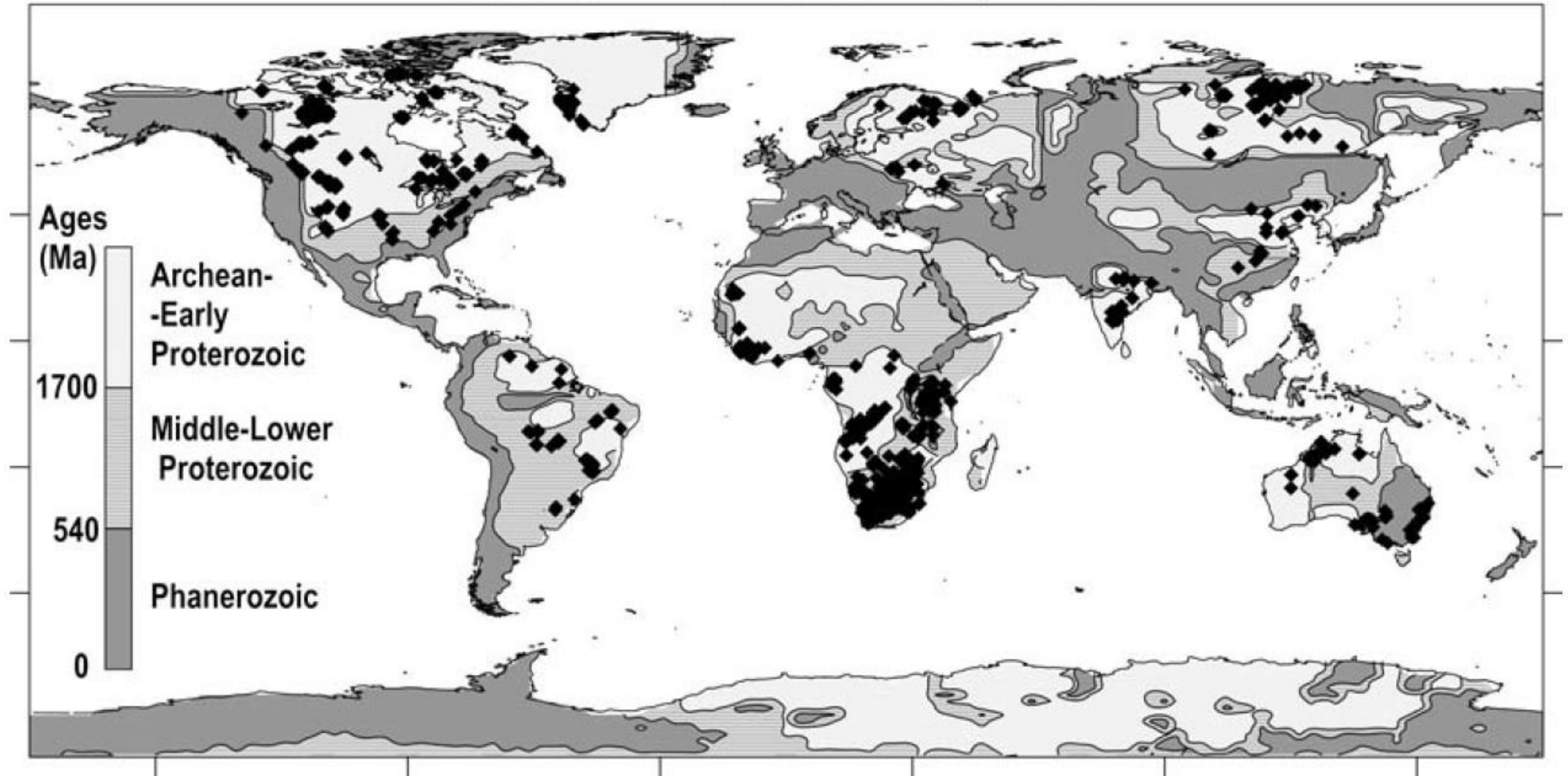
Sensitivity Analysis for the Geothermal Modeling

Change of Model Parameter	Temperature		Lithospheric Thickness	Mantle Heat Flow
	at $z = 50$ km	at $z = 100$ km		
Average crustal heat production 20% higher	9–13% (50–70°C) lower	11–16% (100–130°C) lower	15–30% (25–80 km) greater	8–10% (4–5 mW m ⁻²) lower
Average crustal conductivity 10% higher	8% (30–60°C) lower	5% (30–60°C) lower	3–6% (5–10 km) greater	the same
Upper mantle conductivity 3.3 W m ⁻¹ K ⁻¹ (rather than 4.0 W m ⁻¹ K ⁻¹)	2–3% (10–15°C) higher	8% (50–80°C) higher	3–8% (10–15 km) lower	the same
Surface heat flow 5% higher	7–8% (30–50°C) higher	8–9% (50–90°C) higher	10% (10–25 km) lower	2–3% (2–3 mW m ⁻²) higher

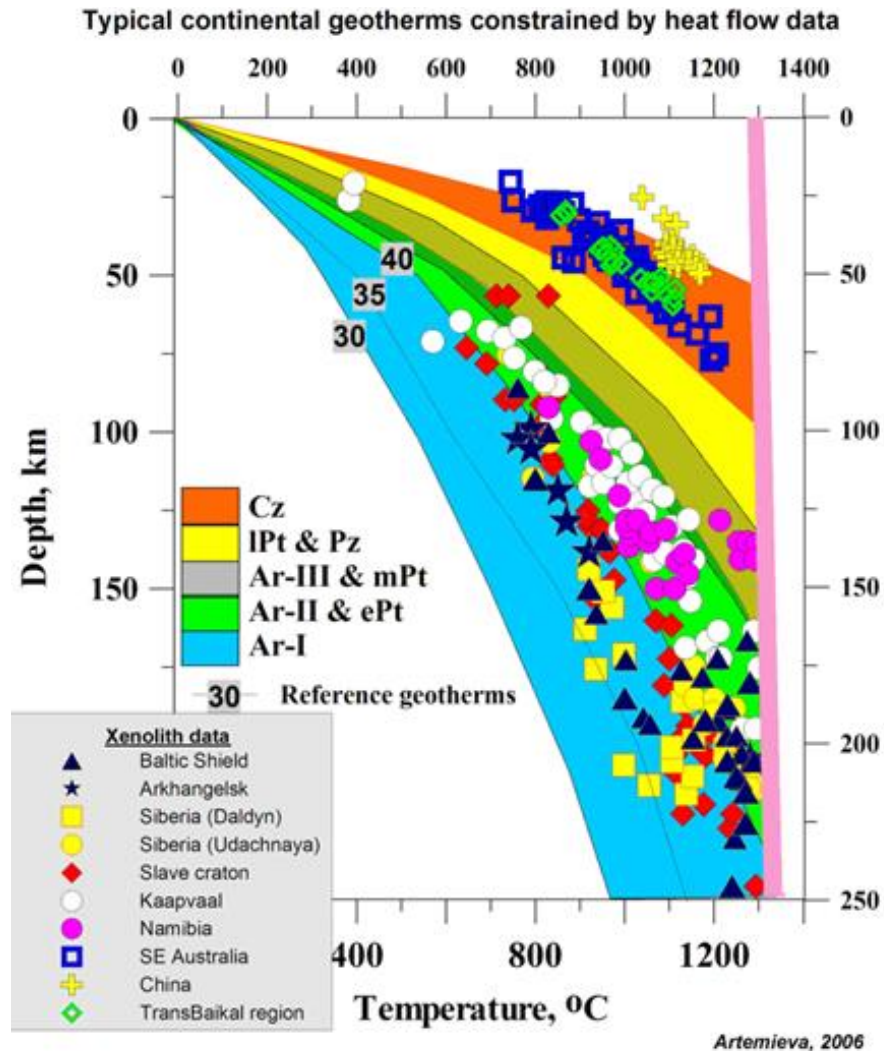
Xenolith data

Xenoliths are pieces of crustal and mantle rocks entrapped by magmas from the margins of magma chambers/conduits, which provide a direct (non-uniform) sampling of the lithosphere at the time of eruption.

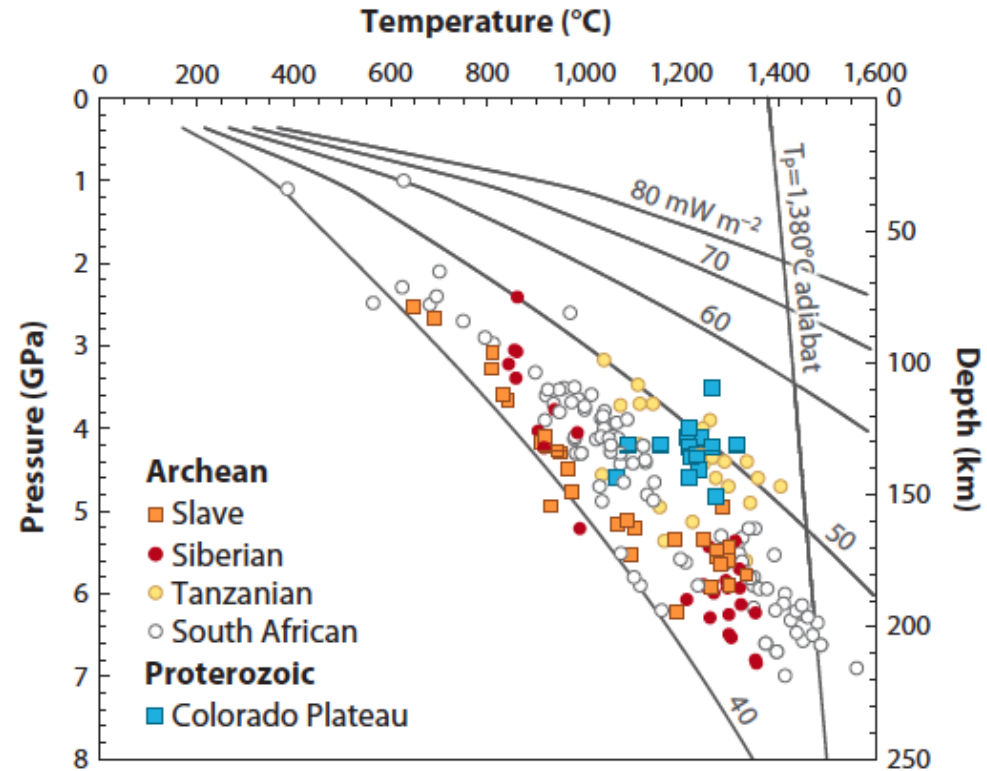
Worldwide kimberlites and lamproites



Xenolith data



(Artemieva, 2009, Lithos, 109)

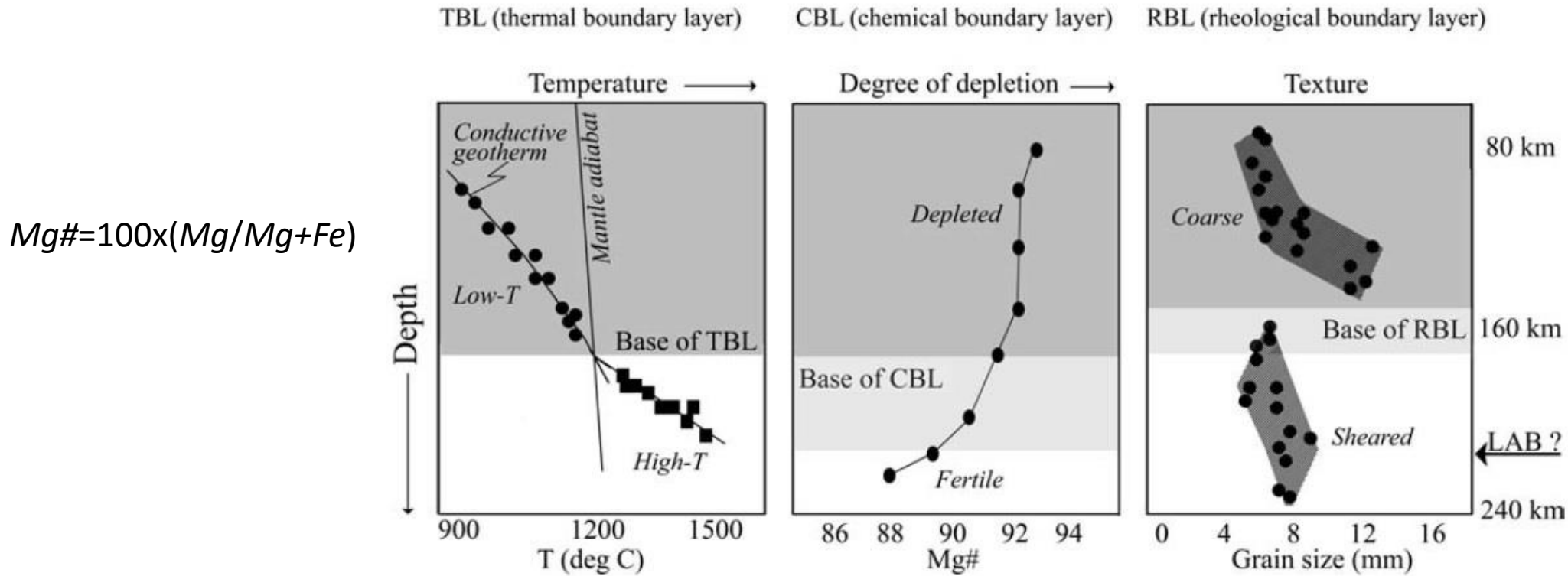


Lee et al. (2011)

- High geothermal gradients oceanic spreading centers (Middle Atlantic Rift) and along island arc
 - Molten volcanic rocks (magma) coming to the surface
- Low gradients in subduction zones
 - Thrusting of (cold and water filled) sediments beneath existing crust
- Tectonically stable (shield) areas and sedimentary basins have average gradients

Xenolith data

The approach of geothermobarometers to constrain P - T conditions in the mantle sampled by xenoliths is based on P - T dependence of the activity of exchange reactions between coexisting minerals (e.g., Al content in the OPX constrain the depth of the xenolith formation).

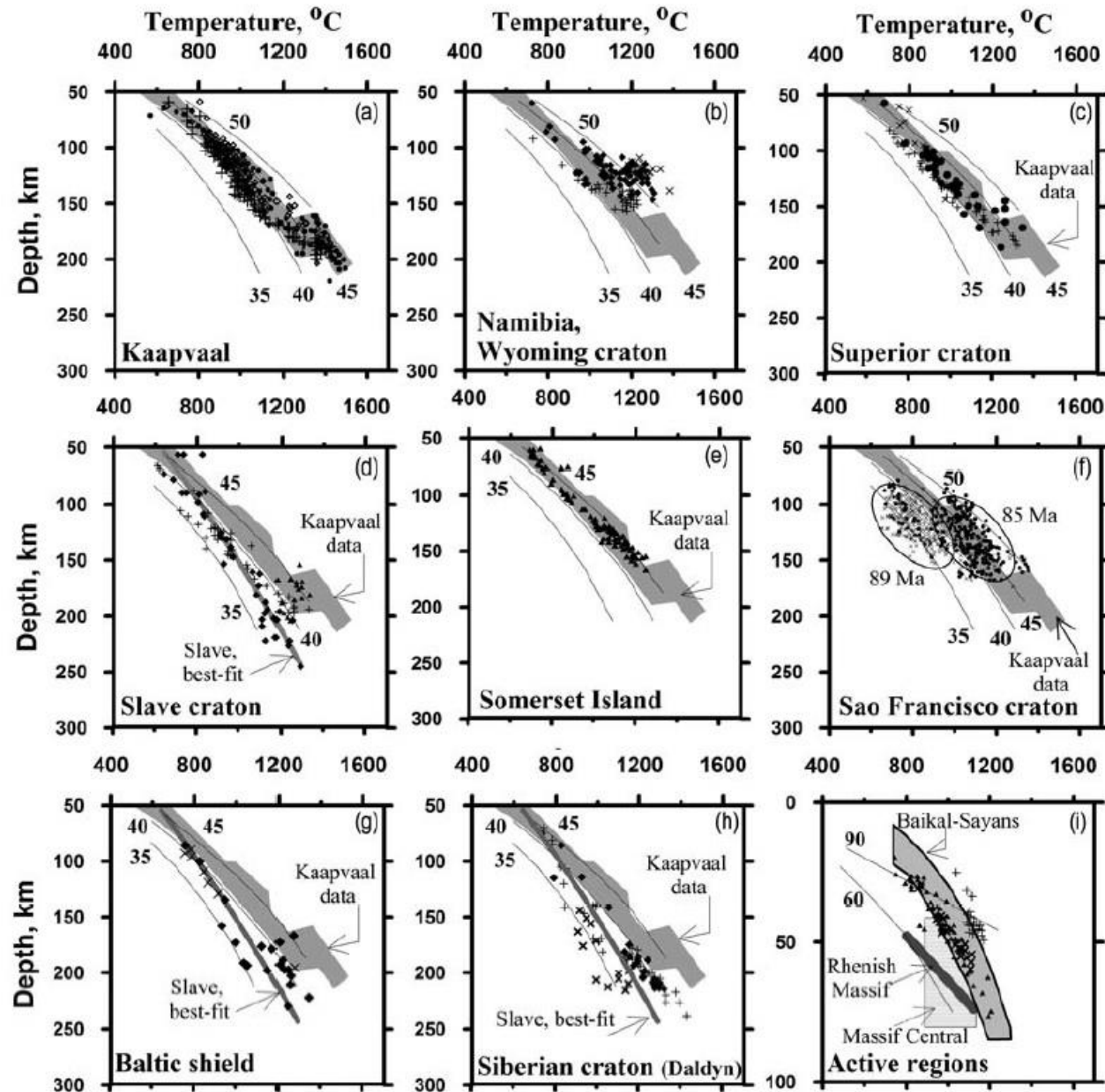


- In some cases the lower part of the mantle sampled by xenoliths exhibits a significant deviation of the T gradient, interpreted as a transition from a pure conductive to a non-conductive heat transfer (sometimes it is an artefact of thermobarometry or a thermal perturbation of the mantle).
- The gradual decrease of Fe depletion with depth may indicate the transition towards the lowermost lithosphere metasomatized by melts and fluids from the convective mantle.
- Low- T are usually coarse grained (> 2 mm) and show a low level of lithosphere deformation, while high- T xenoliths are finer grained and deformed (sheared). The latter are associated with mantle zone of reduced viscosity, close to the asthenosphere.
- The LAB does not necessarily correspond to any of the TBL, CBL, or RBL.

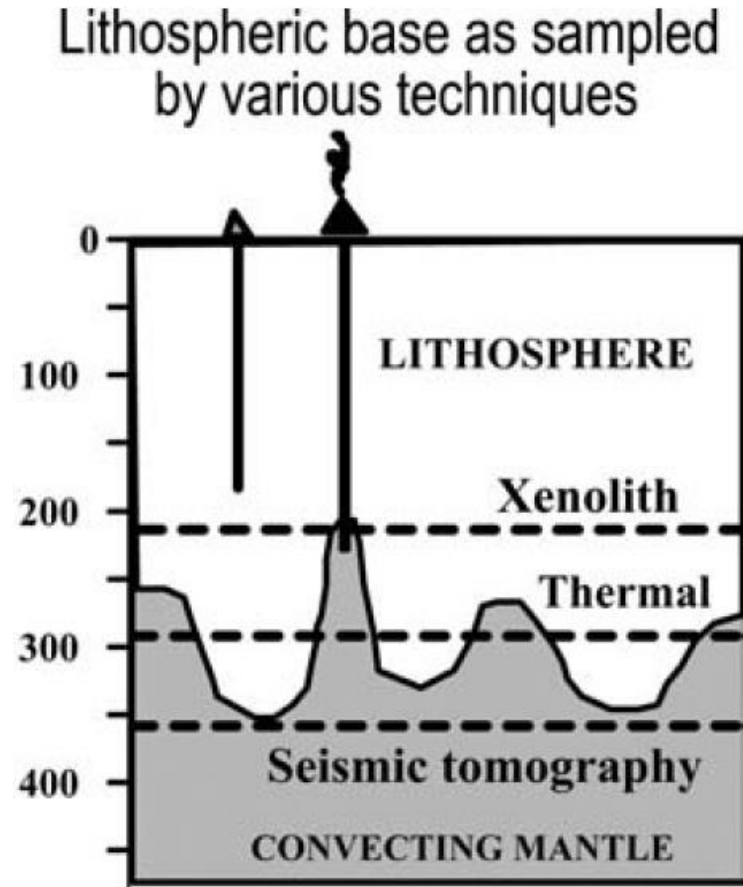
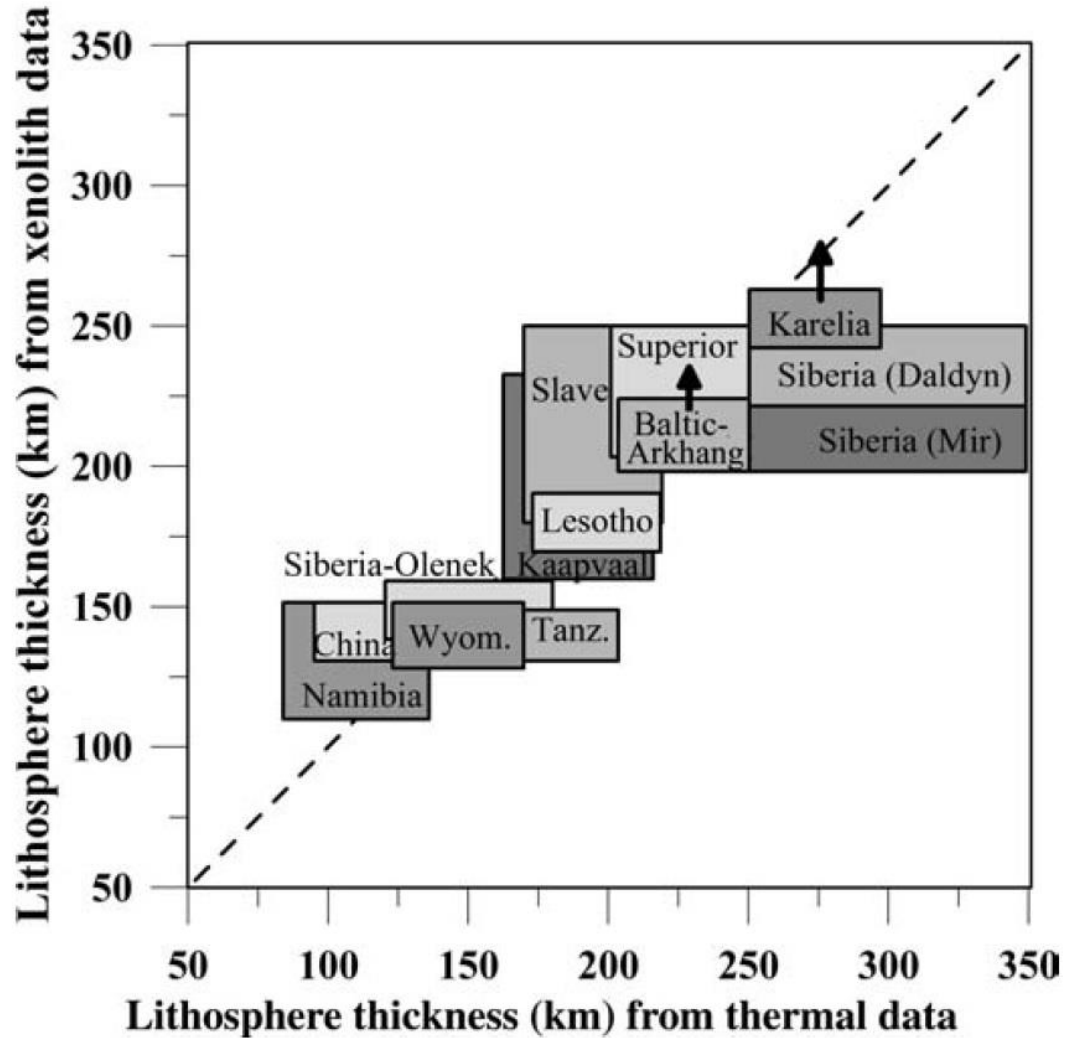
Xenolith data (Geotherms)

Two representative geotherms for Archean lithosphere, leading to two different lithospheric thickness:

- 40-45 mWm⁻² (South Africa, South America and Superior Province), lithospheric thickness about 220 km.
- 37 mWm⁻² (Slave, Fennoscandia, and Siberian craton), lithospheric thickness about 300 km.

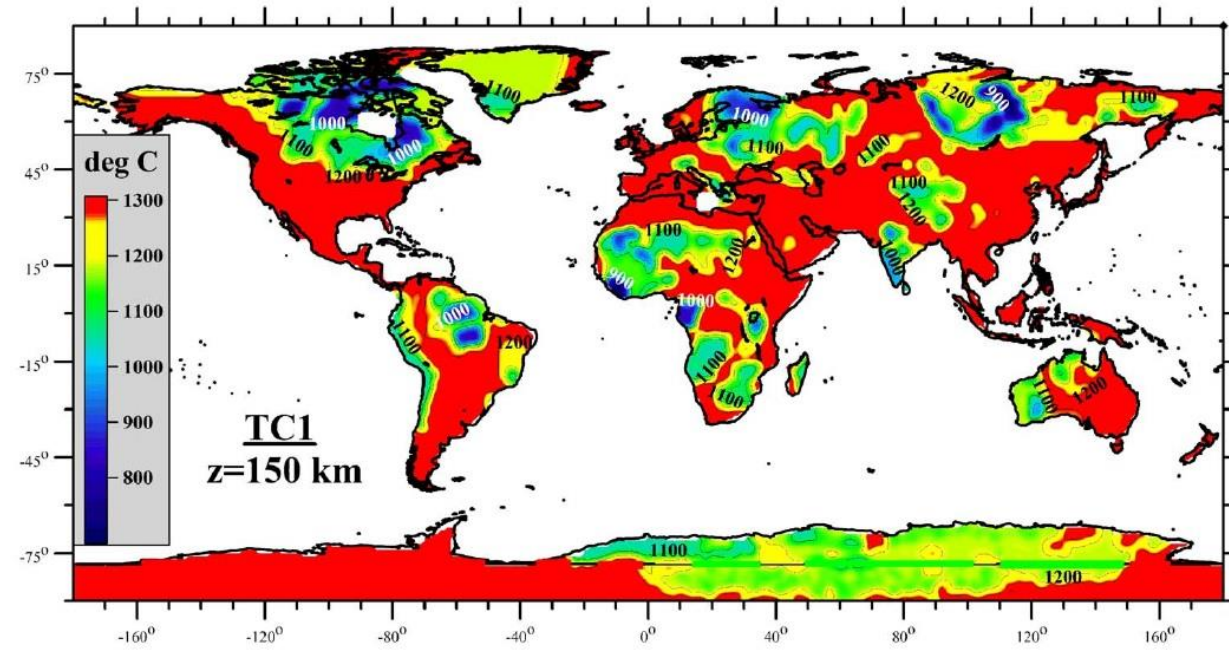
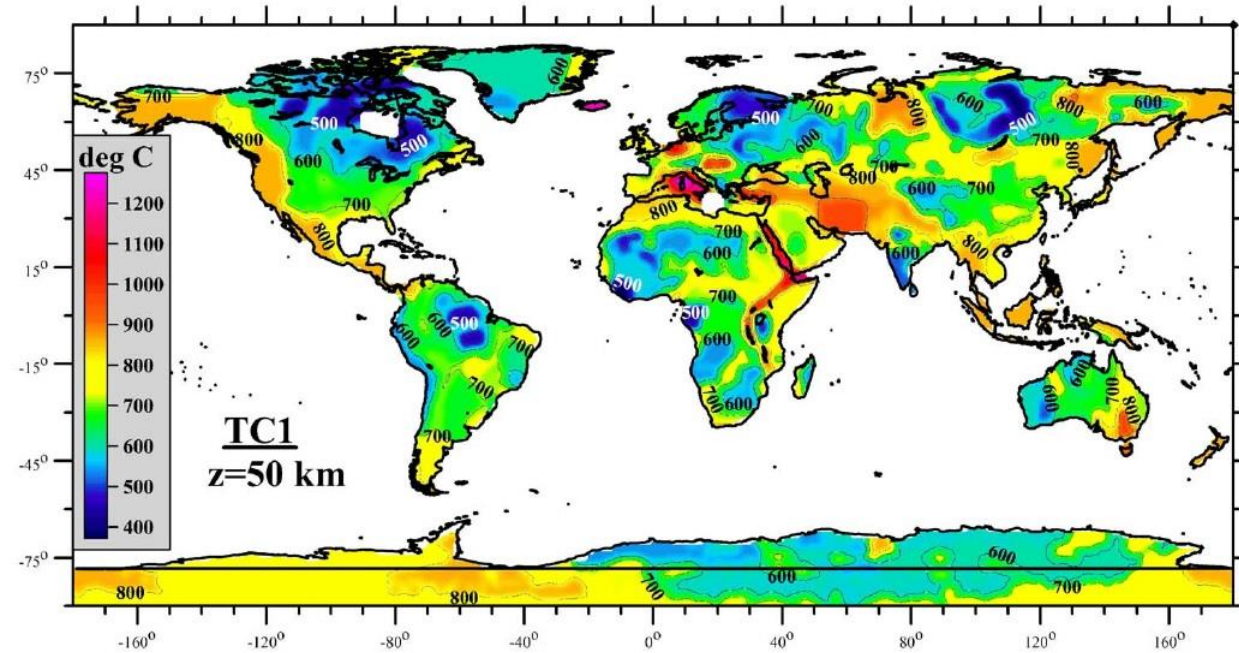


Xenolith data (Lithospheric Thickness)



- Different geophysical methods and petrologic xenolith-based data sample different depths in the upper mantle, leading to significant discrepancies in lithospheric thickness estimated by different methods.

Global Thermal Model (heat flow data, electromagnetic, and xenolith data)

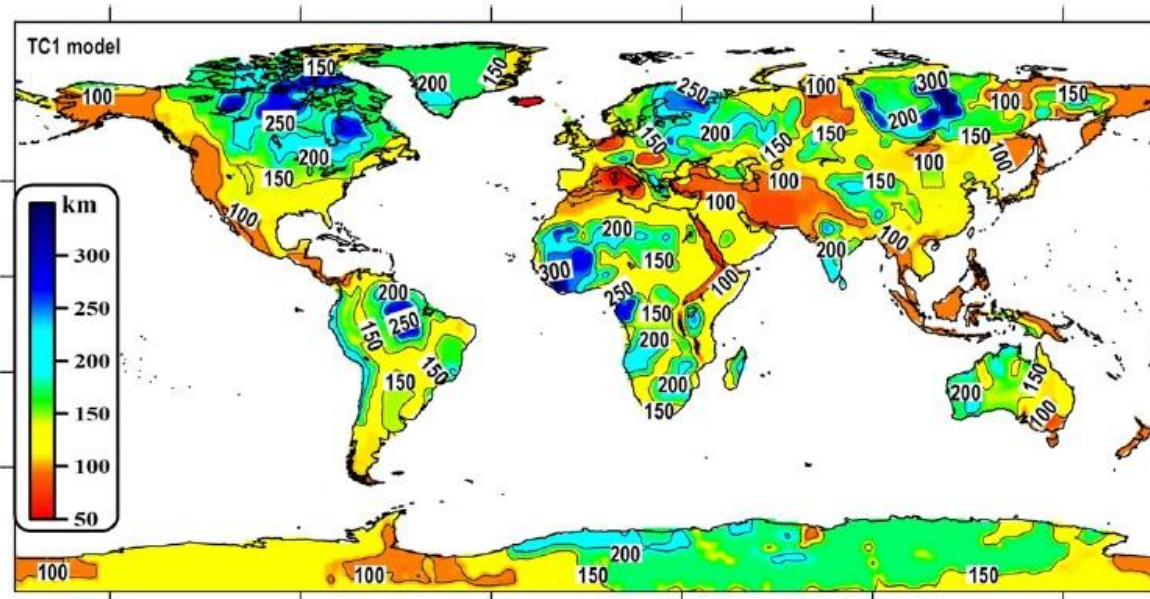


Artemieva, 2006, Tectonophysics, 416

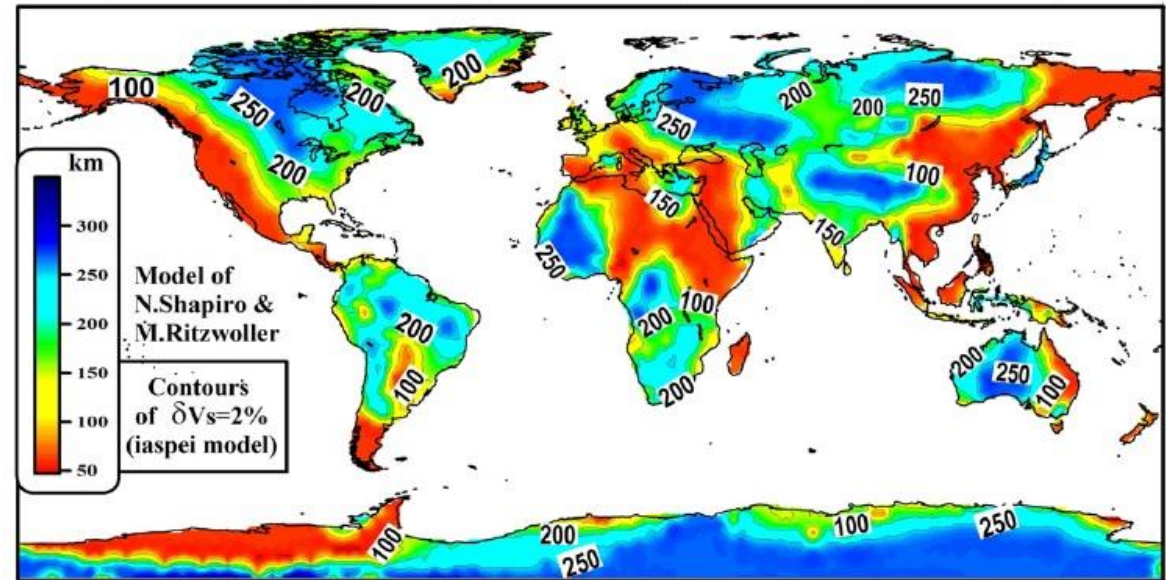
- In tectonically active regions, T at 50 km depth are between 900-1100 °C and the lithosphere thermal thickness is 60-80 km
- Moho T varies from 300-500°C in the cratons 500-800°C in Meso-Cenozoic regions.

Thermal Lithosphere vs Seismic Lithosphere (heat flow data, electromagnetic, and xenolith data)

Thermal Lithospheric Thickness



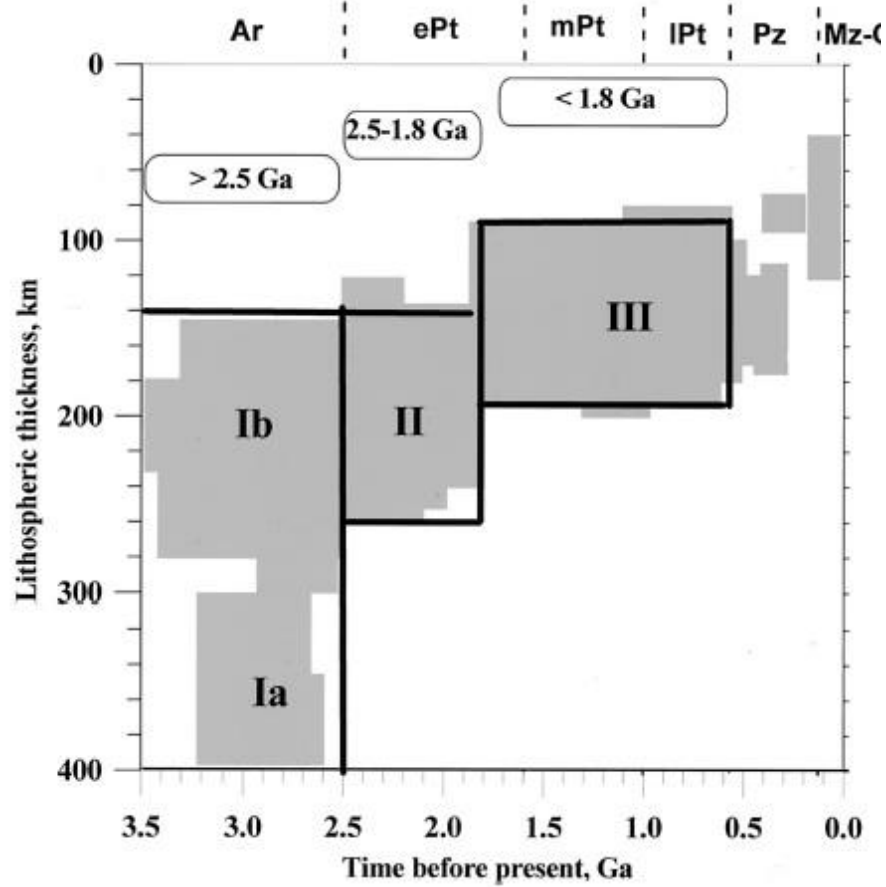
Lithospheric Thickness from surface-wave seismic tomography



Artemieva, 2009, Lithos, 109

- **Thermal Lithospheric Thickness:** determined by the intersection of a lithospheric geotherm with a mantle adiabat $T_m \sim 1350^\circ\text{C}$ or at $T \sim 0.8T_m$ ($\sim 1100^\circ\text{C}$), at the top of the transitional layer from high to low viscosity. It is usually 40-50 km shallower than the seismological boundary detected from seismic tomography (based of the convective boundary).
- **Seismic Lithospheric Thickness:** the lithospheric base is defined here as the depth where V_s velocity in the upper mantle is $2.0 \pm 0.5\%$ higher.

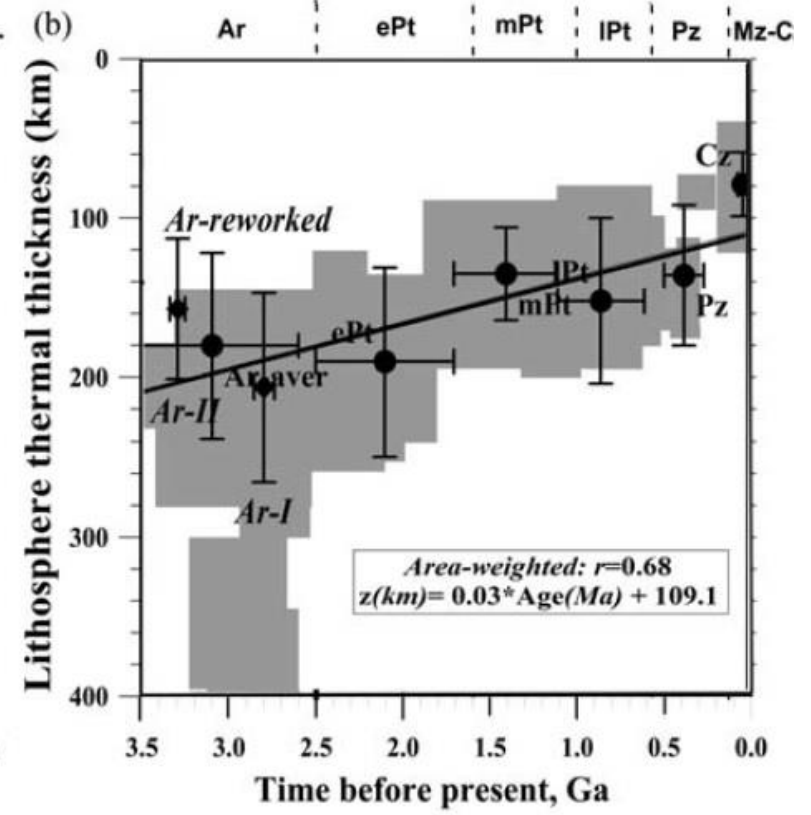
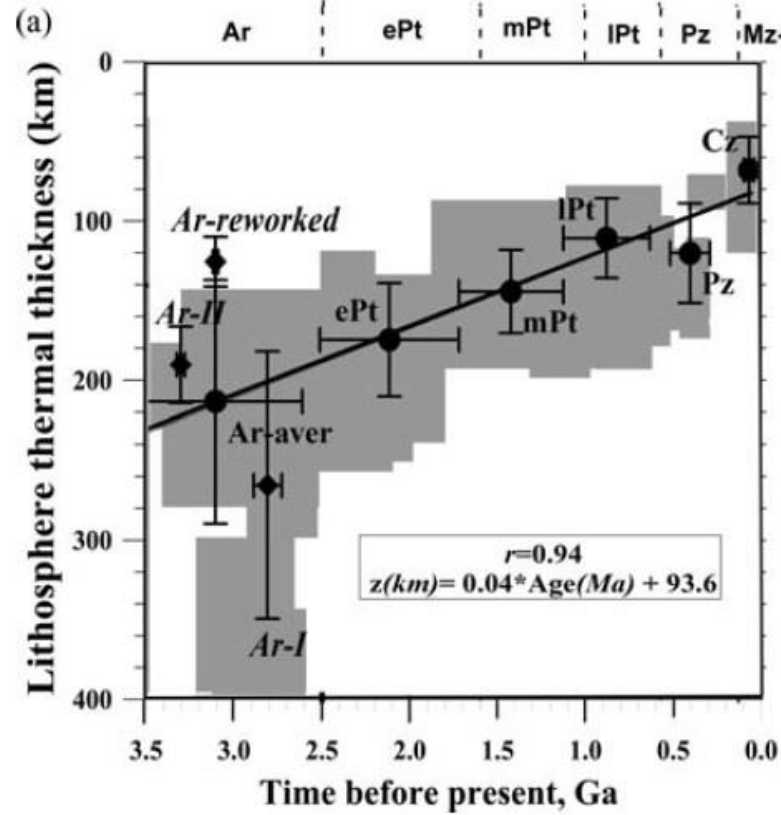
Lithospheric Thickness vs Age



Artemieva, 2006, Tectonophysics, 416

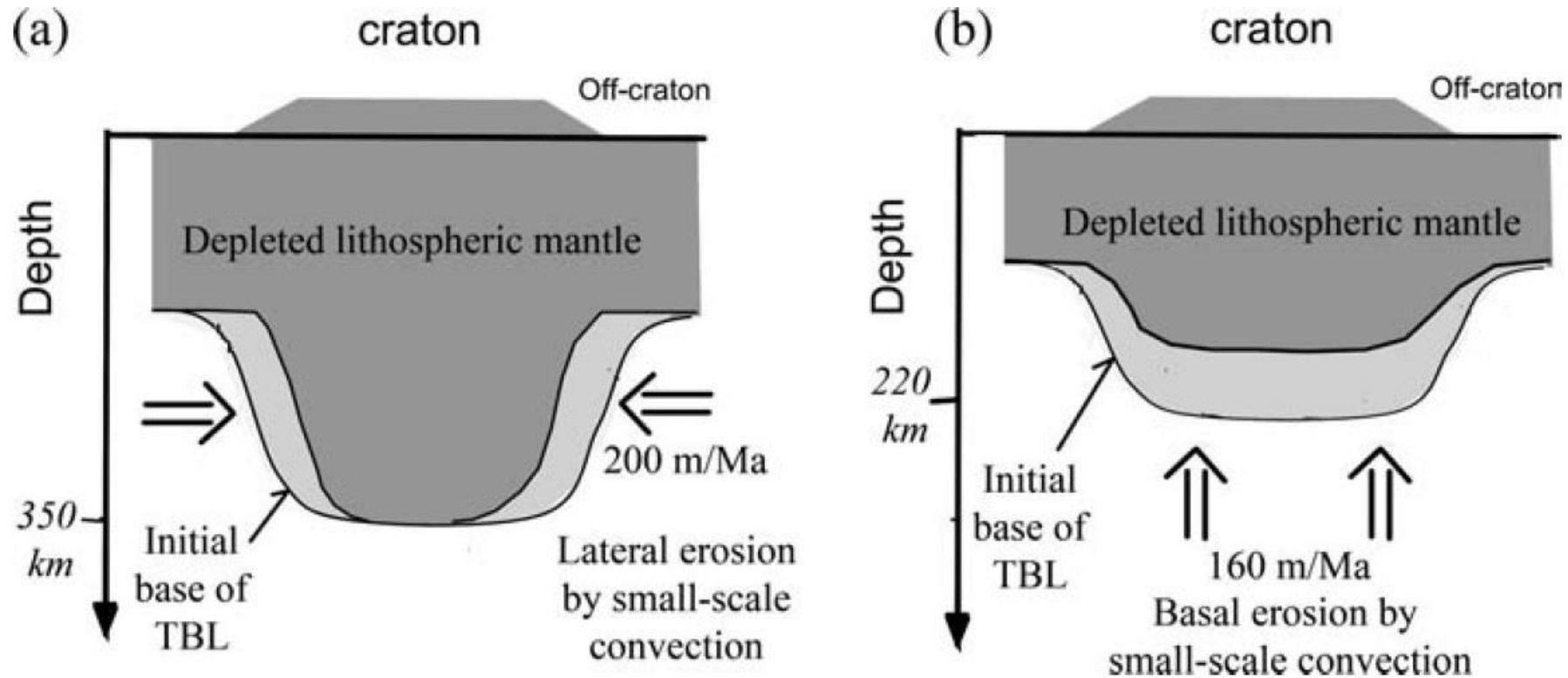
$$L=0.04t(\text{Myr})+93.6 \text{ (all continents)}$$

$$L=0.03t(\text{Myr})+109.1 \text{ (area-weighted data)}$$



- These relationships are empirical and do not work for very young active areas or in case of underthrust of old (Archean) terranes.

Archean Lithospheric Thickness



- Paleo-Precambrian cratons surrounded by Proterozoic mobile belts (as in South Africa, South America, western Australia, and India) have lithospheric thickness around 200–220 km, while the cratons without surrounding Proterozoic mobile belts (as in North America, Siberia, Europe, and West Africa) are characterized by thick lithospheric roots (250–350 km).
- In the case of thick (~350 km) lithosphere, small-scale convection at its base is sluggish and the basal part of the lithosphere is mainly destabilized by lateral erosion.
- The cratons with thin (200–220 km) lithosphere are older (>3.2–3.0 Ga) than the cratons with thick lithosphere. The lower part of the lithosphere could have been removed during adjacent Proterozoic orogenic activity. Alternatively, thick cratonic roots with ages of 2.9–2.6 Ga could be formed by Archean–Paleoproterozoic plate tectonic processes.

Radiogenic Heat Generation and seismic velocities

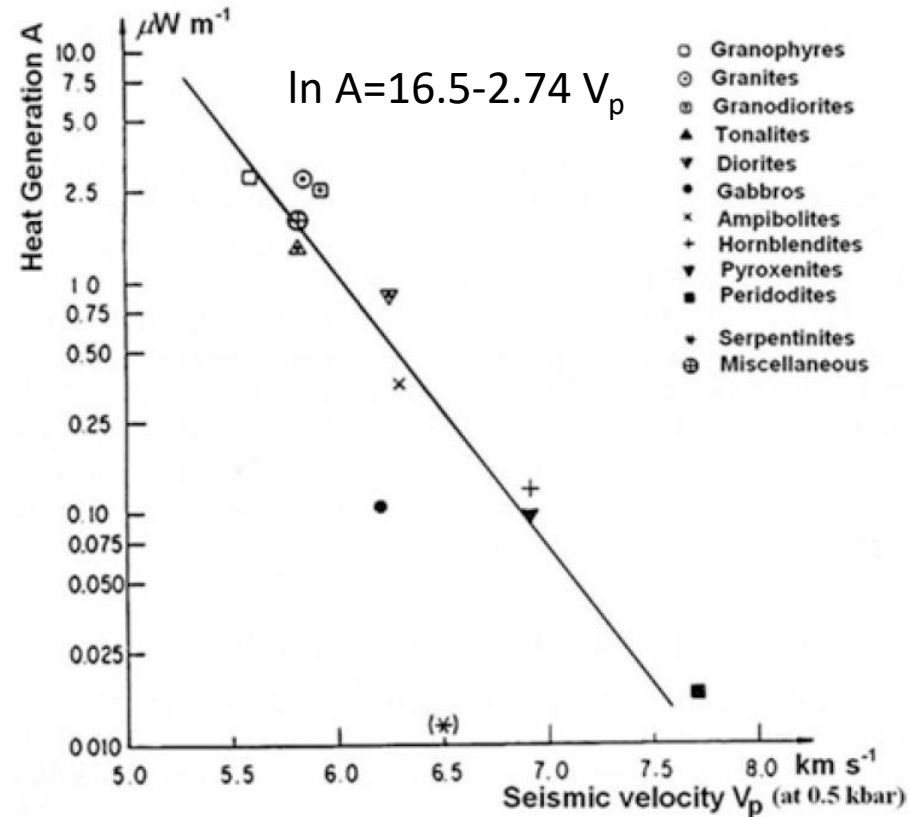
$$\ln A = B - 2.17v_p \quad \text{for } 6.0 < v_p < 8.2 \text{ km s}^{-1} \quad \text{Rybach and Buntentbath (1984)}$$

B = 12.6 for the Precambrian and 13.7 for the Phanerozoic crust

Other relationships: $\ln A = 13.92 - 2.38V_p$ $\ln A > 8.85 - 1.33V_p$

$$A(v_p) = a \exp(-bv_p) \quad \text{for } v_p \text{ range of } 5.0\text{--}8.0 \text{ km/s}$$

Rybach (1978) a and b are dependent on pressure



(after Rybach, 1988)

Heat flow, seismic velocities, and electrical conduction

Seismic velocities varies with temperature and temperature of the upper mantle depends on crustal heat flow.

$$Q=1150-135V_p$$

$$Q=21.45t_r+65.3$$

t_r =travel time residuals

Cull and Denham, 1979

$$Q^* = \ln \frac{T_L + c}{T_U + c} \times \frac{1}{a(t_L - t_U)}$$

Q^* =heat flow in relative Bolderij units (1BU = 77mWm⁻²)

T_L and T_U = temperatures (°C) at the bottom and top of a sub-surface interval

t_L and t_U = one-way sonic travel times (s) to the bottom and top of the interval

$a=1.039$

$c=80.031$

Heat flow is correlated with the depths of electrically conductivity layers in the crust (FCL), coinciding with the onset of granitization and melting in the crust and upper mantle (ICL), related to partial melting at top of the asthenosphere.

$$h=h_0q^{-a}$$

$h_0=4493$ km $a=1.30$ for FCL

$h_0=36167$ km $a=1.46$ for ICL

Dependance of seismic velocities in the upper mantle

Anharmonicity: refers to the behaviour of materials in which elastic properties change because of temperature (or pressure) caused by the deviation of lattice vibration from the harmonic oscillator. This process produces thermal expansion (without energy dissipation) and thus elastic properties of materials vary due to the change in mean atomic distances.

Anelasticity: a dissipative process involving viscous deformation. The degree to which viscous deformation affects seismic wave velocities is measured by the attenuation parameter and depends on the frequency of seismic waves and temperature. Seismic attenuation is described by the “quality factor” Q which quantifies the amount of energy ΔE lost per cycle.

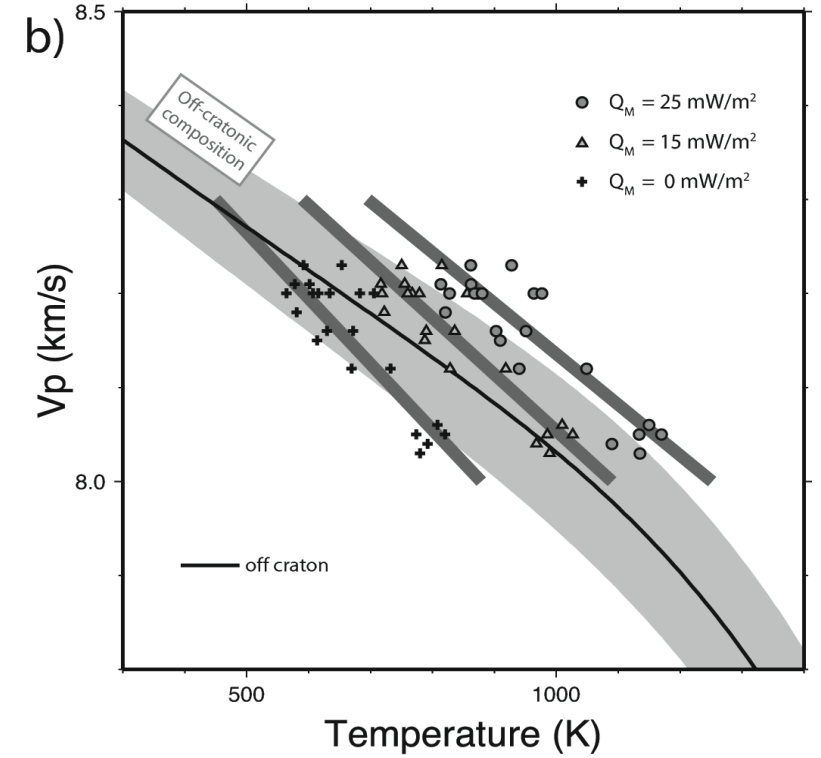
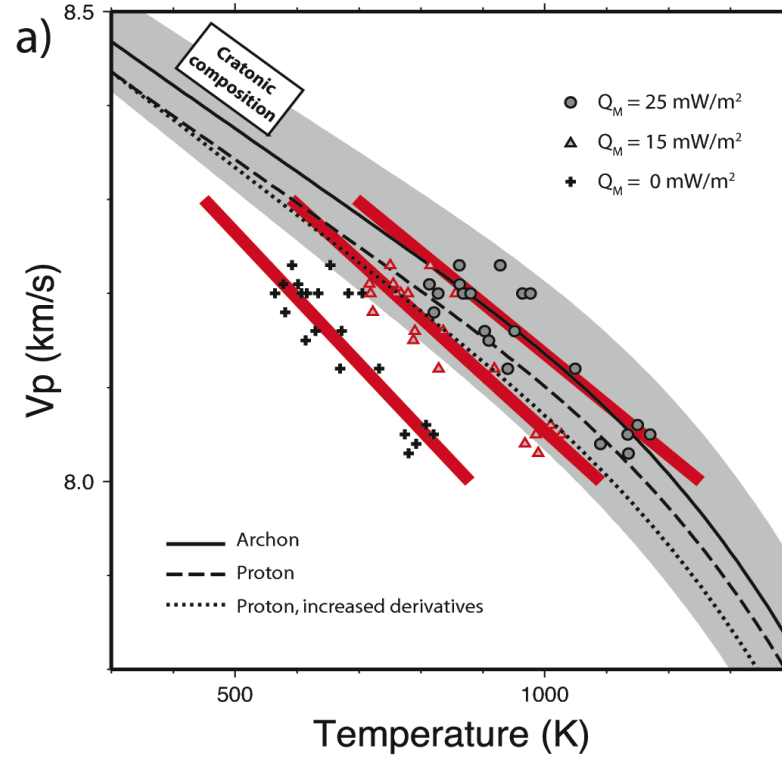
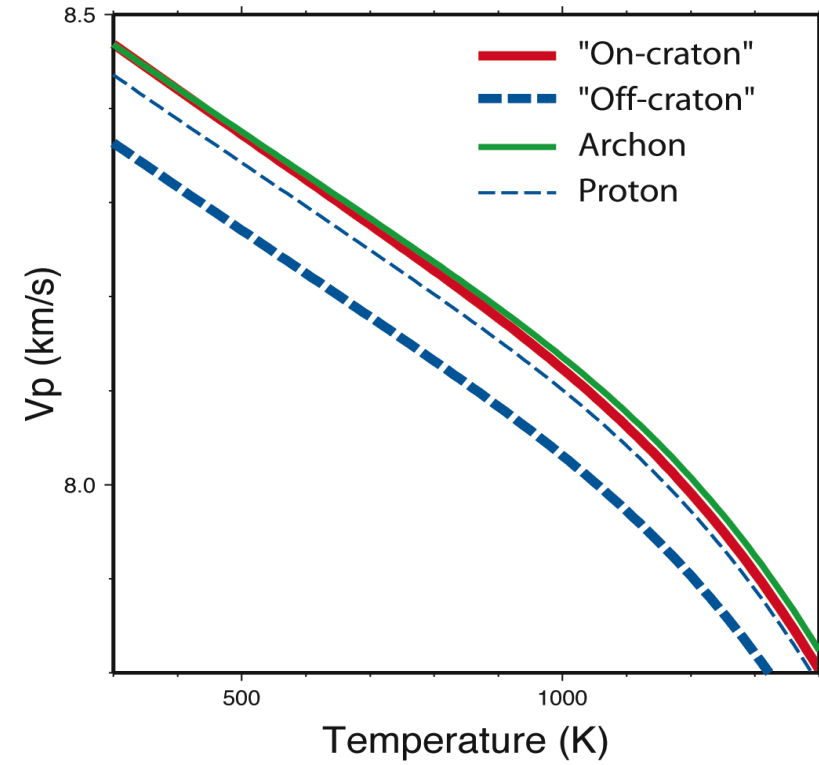
Composition: A decrease in Mg# by 4–5 units (corresponding to a typical difference between Archean to Phanerozoic lithospheric mantle) results in a 1% S velocity decrease, in a ~1.4% density increase and in a mantle temperature variation by 220 °C.

Melt: ca. 5% of melt lead to more than a 10% velocity decrease. The amount of melt even beneath the midocean ridges is only ca. 2%, while in the continental lithospheric mantle is even smaller. Indeed, interconnected melt is gravitationally unstable and migrates upwards even at concentrations of $\ll 1\%$.

Fluids: They may have an indirect effect on velocities by affecting the solidus temperature and enhance anelasticity. We should consider that the amount of water does not exceed 0.03 wt.% of olivine, but at the sites of paleosubduction zones the amount of water in the mantle can increase by 3–10 times due to its downward transport.

Seismic anisotropy: or the dependence of seismic wave speeds on the propagation direction or polarization of the waves. Deformation in the Earth often leads to seismic anisotropy, either through the crystallographic or lattice preferred orientation (CPO, LPO) of anisotropic constituent minerals, or through the shape preferred orientation (SPO) of materials with distinct isotropic elastic properties (e.g., melt). Differences in propagation speed between surface waves that are polarized differently (Rayleigh waves vs. Love waves) contain information about radial anisotropy, while the dependence of Rayleigh (or Love) wave velocities upon propagation direction contains information about azimuthal anisotropy.

P-wave velocity as a function of temperature and composition



Conversion of seismic velocity into temperatures

Anharmonicity

- For pressures < 6 GPa, elastic parameters, M (K, μ), and density, ρ , can be computed at a given conditions (P, T), from their values at a reference state (P_0, T_0), using the infinitesimal strain approximation:

$$M(P, T) = M(P_0, T_0) + (T - T_0) \frac{\partial M}{\partial T} + (P - P_0) \frac{\partial M}{\partial P}$$

$$\rho(P, T) = \rho(P_0, T_0) \left[1 - \alpha_0 (T - T_0) + \frac{(P - P_0)}{K} \right]$$

$$\alpha = \frac{(\partial V / \partial T)_P}{V_0}$$

M =Elastic Modulus K =Bulk Modulus

- The Voigt-Reuss-Hill averaging scheme approximates the parameters for a combination of minerals by taking the average of the mean elastic parameters for a constant stress (Reuss) and a constant strain (Voigt) condition:

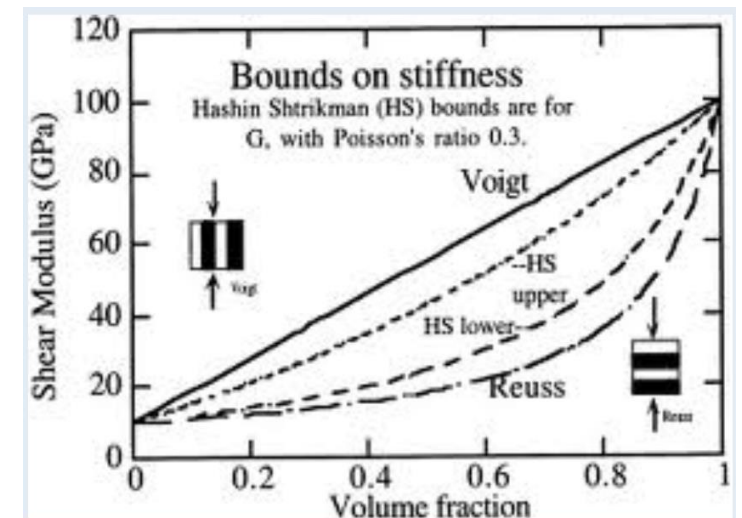
$$\langle \rho \rangle = \sum \lambda_i \rho_i$$

λ_i =volumetric proportion of mineral i

$$\langle M \rangle = \frac{1}{2} (M^{\text{voigt}} + M^{\text{reuss}})$$

$$M^{\text{voigt}} = \sum \lambda_i M_i ; M^{\text{reuss}} = \left(\sum \frac{\lambda_i}{M_i} \right)^{-1}$$

Goes et al., 2000, JGR

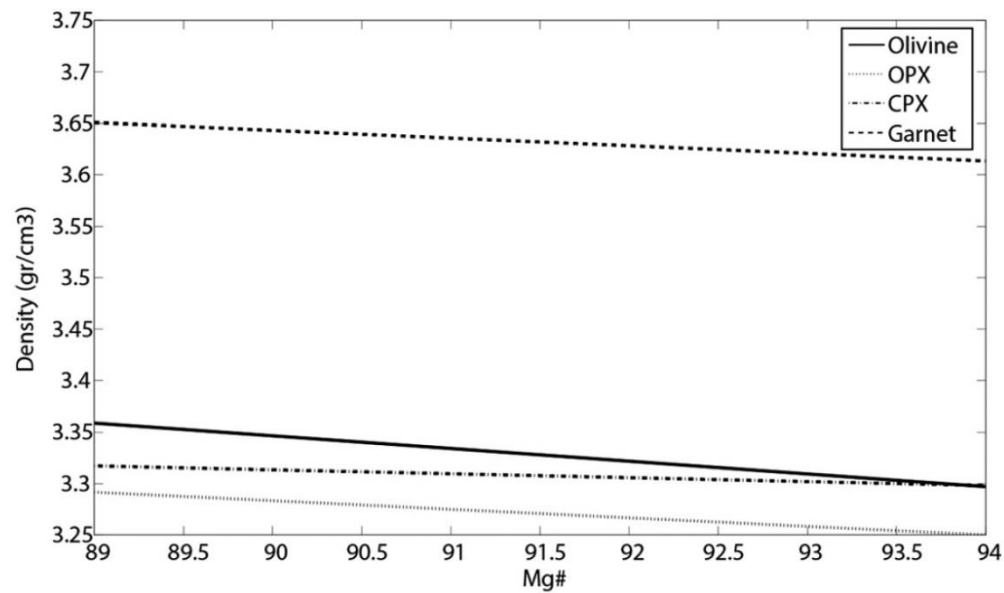


Conversion of seismic velocity into temperatures elastic parameters of mantle minerals

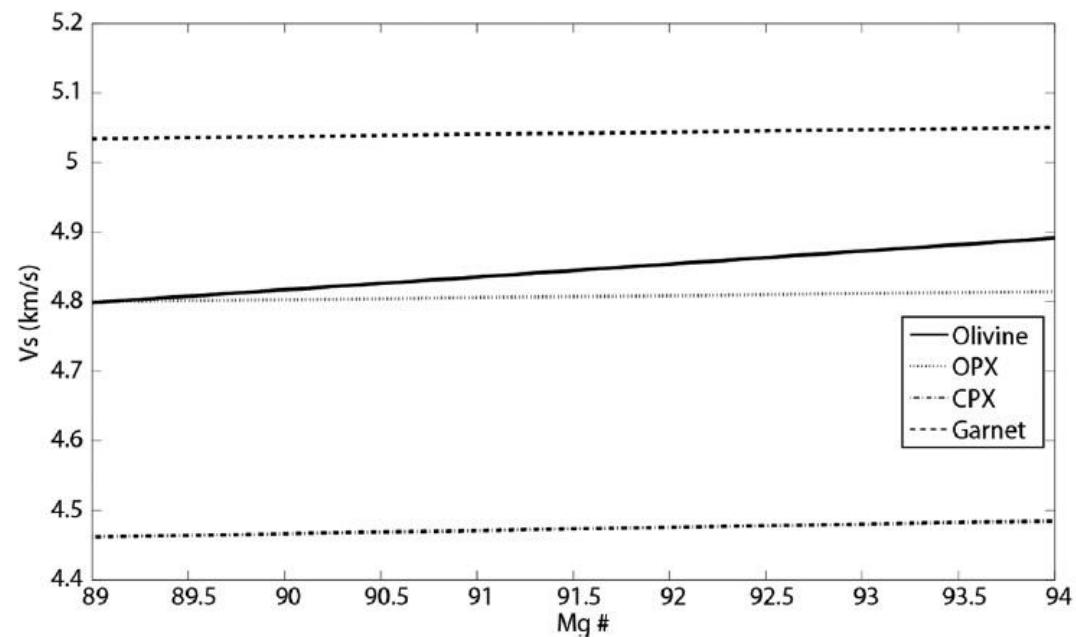
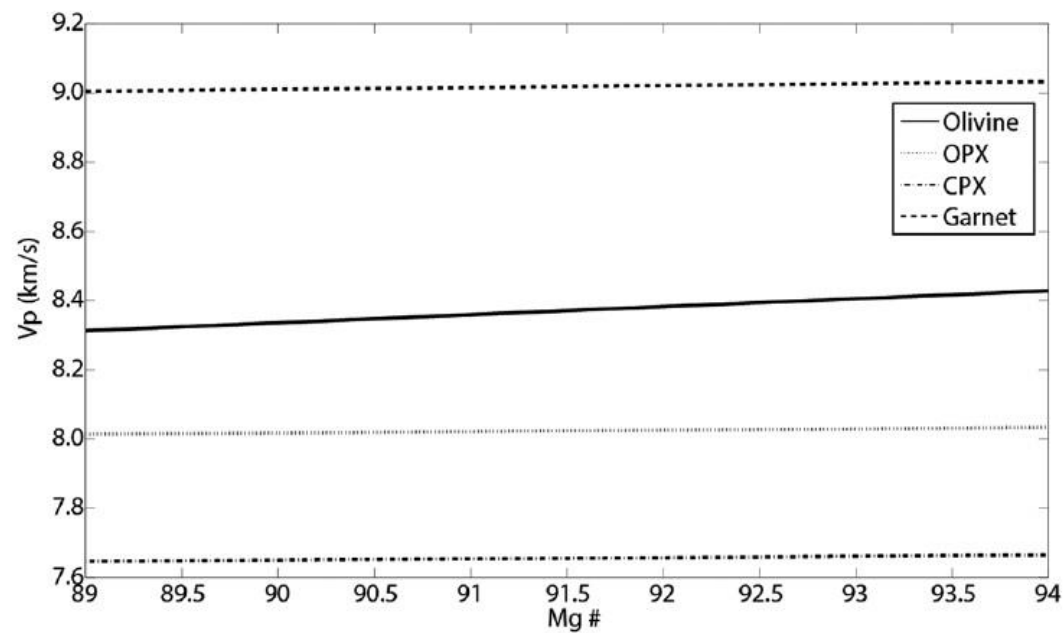
Mineral	ρ (g/cm)	K_S (GPa)	G (GPa)	K'_S	G'	$\partial K_S/\partial T$ (GPa/K)	$\partial G/\partial T$ (GPa/K)
Olivine	$3.222 + 1.182X_{Fe}$	129 ($\pm 1\%$)	$81 - 31X_{Fe}$ ($\pm 1\%$)	4.2 ($\pm 3\%$)	1.4 ($\pm 7\%$)	-0.017 ($\pm 17\%$)	-0.014 ($\pm 17\%$)
Wadsleyite (β -phase)	$3.472 + 1.24X_{Fe}$	172 ($\pm 1\%$)	$112 - 40X_{Fe}$ ($\pm 1.5\%$)	4.5 ($\pm 5\%$)	1.5 ($\pm 10\%$)	-0.014 ($\pm 25\%$)	-0.014 ($\pm 25\%$)
Ringwoodite (γ -phase)	$3.548 + 1.30X_{Fe}$	$185 + 35X_{Fe}$ ($\pm 1\%$)	$120.4 - 28X_{Fe}$ ($\pm 1.5\%$)	4.1 ($\pm 10\%$)	1.3 ($\pm 15\%$)	-0.024 ($\pm 20\%$)	-0.015 ($\pm 20\%$)
Clinopyroxenes Di-cEn-He	$3.277 + 0.38X_{Fe}$	$105 + 12X_{Fe}$ ($\pm 1\%$)	$67 - 6X_{Fe}$ ($\pm 2\%$)	$6.2 - 1.9X_{Fe}$ ($\pm 10\%$)	1.7 ($\pm 15\%$)	-0.013 ($\pm 25\%$)	-0.010 ($\pm 25\%$)
Jadeite	3.32	126 ($\pm 1\%$)	84 ($\pm 2\%$)	5.0 ($\pm 10\%$)	1.7 ($\pm 15\%$)	-0.016 ($\pm 20\%$)	-0.013 ($\pm 25\%$)
Orthopyroxenes En-Fs	$3.215 + 0.799X_{Fe}$	$109 + 20X_{Fe}$ ($\pm 2\%$)	$75 + 10X_{Fe}$ ($\pm 2\%$)	7.0 ($\pm 20\%$)	1.6 ($\pm 15\%$)	-0.027 ($\pm 25\%$)	-0.012 ($\pm 25\%$)
Garnet Py-Mj-Alm	$3.565 + 0.76X_{Alm} - 0.05X_{Mj}$	$171 + 15X_{Alm} - 5X_{Mj}$ ($\pm 1\%$)	$92 + 7X_{Alm} - 5X_{Mj}$ ($\pm 2\%$)	$4.4 + 1.4X_{Mj}$ ($\pm 10\%$)	$1.4 + 0.3X_{Mj}$ ($\pm 15\%$)	-0.019 ($\pm 20\%$)	-0.010 ($\pm 25\%$)
Ca-Garnet (Grossular)	3.597	168 ($\pm 1\%$)	107 ($\pm 1\%$)	5.2 ($\pm 10\%$)	1.6 ($\pm 15\%$)	-0.016 ($\pm 20\%$)	-0.012 ($\pm 25\%$)
Na-majorite	3.926	187 ($\pm 3\%$)	115 ($\pm 3\%$)	5.0 ($\pm 15\%$)	1.6 ($\pm 15\%$)	-0.016 ($\pm 25\%$)	-0.015 ($\pm 25\%$)
Mg-perovskite	$4.107 + 1.07X_{Fe}$	263 ($\pm 1\%$)	175 ($\pm 2\%$)	4.0 ($\pm 5\%$)	1.8 ($\pm 15\%$)	-0.017 ($\pm 20\%$)	-0.029 ($\pm 20\%$)
Ca-perovskite	4.210	236 ($\pm 2\%$)	165 ($\pm 2\%$)	4.4 ($\pm 10\%$)	2.5 ($\pm 20\%$)	-0.022 ($\pm 25\%$)	-0.023 ($\pm 25\%$)
Mg-wustite	$3.584 + 2.28X_{Fe}$	162 ($\pm 1\%$)	$130 - 77X_{Fe}$ ($\pm 2\%$)	4.0 ($\pm 10\%$)	2.35 ($\pm 20\%$)	-0.021 ($\pm 20\%$)	-0.024 ($\pm 25\%$)
Ilmenite	$3.810 + 1.1X_{Fe}$	212 ($\pm 1\%$)	$132 - 41X_{Fe}$ ($\pm 2\%$)	5.6 ($\pm 20\%$)	1.7 ($\pm 15\%$)	-0.017 ($\pm 25\%$)	-0.017 ($\pm 25\%$)
Coesite	2.911	98 ($\pm 1\%$)	61.7 ($\pm 1\%$)	4.3 ($\pm 20\%$)	1.5 ($\pm 20\%$)	-0.015 ($\pm 30\%$)	-0.015 ($\pm 30\%$)
Stishovite	4.289	294 ($\pm 1\%$)	217 ($\pm 1\%$)	5.3 ($\pm 15\%$)	1.8 ($\pm 15\%$)	-0.034 ($\pm 20\%$)	-0.018 ($\pm 25\%$)
Corundum	3.988	257 ($\pm 2\%$)	162 ($\pm 2\%$)	4.4 ($\pm 15\%$)	1.8 ($\pm 15\%$)	-0.014 ($\pm 25\%$)	-0.019 ($\pm 25\%$)
Hydrous wadsleyite	$3.300 + 1.24X_{Fe}$	153 ($\pm 3\%$)	$105 - 40X_{Fe}$ ($\pm 4.5\%$)	4.0 ($\pm 20\%$)	-	-	-
Hydrous ringwoodite	$3.470 + 1.30X_{Fe}$	$155 + 35X_{Fe}$ ($\pm 3\%$)	$108.0 - 28X_{Fe}$ ($\pm 3\%$)	5 ($\pm 20\%$)	-	-	-

ρ : density; K_S : bulk modulus; G : shear modulus, K'_S and G' : pressure derivatives of the moduli; $\partial K_S/\partial T$ and $\partial G/\partial T$: temperature derivatives of the moduli; X_{Fe} : mole fraction of iron; X_{Alm} , X_{Mj} : mole fractions of almandine and majorite in garnet solid solution. Di: diopside; cEn: clinoEnstatite; He: hedenbergite; En: enstatite; Fs: ferrosilite; Py: pyrope, Mj: majorite; Alm: almandine. Entries in italics are non-experimental values (elasticity systematics).

Minerals velocity and density dependence on composition



Tesauro et al., 2014, G3



Conversion of seismic velocity into temperatures

Anelasticity

$$Q_S = B\omega^a \exp\left(\frac{aH(P)}{RT}\right) \quad \text{with} \quad H(P) = E + PV$$

A is a normalization factor, ω the seismic frequency, a the exponent describing the frequency dependence of the attenuation, T the temperature, R the gas constant, H the activation enthalpy, V the activation volume and E the activation energy

The dimensionless factor g is a function of the activation enthalpy H , the melting temperature T_m and the gas constant R

$$Q_P^{-1} = (1-L)Q_K^{-1} + LQ_\mu^{-1} \quad L = (4/3)(V_S/V_P)^2$$

Q_k is a constant (1000 in the upper mantle and 10000 in the lower mantle)

Homologous Temperature Approach:
$$g = \frac{H(P)}{RT_m(P)}$$

Anelasticity parameters

Homologous temperature	$B^{a,b}$	g^a	a
Q1	0.5, 10	20, 10	0.2
Q2	0.8, 15		
Q3	1.1, 20		
Q4	0.035, 2.25	30, 15	0.2
Q5	0.056, 3.6		
Q6	0.077, 4.95		

a First value for upper-mantle, second for lower-mantle.

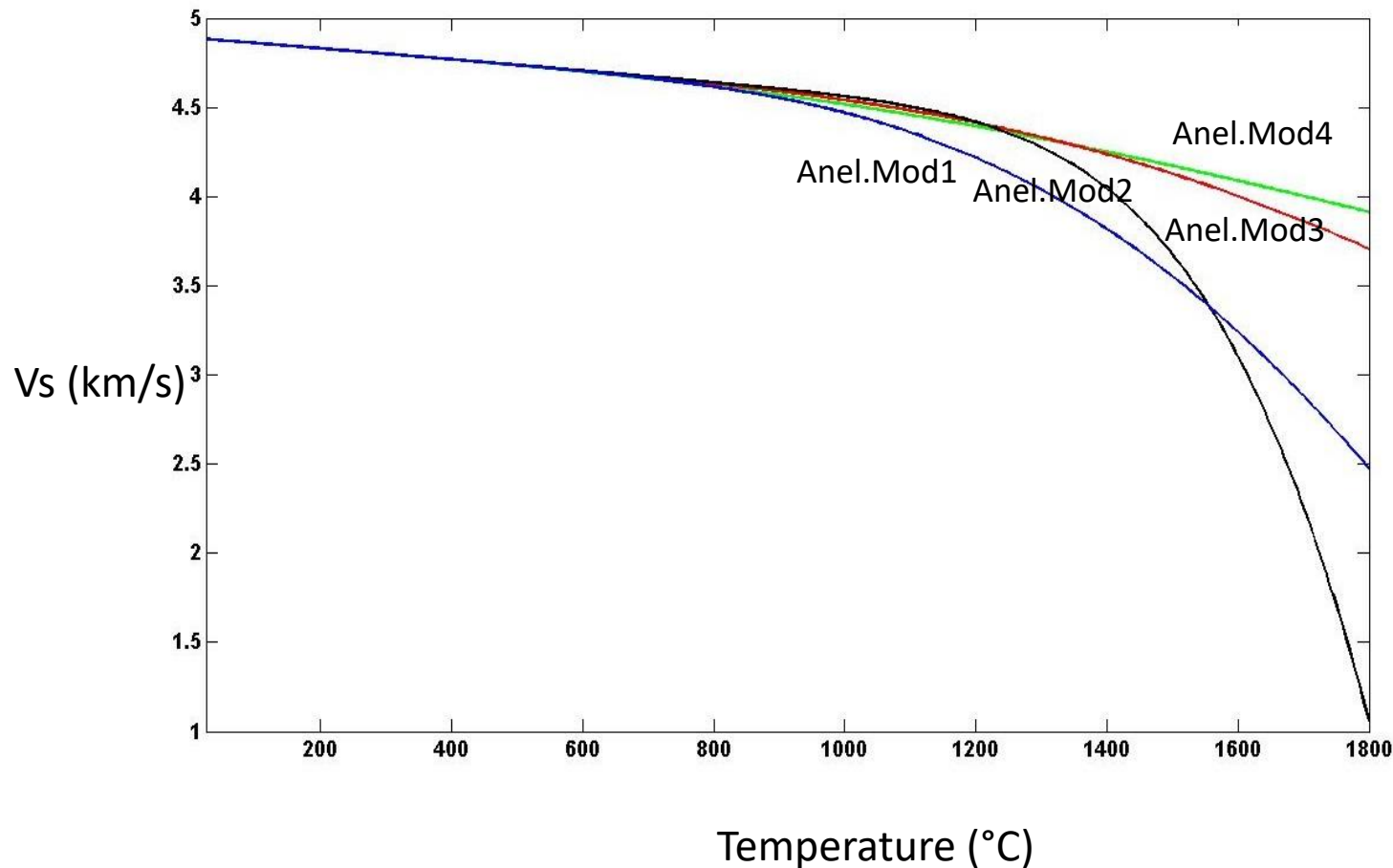
b Value is constrained by radial seismic attenuation models.

Cammarano et al., 2003, EPSL

Conversion of seismic velocity into temperatures

Seismic velocity and temperature are linearly inversely correlated up to a temperature of about 900°C due to the anharmonicity effect.

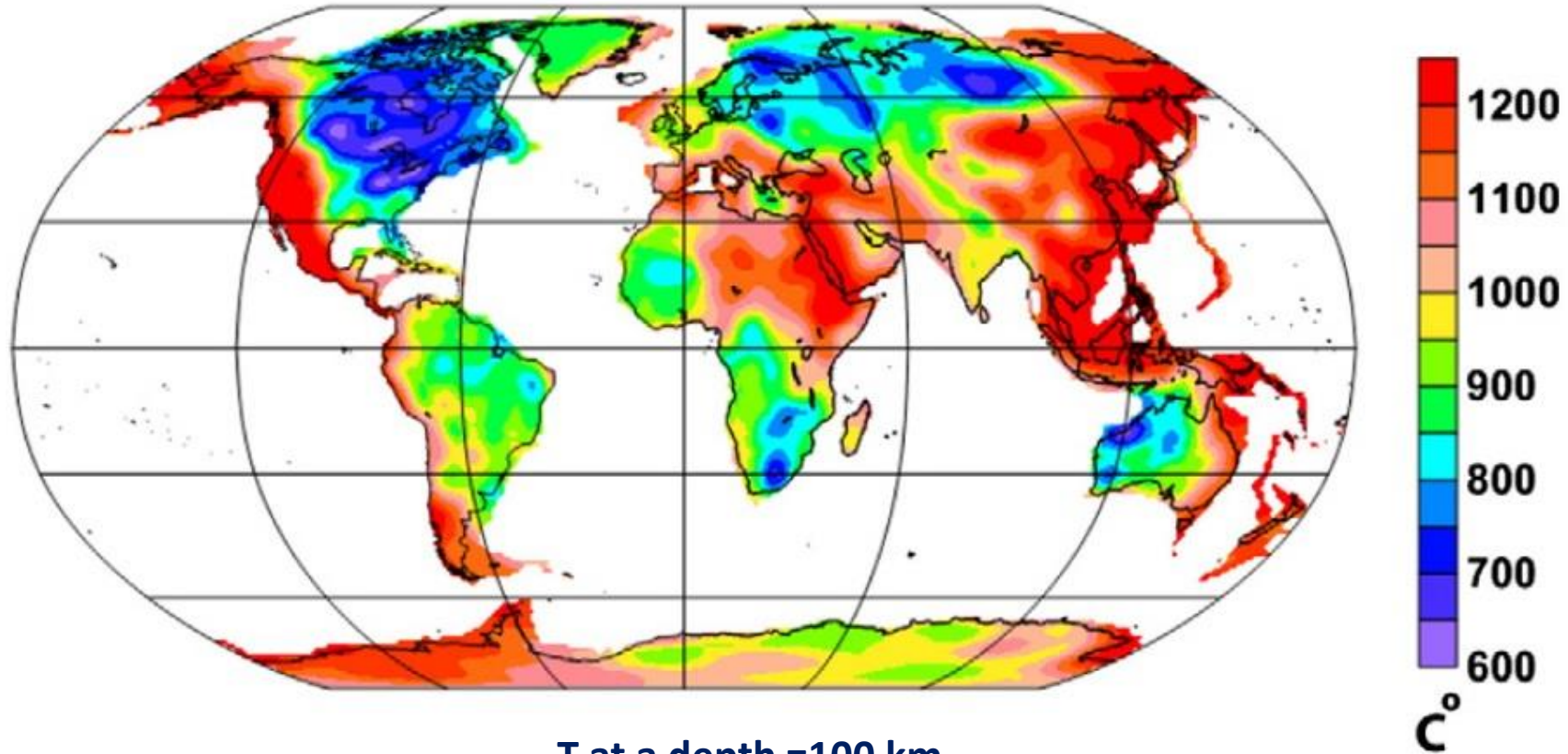
At higher temperatures it starts the effect of anelasticity: no linear correlation between velocity and temperatures



$$V(P, T, X, \omega) = V_{anh}(P, T, X) \left[1 - \frac{Q^{-1}(\omega, T)}{2 \tan(\pi a/2)} \right]$$

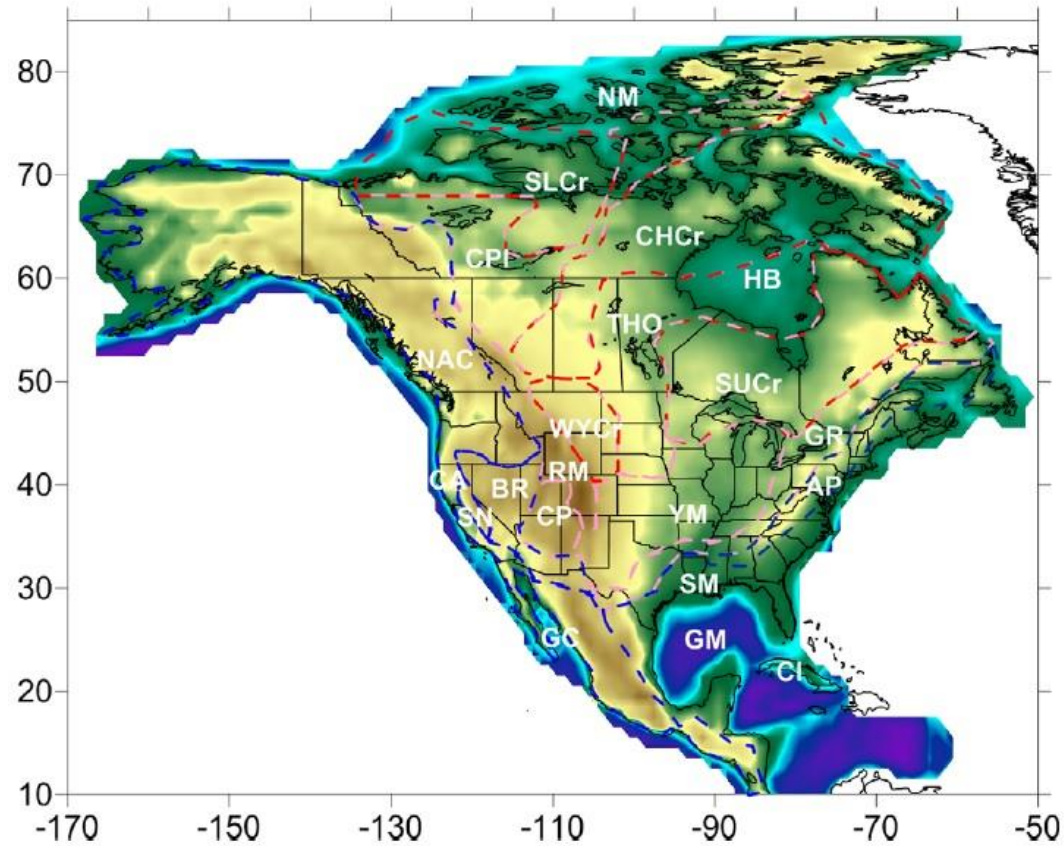
V_{ahn} = Synthetic Velocity (anharmonicity effect)

Global Thermal Model (inversion of seismic velocities into temperatures)



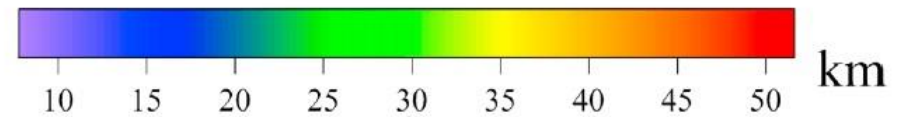
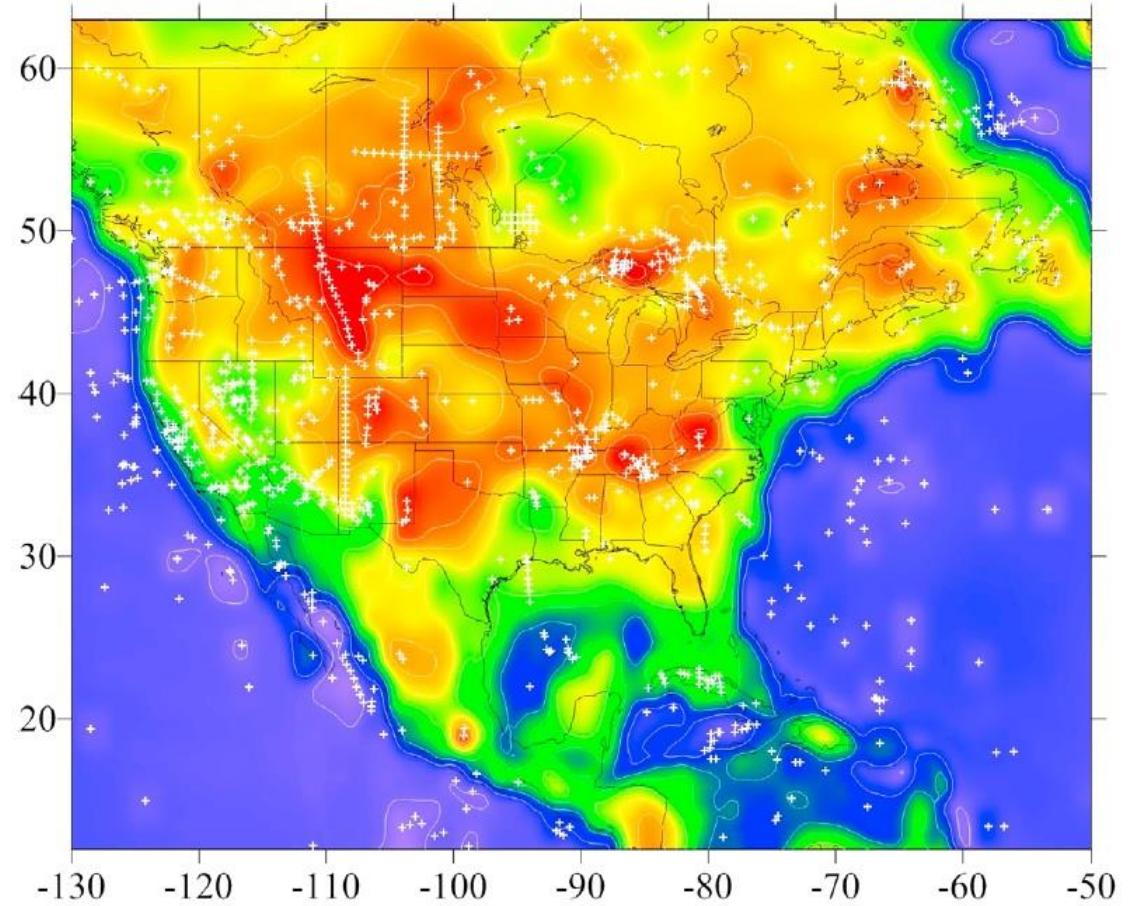
Tesauro et al., 2013, Tectonophysics, 602

Case of Studies: North American Continent (steady state conditions partially or not applicable)



--- Phanerozoic
 --- Proterozoic
 --- Archean

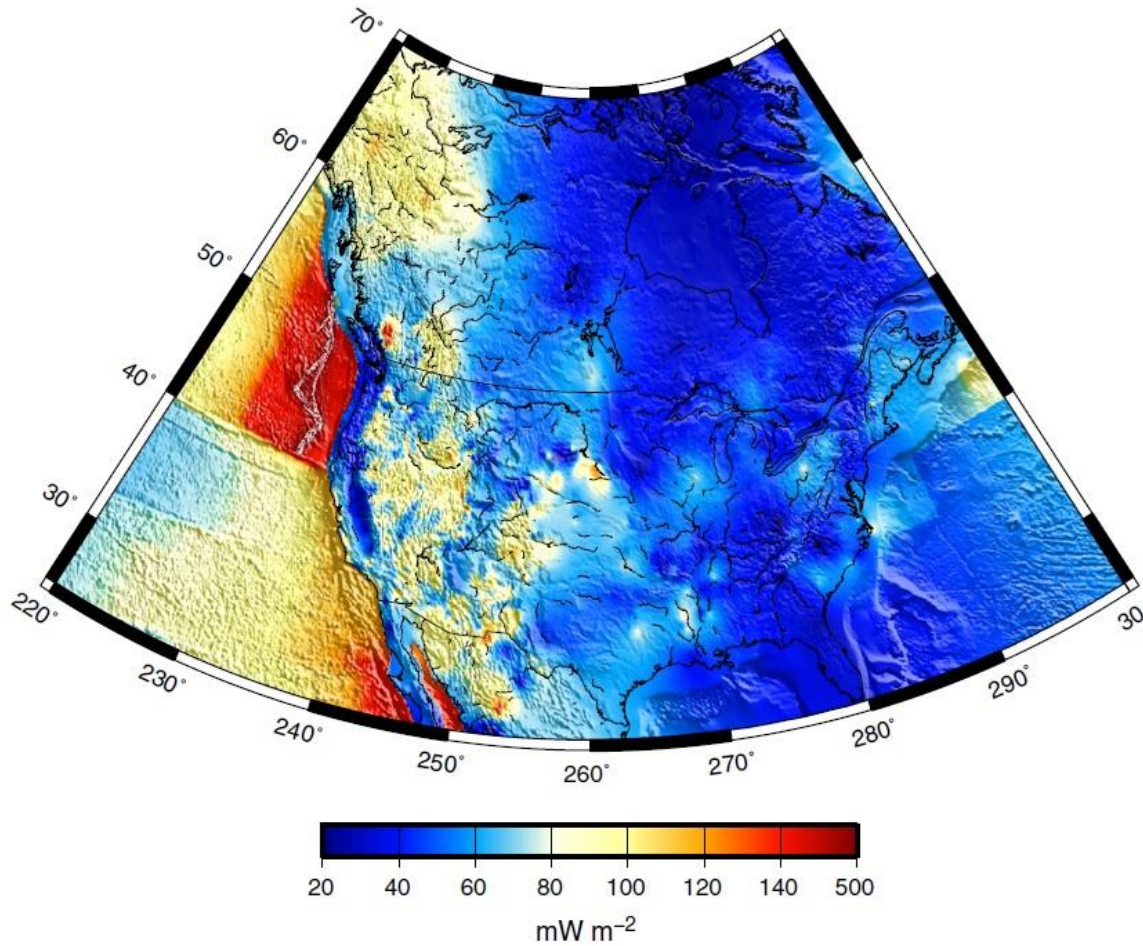
Tesauro et al., 2014, Tectonophysics, 631



Mooney and Kaban, 2010, JGR, 115

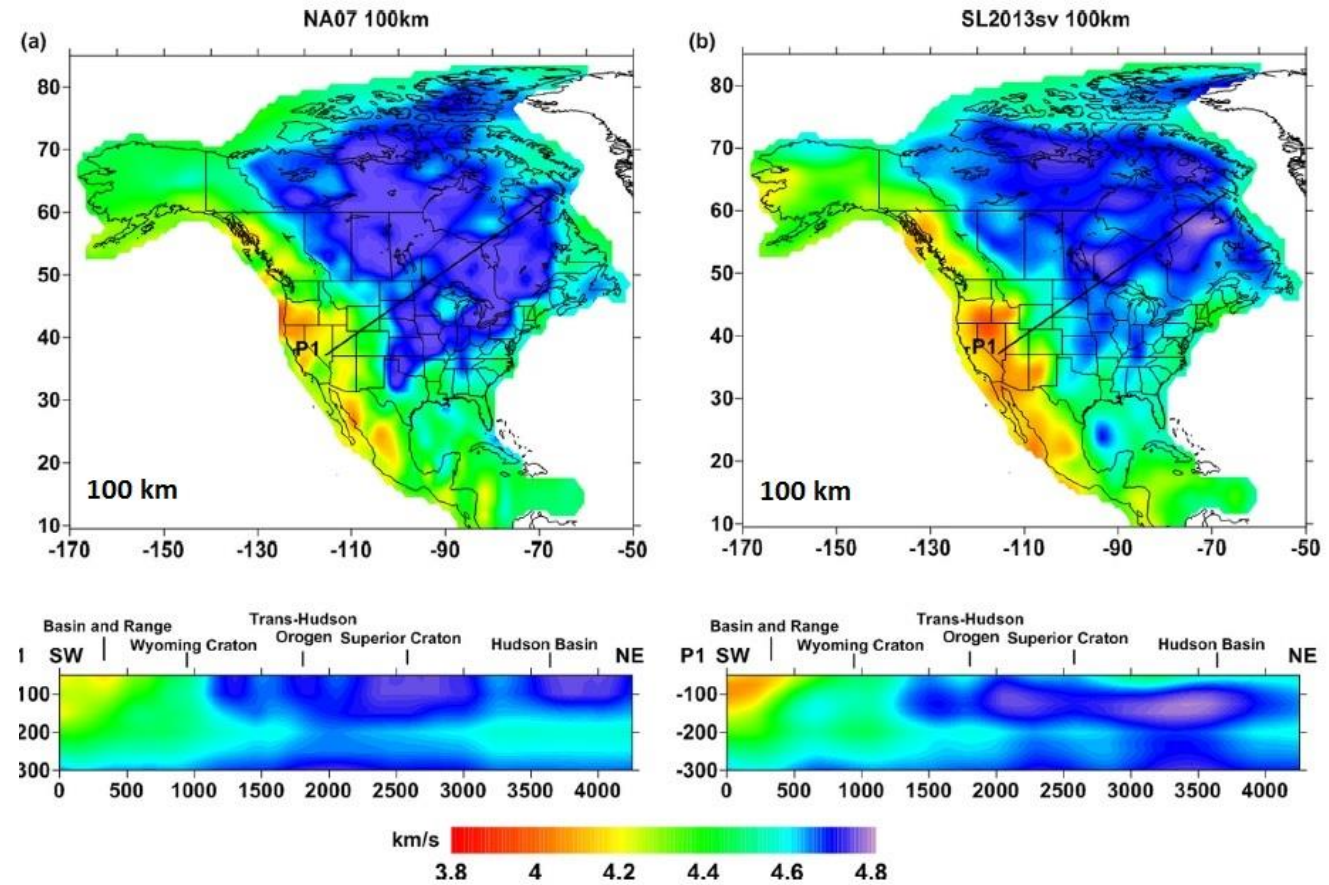
Case of Studies: North American Continent (steady state conditions partially or not applicable)

Heat Flow Values



Mareschal and Jaupart, 2013, Tectonophysics 609

S-Wave Tomography Model

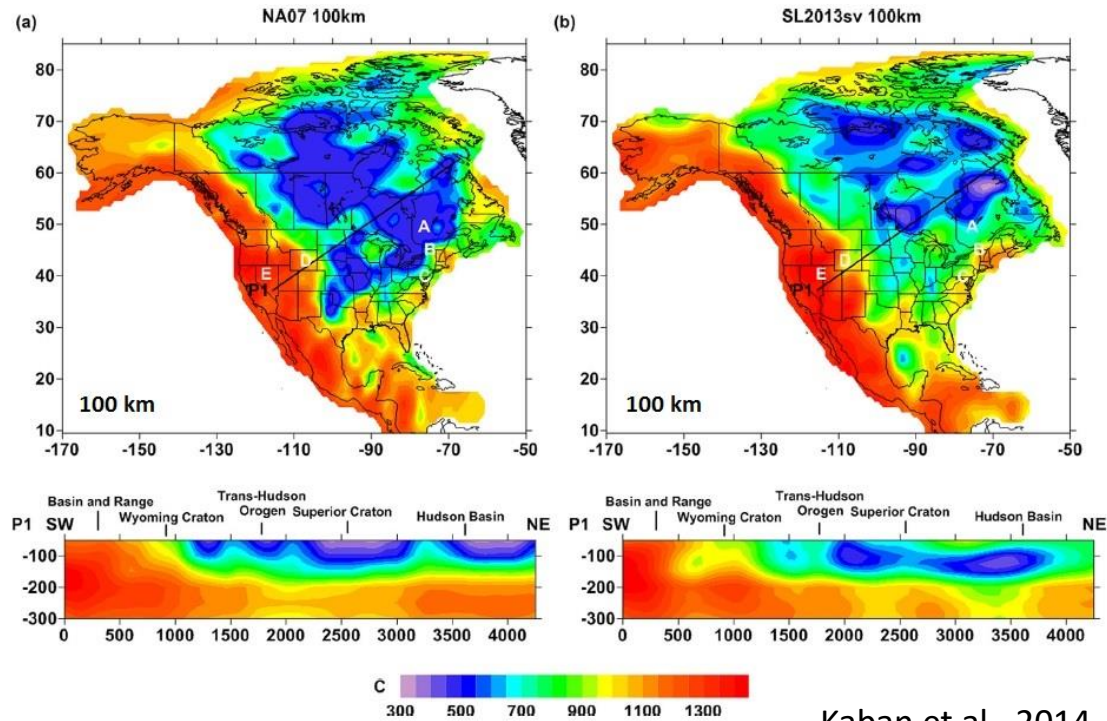


Bedle and van der Lee, 2008

Schaeffer and Lebedev, 2013

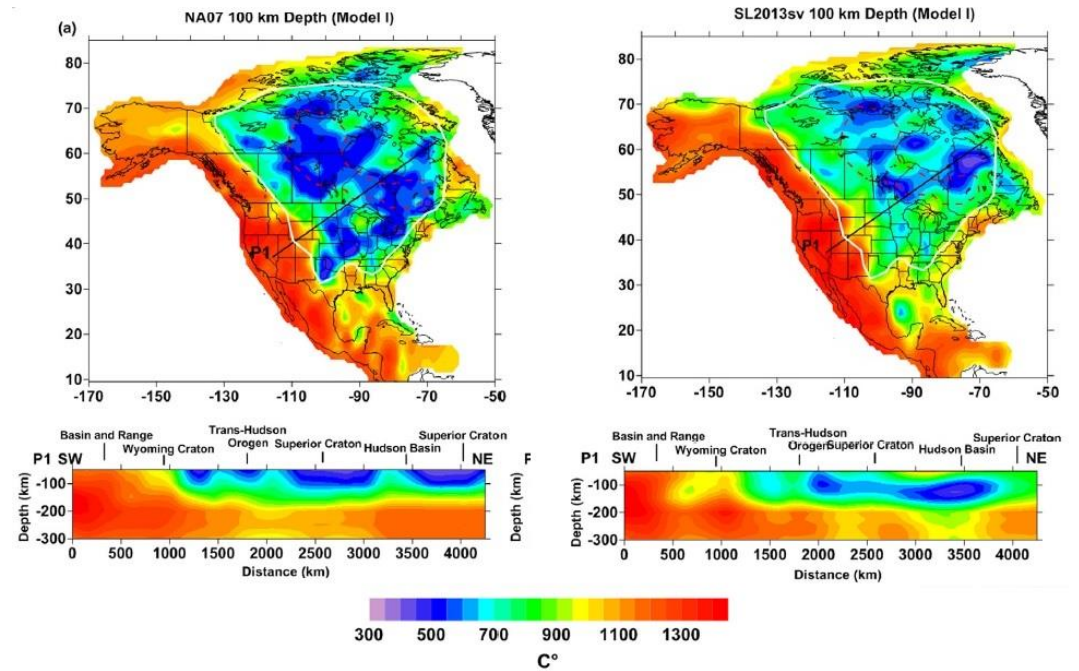
Case of Studies: North American Continent (steady state conditions partially or not applicable)

A



Kaban et al., 2014, G3

B



Tesauro et al., 2014, G3

A: Mantle temperatures obtained from seismic tomography inversion, using a uniform composition (fertile upper mantle).

B: Mantle temperatures obtained from seismic tomography inversion, accounting for depletion.

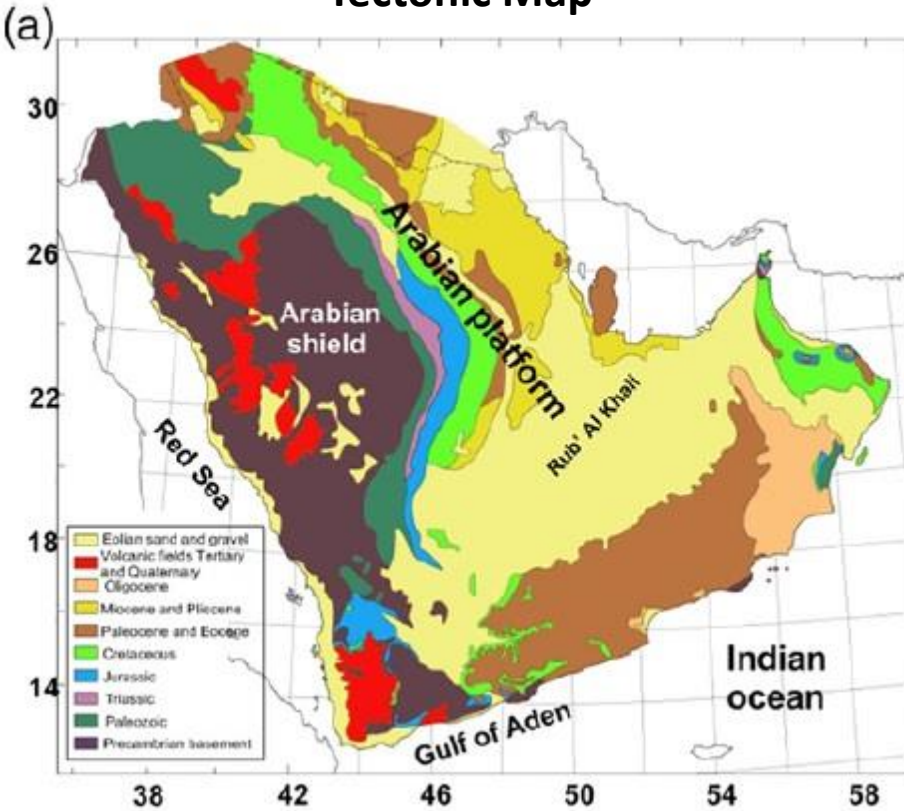
Fertile Upper Mantle (%)

Depleted Upper Mantle (%)

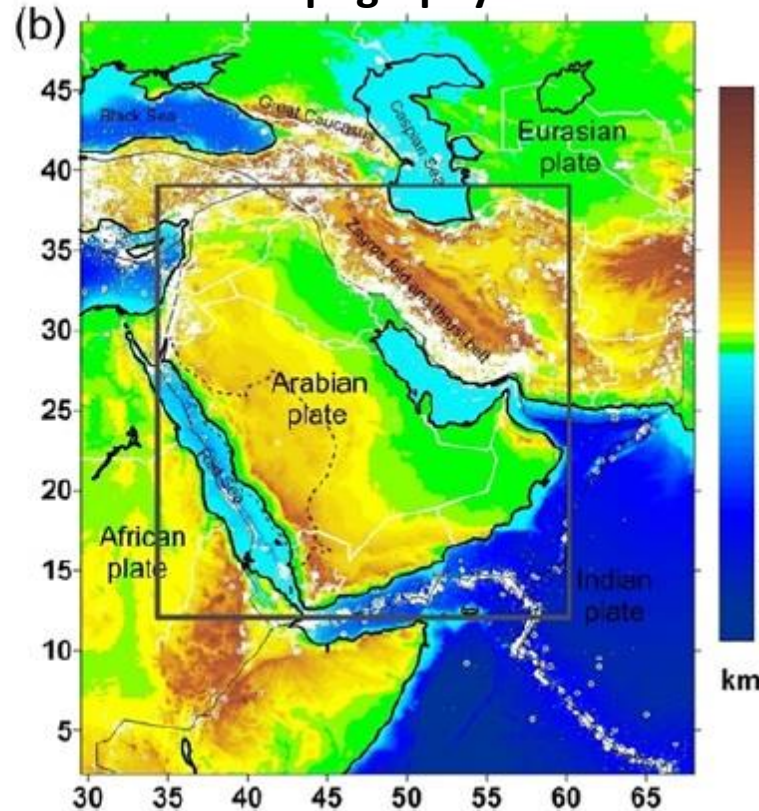
OI	OPX	CPX	Gr	Mg#	OI	OPX	CPX	Gr	Mg#
58.5	15	11.5	15	89	69.5	21	4	5.5	94

Case of Studies: Arabian Plate (steady state conditions partially or not applicable)

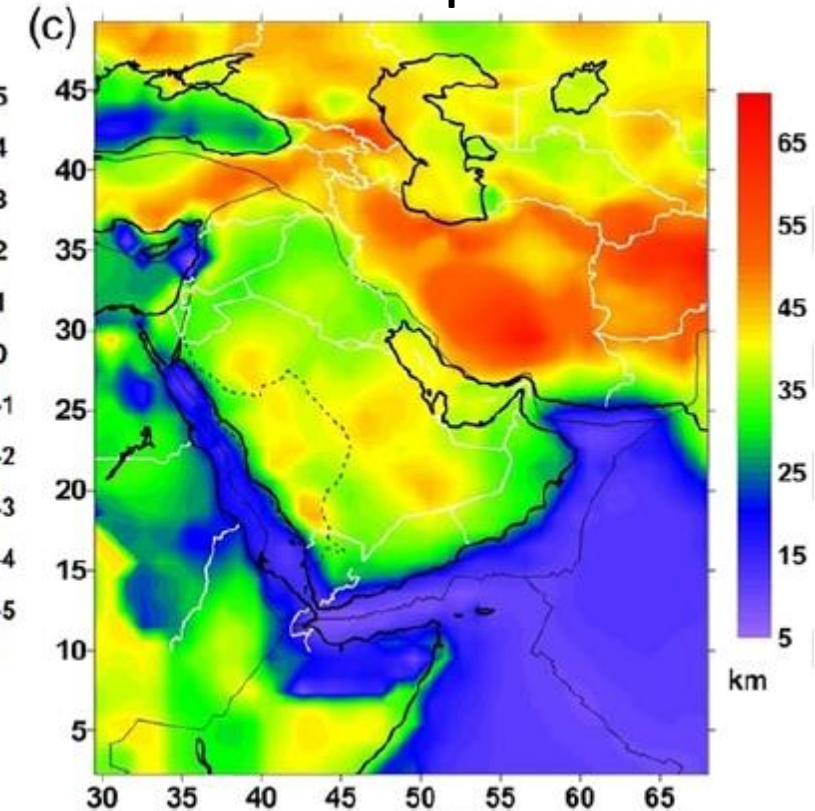
Tectonic Map



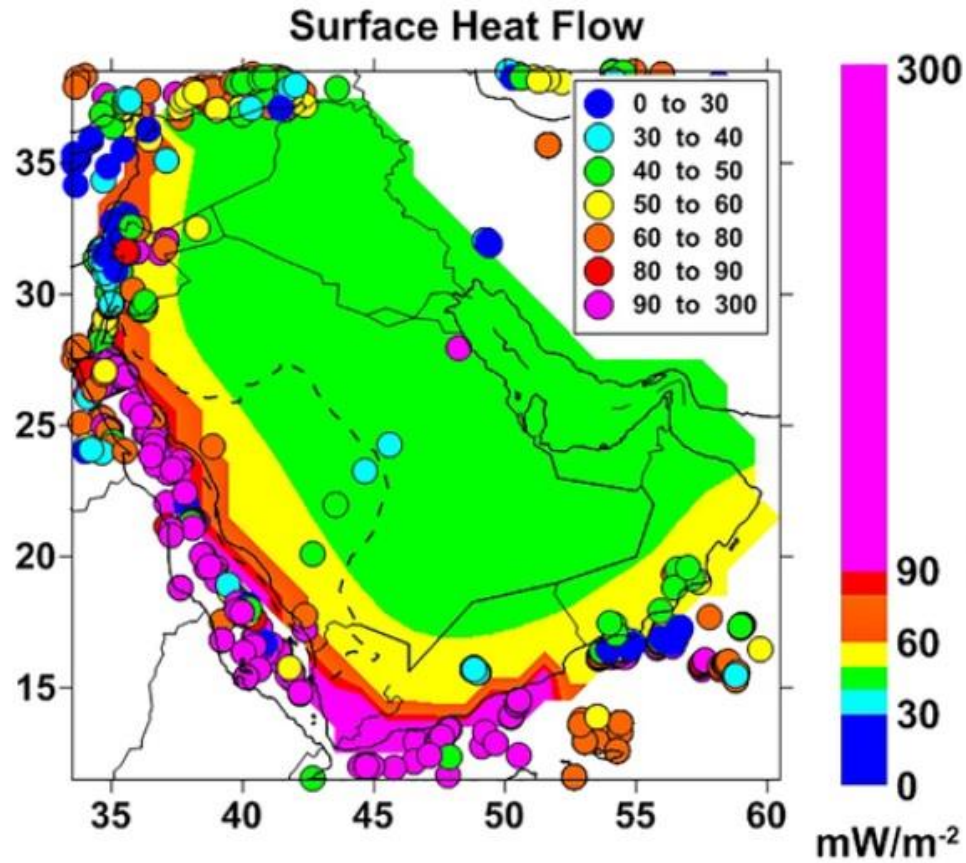
Topography



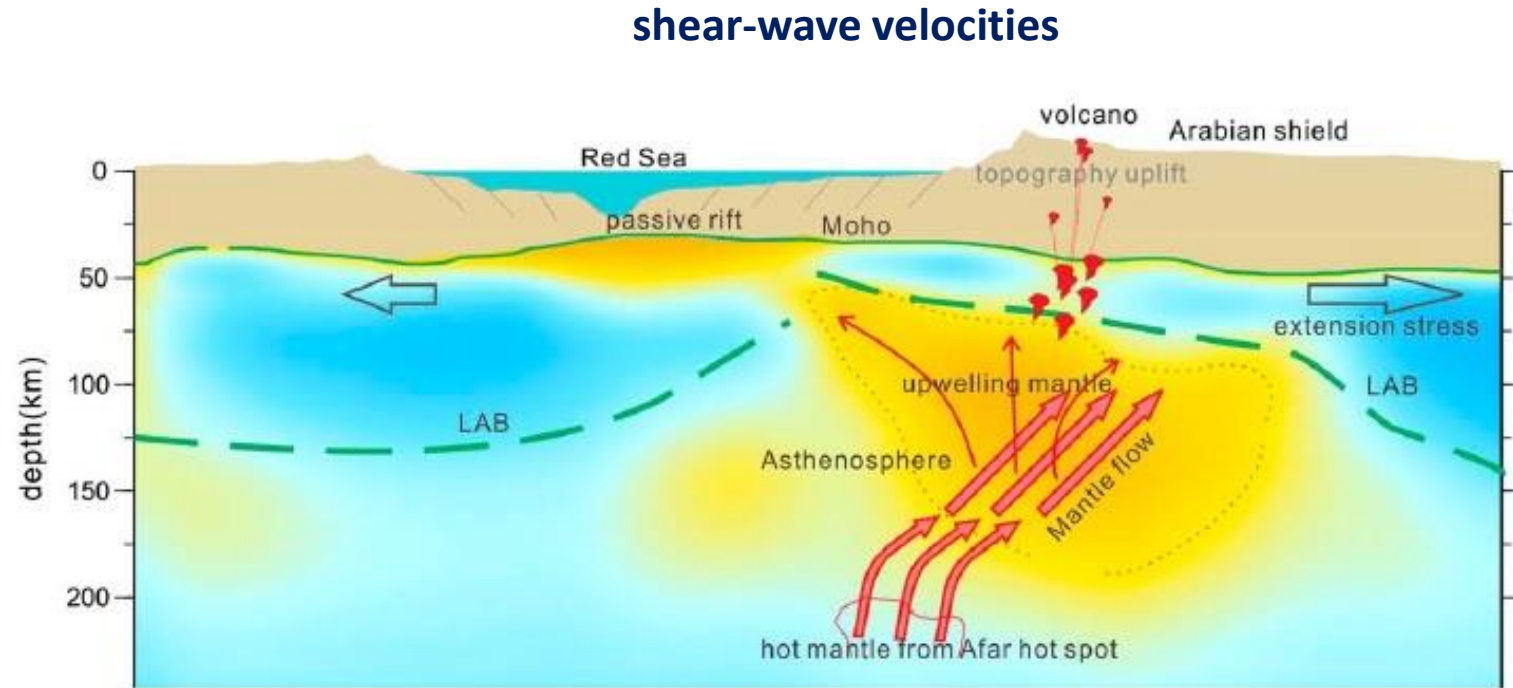
Moho Depth



Case of Studies: Arabian Plate (steady state conditions partially or not applicable)



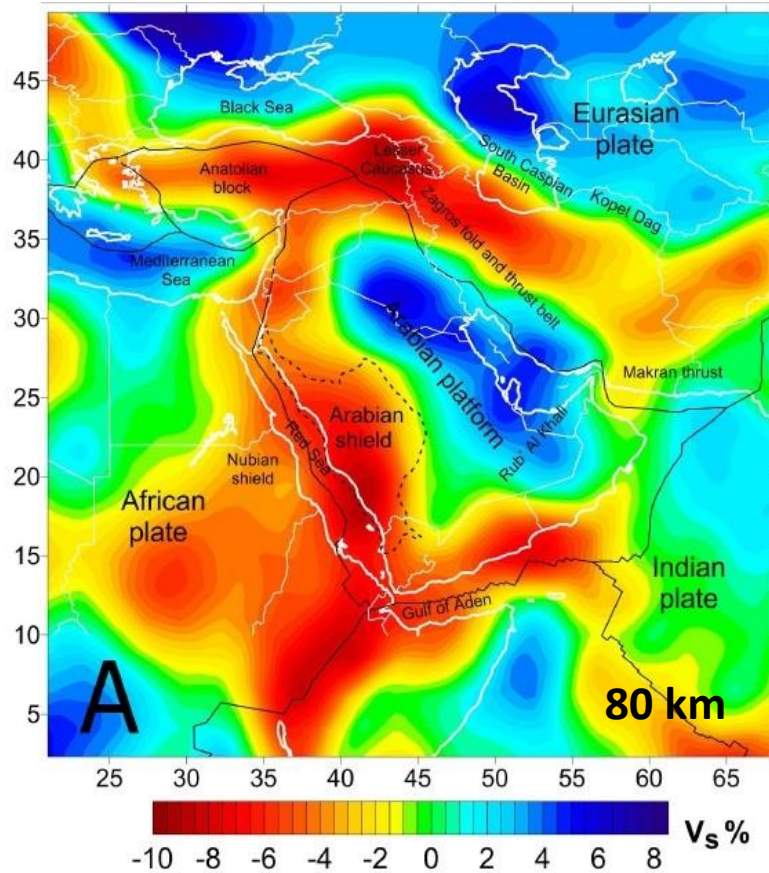
Tesauro et al., 2018, Tectonophysics



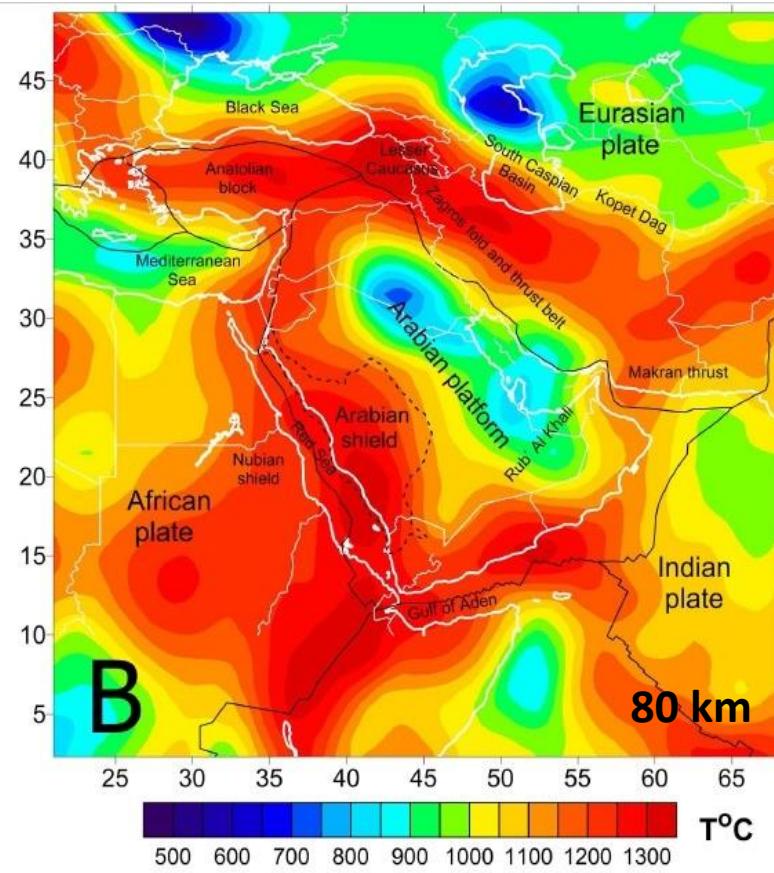
Yao et al., 2017, JGR

Case of Studies: Arabian Plate (steady state conditions partially or not applicable)

S-wave tomography model *SL2013sv*
(Schaeffer and Lebedev, 2013)



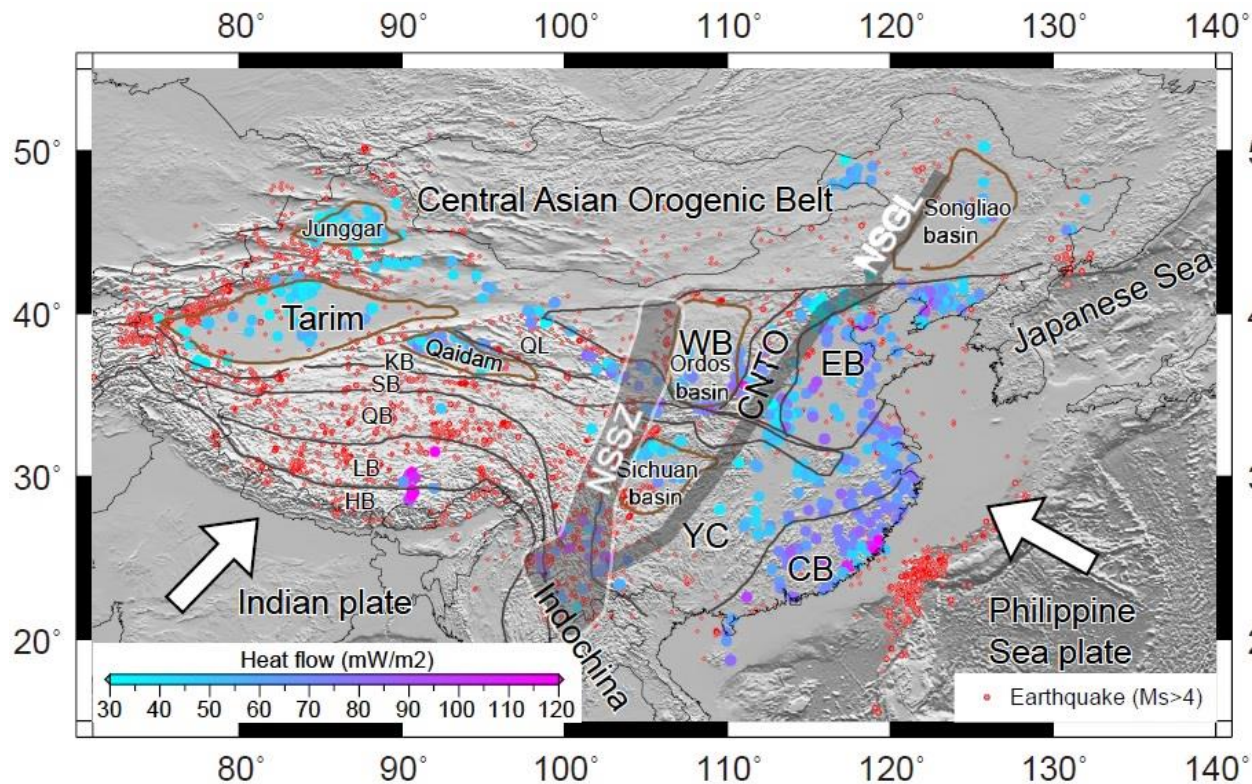
Upper Mantle Temperature
(Kaban et al., 2016), G3



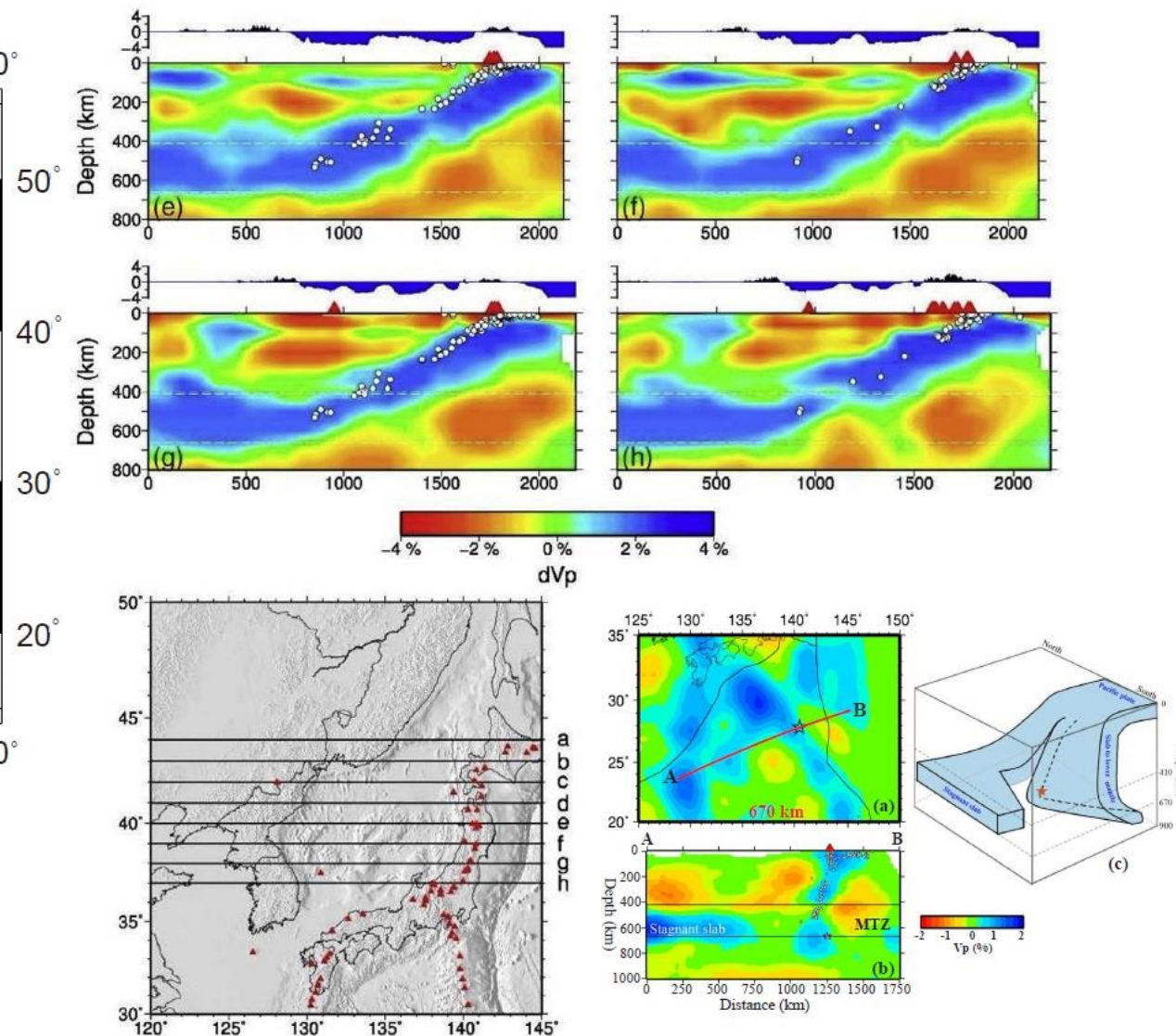
Tesauro et al., 2018, Tectonophysics (in press)

- According to the surface heat flow data, the Precambrian Crust of the Arabian Plate is cold ($Q < 65 \text{ mWm}^{-2}$)
- Seismic velocity models and their conversion into temperature, show that the upper mantle of the Shield is anomalously hot

Case of Studies: Mainland China (steady state conditions partially or not applicable)

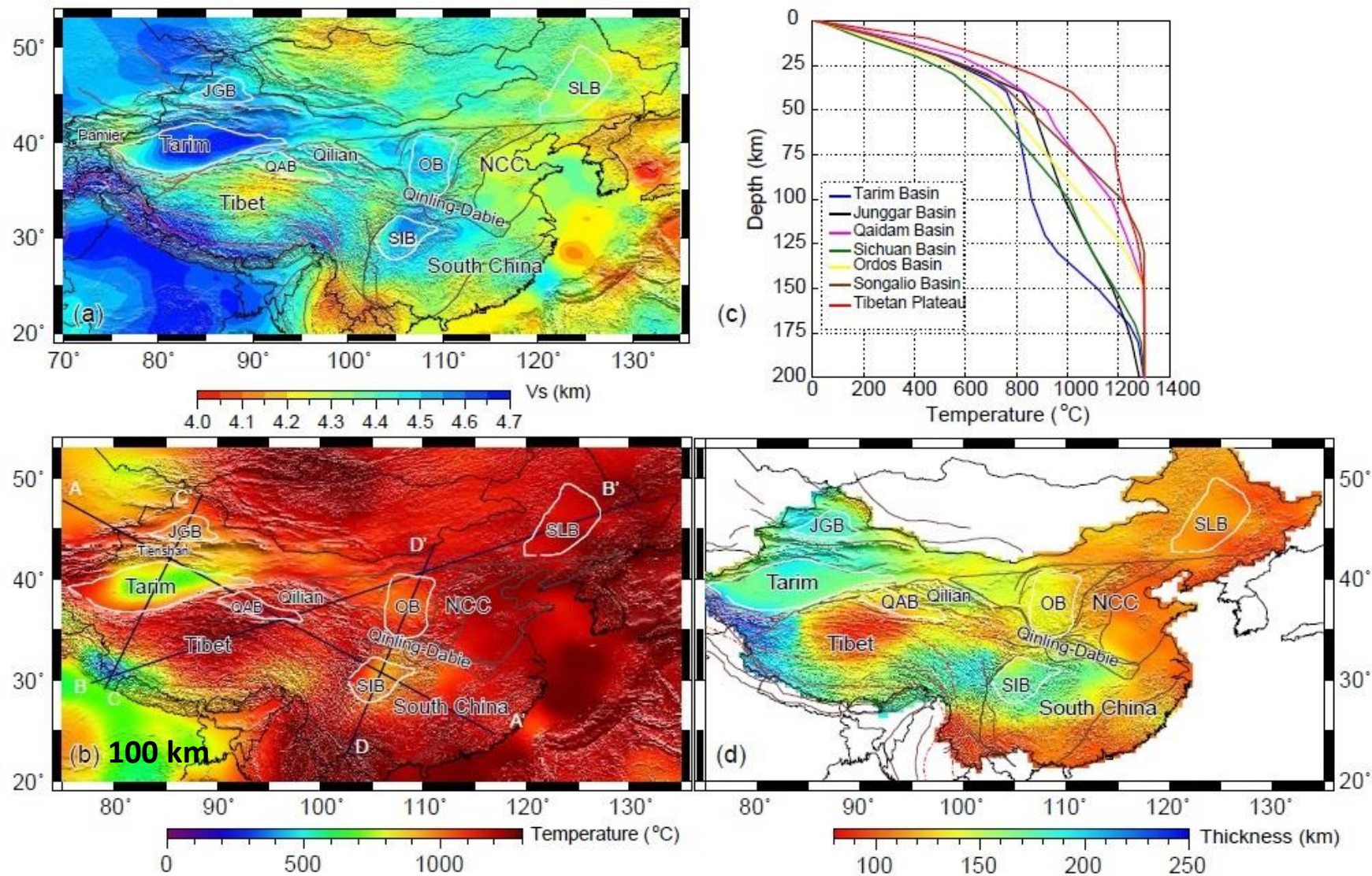


Deng and Tesauro, 2016 Tectonics



Zhao et al. , 2017 J. Asian Earth Sci.

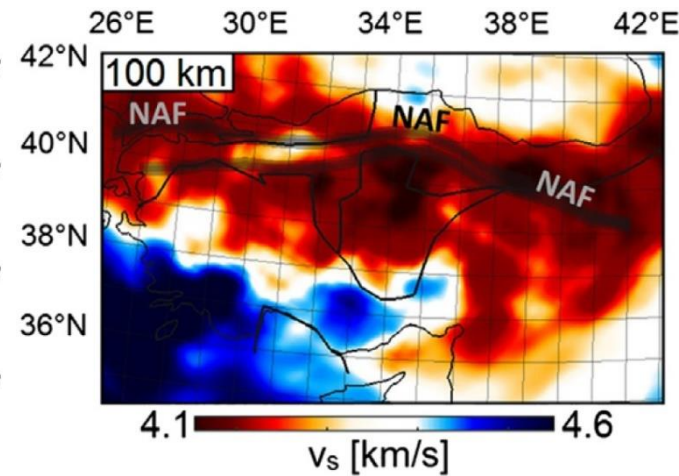
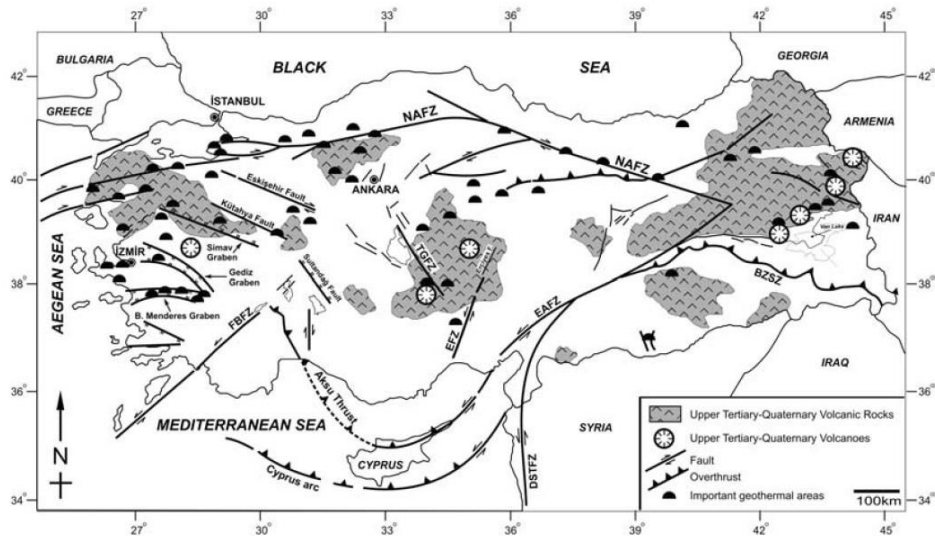
Case of Studies: Mainland China (steady state conditions partially or not applicable)



Curie Temperatures

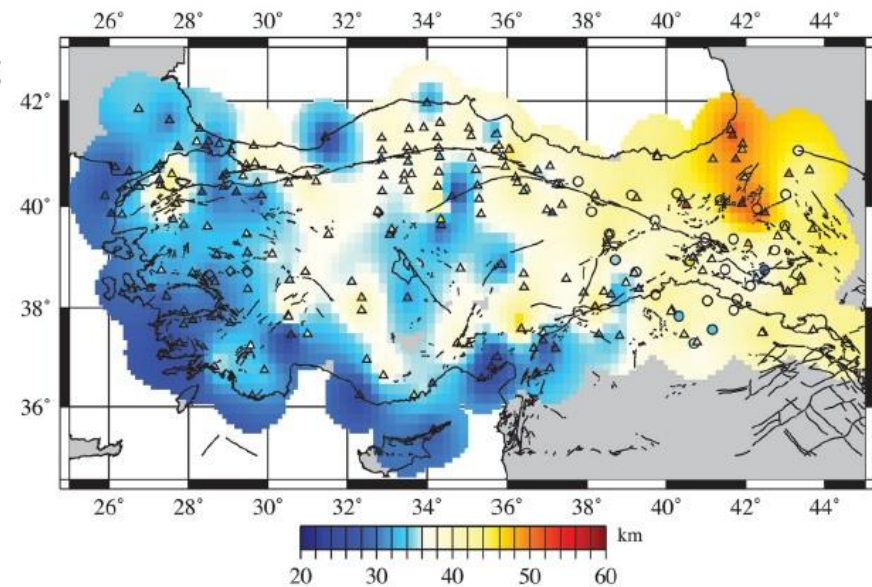
- The Curie temperature is the temperature at which a mineral loses its ferromagnetic properties becoming paramagnetic and the depth at which this occurs is called Curie point depth (CPD). Above the CPD surface (referred to as the magnetite), iron(II) oxide present in rocks are unstable and iron(III) oxide present in rocks are stable, but below the CPD surface, this condition is inverted.
- Usually we refer to the Curie T of the pure magnetite ($\sim 580^\circ\text{C}$, with a range of 848-853 K), but different rocks have different Curie T , e.g., ~ 100 - 540°C for titanomagnetites, depending on their TiO_2 content, 100 - 300°C , for ferromagnetic minerals within andesites and alkali-basalts, 300° - 450°C for intermediate to mafic compositions, and 770°C for pure iron.
- The CPD usually does not correspond to the depth of the bottom edges of magnetic bodies (BEMB), which can be explained by ferric iron (III) instability under high P - T conditions with its transformation to ferrous iron (II), occurring at a $T \sim 843$ (or lower at higher pressure).

Case of study: Turkey

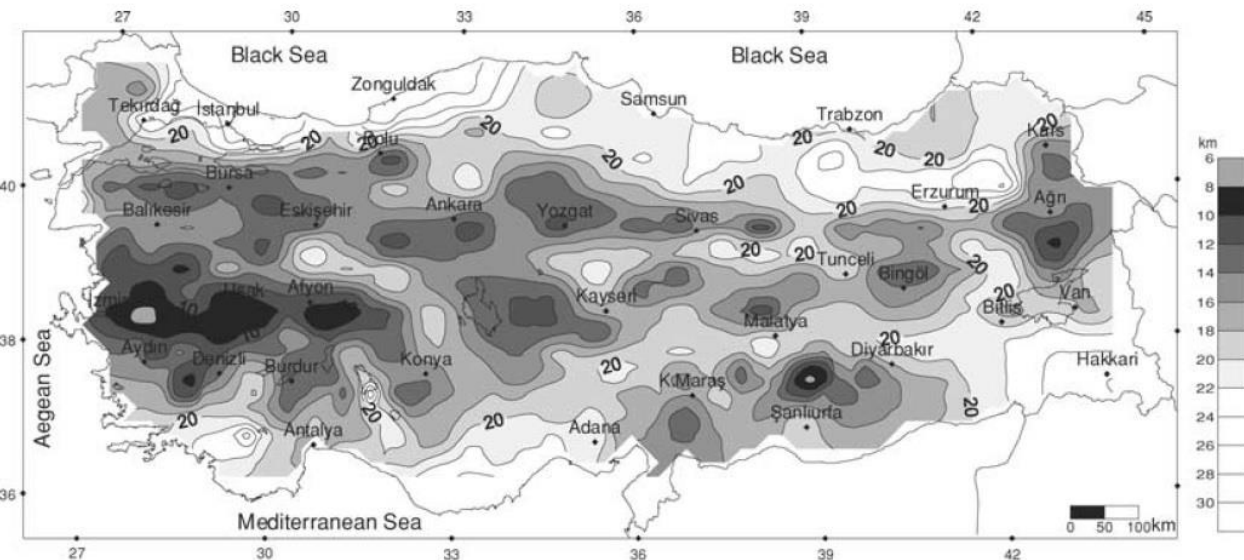


Fichtner et al., EPSL, 373

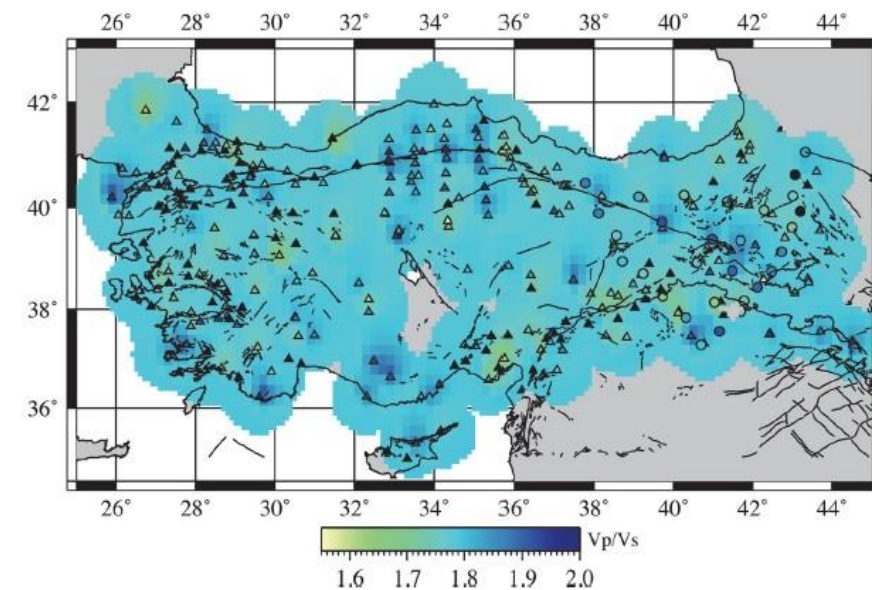
Moho Depth



CPD



Aydin et al., 2005, GJI, 162



Vanacore et al., 2013, GJI, 193

Drawbacks of different approaches estimating thermal conditions of continental lithosphere

Surface Heat Flux data:

- Different data quality (data of low quality are those from shallow boreholes)
- Uneven distribution of surface heat flux data
- Uncertainties in conductivity and heat production values
- Wrong assumption on pure conductive origin of surface heat flow (e.g., tectonically active region)
- Heat flux data may reflect the past thermal regime because of the low thermal conductivity of the lithosphere.

Xenolith data:

- Xenolith data are restricted to specific tectonic settings
- Xenolith have small size (usually < 1m) not representative of the mantle heterogeneity
- Xenoliths may not be representative of the present thermal state of the lithosphere
- Chemical reactions between xenoliths and host magmas further complicate petrologic interpretations
- The maximum depth sampled by xenoliths is ~ 250 km (not necessarily corresponding to the depth of the lithosphere).

Inversion of seismic velocity into temperatures:

- There are many uncertainties affecting the seismic tomography models (e.g., the amplitude of velocity perturbations can vary significantly from a model to another), which cause uncertainties of temperature.
- There are other factors rather than temperatures on which the seismic velocities depend (e.g., composition, melt, water, anisotropy).
- There are uncertainties on the values of elastic parameters and densities of the minerals.

References

Main readings:

Books:

- Artemieva, 2011, Chapter 4, Thermal regime of the lithosphere from heat flow data, *The lithosphere an interdisciplinary approach*, Cambridge and University Press.
- Artemieva, Chapter 5, Thermal state of the lithosphere from non-thermal data, *The lithosphere an interdisciplinary approach*, Cambridge and University Press.
- Davies, 1999, Chapter 7, Heat, *Dynamic Earth Plates, Plumes and Mantle Convection*, Cambridge and University Press.
- Goes et al., 2020, Continental lithospheric temperatures: A review, *Physics of the Earth and Planetary Interiors*, 306, 106509
- Jaupart and Mareschal, 2011, Chapter 7, Heat Generation and Transport in the Earth Thermal structure of the continental lithosphere, 146-175.
- Jaupart and Mareschal, 2007, Heat Flow and Thermal Structure of the Lithosphere, *Treatise of Geophysics*, vol.6, 217-251.

Articles:

- Hasterok and Chapman, 2011, Heat production and geotherms for the continental lithosphere, 307, 59-70.
- Goes et al., 2000, Shallow mantle temperatures under Europe from *P* and *S* wave tomography, *JGR*, 105, 11153-11169.
- Jaupart et al., 2016. Radiogenic heat production in the continental crust. *Lithos* 262, 398–427.

References

Further readings:

- Artemieva, 2009, The continental lithosphere: Reconciling thermal, seismic, and petrologic data, *Lithos*, 109, 23–46.
- Artemieva and Mooney, 2001, Thermal thickness and evolution of Precambrian lithosphere: A global study, *J. Geophys. Res.* 106B, 16387-16414.
- Artemieva, 2006, Global 1°×1° thermal model TC1 for the continental lithosphere: Implications for lithosphere secular evolution, *Tectonophysics*, 416, 245–277.
- Aydin et al., 2005, Curie-point depth map of Turkey, *GJI*, 162, 633-640.
- Bedle and van der Lee, 2008, S velocity variations beneath North America, *JGR* 14, B07308.
- Cammarano et al., 2003, Inferring upper-mantle temperatures from seismic velocities, *EPSL*, 197–222
- Deng and Tesauro, 2016, Lithospheric strength variations in Mainland China: Tectonic implications, *Tectonics*, 35.
- Fichtner et al., 2013, The deep structure of the North Anatolian Fault Zone *EPSL*, 373, 109-117.
- Kaban et al., 2014, Density, temperature, and composition of the North American lithosphere—New insights from a joint analysis of seismic, gravity, and mineral physics data: 1. Density structure of the crust and upper mantle, *G3*, 15.
- Limberger et al., 2018, Geothermal energy in deep aquifers: A global assessment of the resource base for direct heat utilization, *Renewable and Sustainable Energy Reviews*, 82, 961-975.
- Mareschal and Jaupart, 2013, Radiogenic heat production, thermal regime and evolution of continental crust, *Tectonophysics* 609, 524-534.
- Mooney and Kaban, 2010, The North American upper mantle: Density, composition, and evolution, *JGR*, 115, B12424.
- Plesa, A.-C., Padovan, S., Tosi, N., Breuer, D., Grott, M., Wicczorek, M. A., et al. (2018). The thermal state and interior structure of Mars. *Geophysical Research Letters*, 45, 12,198–12,209.
- Schaeffer and Lebedev, 2013, Imaging the North American continent using waveform inversion of global and USArray data, *EPSL* 402, 26–41.
- Tesauro et al., 2018, Strength and elastic thickness variations in the Arabian Plate: A combination of temperature, composition and strain rates of the lithosphere, *Tectonophysics* (in press).
- Tesauro et al., 2014, Density, temperature, and composition of the North American lithosphere—New insights from a joint analysis of seismic, gravity, and mineral physics data: 2. Thermal and compositional model of the upper mantle, *G3*
- Tesauro et al., 2013, Global model for the lithospheric strength and effective elastic thickness, *Tectonophysics*, 602, 78-86.
- Vanacore et al., 2013, Moho structure of the Anatolian Plate from receiver function analysis, *GJI*, 193, 329–337.
- Yao et al., 2017, Upper mantle velocity structure beneath the Arabian shield from Rayleigh surface wave tomography and its implications, *JGR*, 122.
- Zhao et al. , 2017, Seismic imaging of the Asian orogens and subduction zones, *J. Asian Earth Sci.*, 145, 349-367.